Table of Contents - Issue 32, 2013

Full papers:

Journal of Pyrotechnics

Journal of Pyrotechnics.

8 Aragon Place, Kimbolton, Huntingdon, Cambridgeshire UK

tel: +44 (1480) 878620 email: jpyro@carndu.com

Shellcalc© – 10 years on. A review of progress and application

Tom Smith
CarnDu Limited, 8 Aragon Place, Kimbolton, Huntingdon, Cambs PE28 0JD, UK
email: tom@carndu.com

Abstract: *Shellcalc© was originally developed by John Harradine and published by him and the author of this paper in the Journal of Pyrotechnics. Shellcalc© has been significantly developed since its original publication and now provides a wide range of simulations. The program has been used to model potential hazards from firework comets and shells in a variety of very high profile events around the world by the author and others, in order to place constraints on types that may be used under a variety of conditions. The development of the program is discussed and examples of its use are illustrated.*

Keywords: *Shellcalc©, shells, comets, trajectory, fall-out, debris*

Introduction

In the 10 years since Shellcalc© was originally developed by John Harradine, and the eight years since the original publication[1] appeared in the *Journal of Pyrotechnics*, there have been many developments both in the program itself, and in its application.

The number of input parameters has been extended and includes:

- Measured shell burst height and diameter
- The ability to fire from above (e.g. on a structure) or below (e.g. in a river valley) ground level
- The ability to fire at a greater range or angles including below horizontal (for firing comets off structures)

The program now displays a variety of information including

- "Blind" shell distance
- Shell burst diameter
- "Normal" fallout distances for expected debris
- "Long burn" fallout distances for long burning effects

The Shellcalc© program has been used by the author to develop risk models for a variety of high profile events including Hong Kong New Year's Eve, the Plymouth Firework Competition, London New Year's Eve and the London Olympics 2012.

This paper explains the features of the newest version of Shellcalc©, and how the program may be used practically.

Original versions

John Harradine, an explosives inspector in Queensland, Australia, developed an Excel© spreadsheet application which he termed Shellcalc©, following the Bray Park[2] and Carmel[3] accidents. The program modelled the trajectories of shells and comets and allows the prediction, for the first time in a practical and easily accessible manner, of where shells might fall if fired and fail to burst ("blinds"), and where they are predicted to burst (in the case of shells) or be extinguished (in the case of comets) from normal functioning under a variety of firing conditions. These include:

- Firing angle
- Relative wind direction
- Wind speed
- Ground terrain
- Air density
- Effective comet diameter and mass (as the comet burns during its flight)

A screenshot from the original Shellcalc© program is shown in Figure 1.

Although this was extremely useful and practical information which was not readily available to the show designer or practitioner at the time, the distance a shell may travel is only one factor in determining an appropriate distance for the shell to be fired from, for instance, buildings or the audience. We do not, wherever possible, refer to such distances as "safety" distances – to do so implies that at such a distance there is no risk to persons or structures. Instead we prefer to examine the

Article Details	***Article No:- 0097***
Manuscript Received:- 11/02/2013	***Final Revisions:- 17/02/2013***
Publication Date:- 17/02/2013	***Article Reference:- 1545***

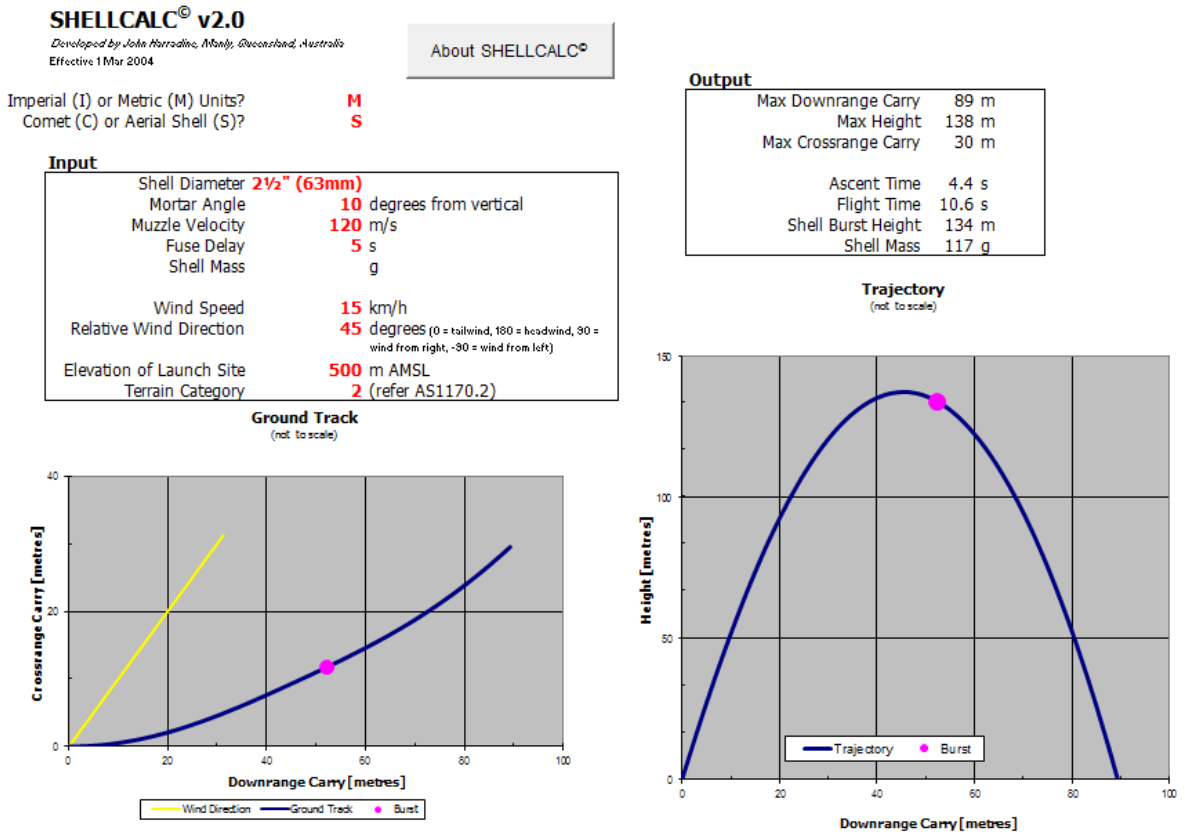

Figure 1. *Screenshot from version 2.0 of Shellcalc©.*

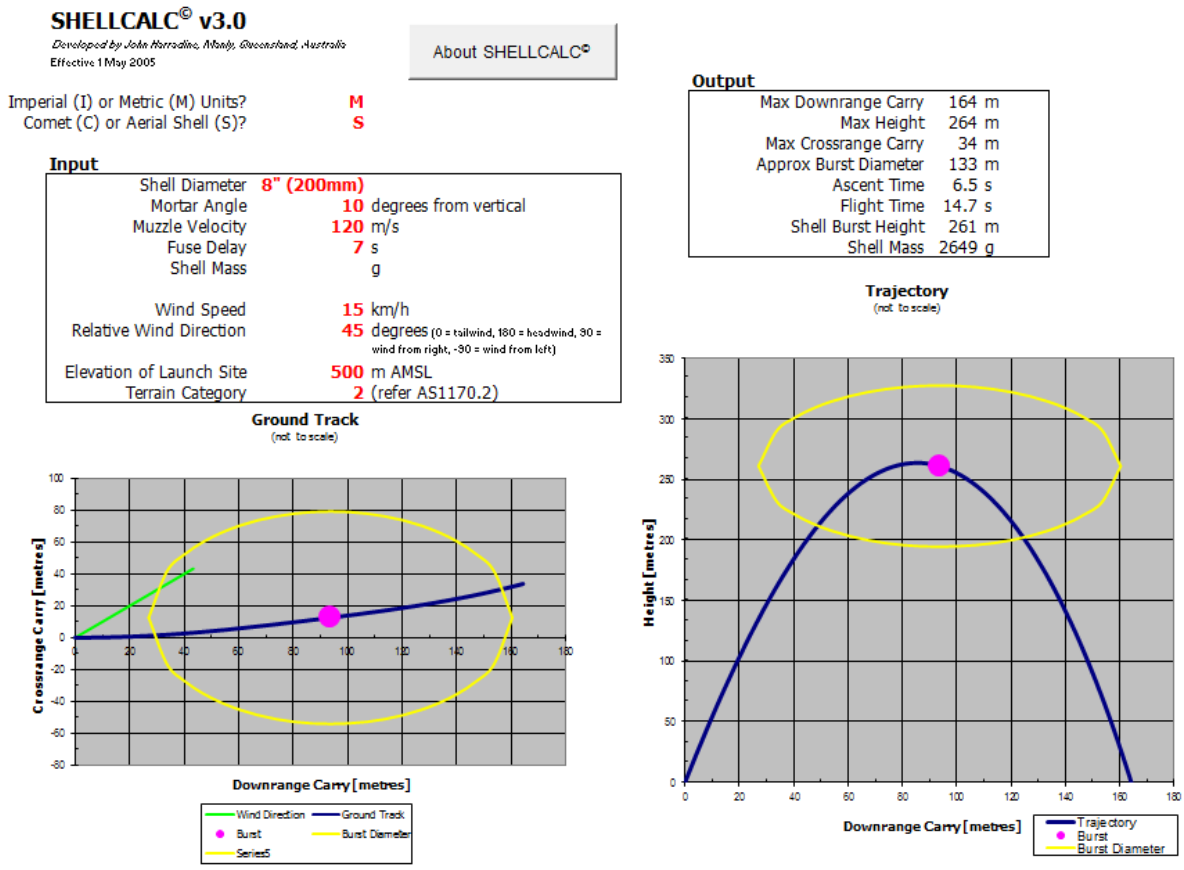

Figure 2. *Screenshot of Shellcalc© version 3 as originally published in the Journal of Pyrotechnics.*

distance at which the risk is at such a level as to be regarded as acceptable.[4]

The first published version of Shellcalc© (version 3) included several minor changes to the original program including an indication of the normal shell burst diameter based on standard data available from Shimizu and others.[5] The actual display of this important parameter on the Excel graph, see Figure 2, may be distorted because of the automatic axis scale calculations by Excel and in the most current version (version 5.18) a fixed scale graphing option has been incorporated and will be discussed below. The screenshot is included for reference only, as this was the first version of Shellcalc© to be available for general use and is the version many readers may be familiar with (although they are encouraged to upgrade).

Shellcalc© version 5.18

The most recent version of Shellcalc© (Version 5.18) incorporates many changes from the original versions which have been requested or developed from use of the program in a variety of display scenarios. The latest version of the program is available from the JPyro archive[6] which also details some of the changes introduced since the publication of the original paper. A more detailed change log for Shellcalc© is given in Table 1.

A screenshot of the newest version is given in Figure 3 above.

The most significant changes and their application are discussed below. Screenshots are all from the latest version of Shellcalc© and all parameters are included so that the situations described can be reproduced. In most cases omitting a parameter forces Shellcalc© to use its "default" values, but supplying the parameter over-rides the Shellcalc© defaults and the program recalculates using the inputted values. It is intended that this feature will be extended in future versions, particularly to mirror the values obtained by test under the CEN Standard for "professional" fireworks – EN 16261.

Conventions and interpretation

Figure 4 shows a 3-dimensional interpretation of the launch and output parameters from Shellcalc©. In this diagram:

- The green arrow represents the wind direction and strength. The longer the green arrow, the higher the wind speed. The wind angle is related

Table 1. *Change log for Shellcalc©*

Change	Introduced in version	Comments (see below for discussion of major changes)
Original version developed by John Harradine	1	Not published
Revised version developed by John Harradine prior to publication	2	Not published
Shell burst shown	3.0	As published in *Journal of Pyrotechnics* in 2005. Shell bursts are illustrative only
Allow shell tumbling and mortar barrelling effects	3.1	Mortar barrelling and tumbling effects prevent the model producing unrealistically short shell travel distances
Allows firing above ground level and allows firing below horizontal	4.10	To permit, for instance, firing from structures
Incorporates greater range of shell sizes and "standard burst diameters"	4.11	
Uses further shell data including V0 from literature	4.12	
Restyled interface and removal of macros. Shows basic "normal fallout"	5.11	Redesigned interface. Removal of macros allows use on a variety of operating systems. Users can print or "screengrab" using normal Excel menus
Added long burn effects (e.g. "Kamuro") to fallout plot	5.12	
Added ability to manually set shell burst height	5.16	Recalculates initial shell velocity to allow custom use of Shellcalc©
Added fixed scale plots for use in presentations and reports	5.17	To allow super-imposition of plots to model multiple firings, or firing from multiple points
Revised parameters for large shells	5.18	Bug fixing

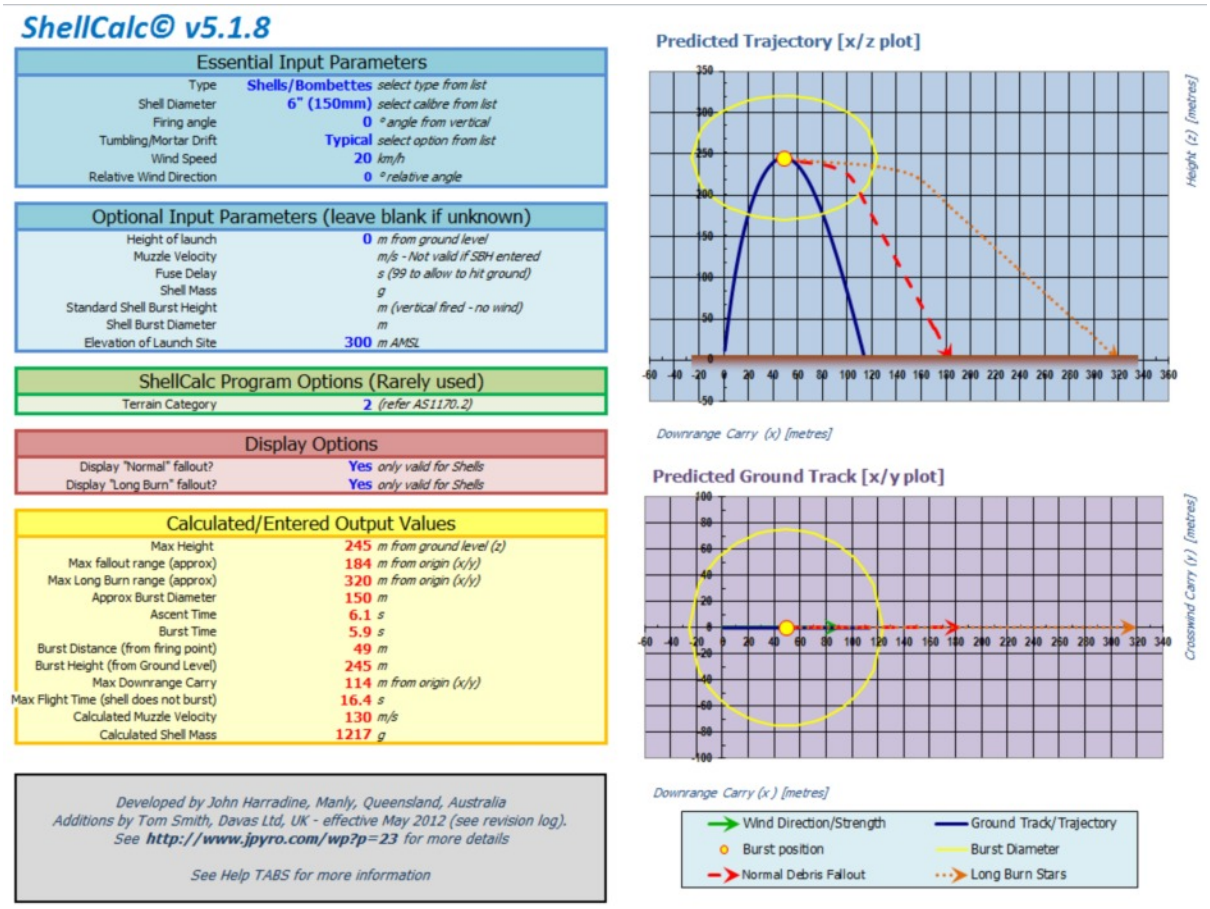

Figure 3. *Screenshot of latest Shellcalc© version.*

to the *x*-axis, so in Figure 4 the relative wind angle is approximately 75 degrees.

- The blue line represents the trajectory of a "blind" shell.
- The red line represents the maximum trajectory of the "normal" fallout. This line is also projected onto the *x*–*y* plane to reproduce that seen in the "Predicted Ground Track *x*/*y* plot" in Shellcalc©.
- The orange line represents the maximum trajectory of lightweight fallout. This line is also projected onto the *x*–*y* plane to reproduce that seen in the "Predicted Ground Track *x*/*y* plot" in Shellcalc©.

It is important to realise that the arrows displayed in Shellcalc© for normal and lightweight debris do not imply that all of the debris takes the trajectory shown. Figure 5 shows typical fallout patterns for normal and lightweight debris. Debris may even fall upwind of the firing point in low velocity winds.

It is also important to appreciate that the calculated values shown in the Shellcalc© output table may appear to contradict the graphical output if the wind is not directly along the *x*-axis (i.e. 0 or 180 degrees). The figure given is the distance from the origin to the calculated debris distance as shown in the *x*–*y* plot and this is the distance that should be used in making hazard and risk calculations.

In some conditions, such as where the wind funnels between buildings or along a valley or river, the debris may travel further and in a somewhat different direction to that calculated.

Shellcalc© should be used to predict the most likely debris distances and to use local knowledge and experience to tailor the results to the particular firing site.

In most cases, of course, it is impractical to use Shellcalc© except as a modelling tool to determine a set of constraints for the site (e.g. maximum shell calibre or effect) under a variety of foreseeable conditions for a particular site. In addition a general fallout table may be derived from Shellcalc© calculations for the firers to refer to on-site to make informed and objective decisions about modifying the display as a result of what conditions prevail at the display firing time.

Shell burst diameter

The display of shell burst diameter is useful to allow visualisation of the functioning of a shell when fired normally and also for the situation where a "blind shell" bursts on impact with the ground as shown in Figure 4. To ensure the model "bursts" the shell on the ground we manually set the shell delay time to 99 seconds (which is obviously too long – but achieves the same effect as manually entering the exact time a shell would reach the ground).

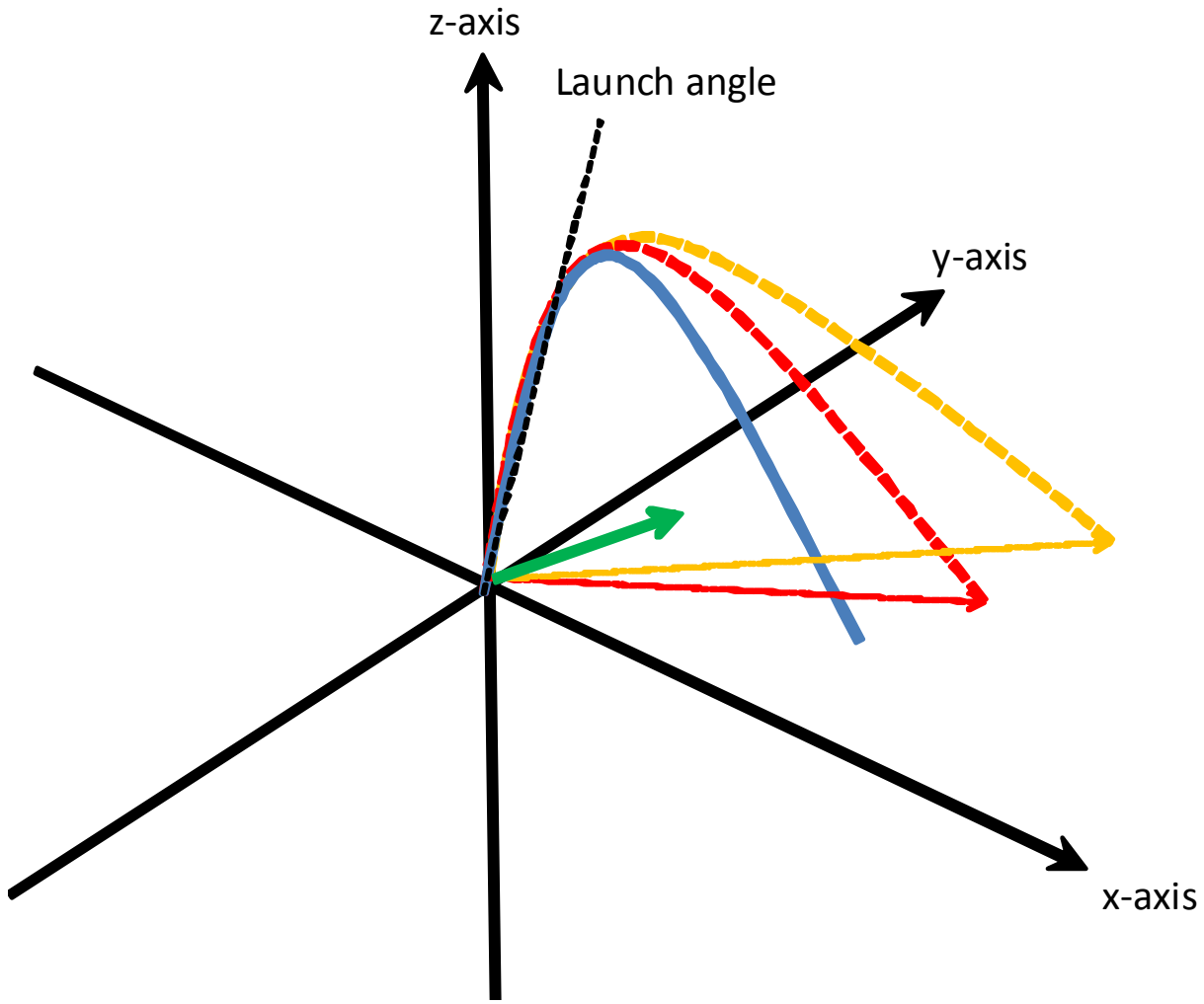

Figure 4. *3-D representation of the Shellcalc© outputs.*

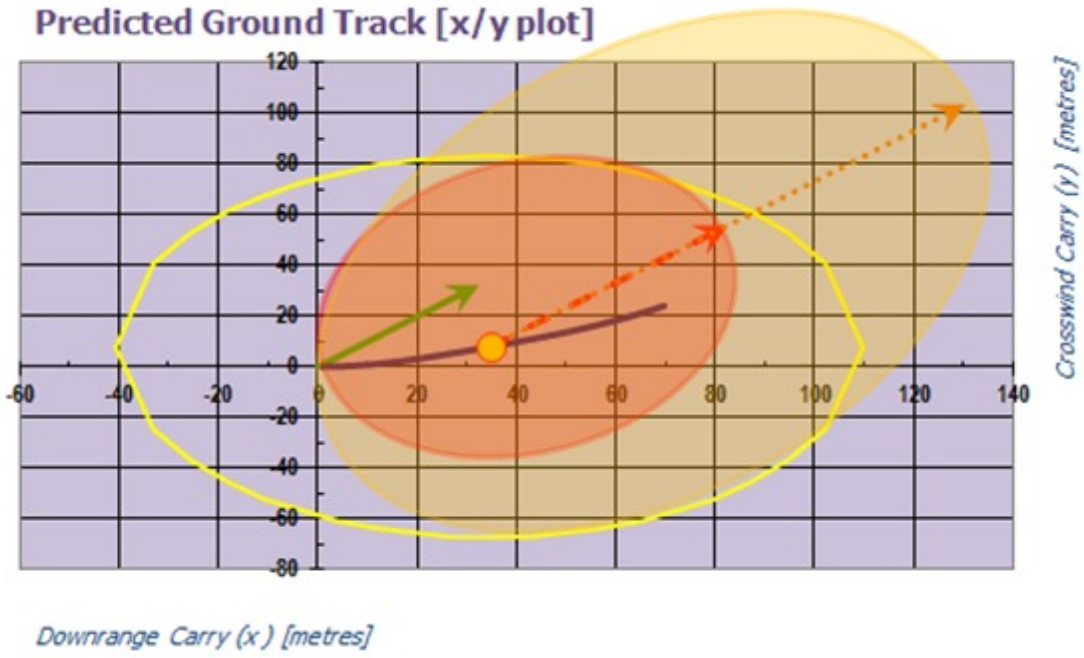

Figure 5. *Overlay of typical fallout patterns on Shellcalc© x/y plot.*

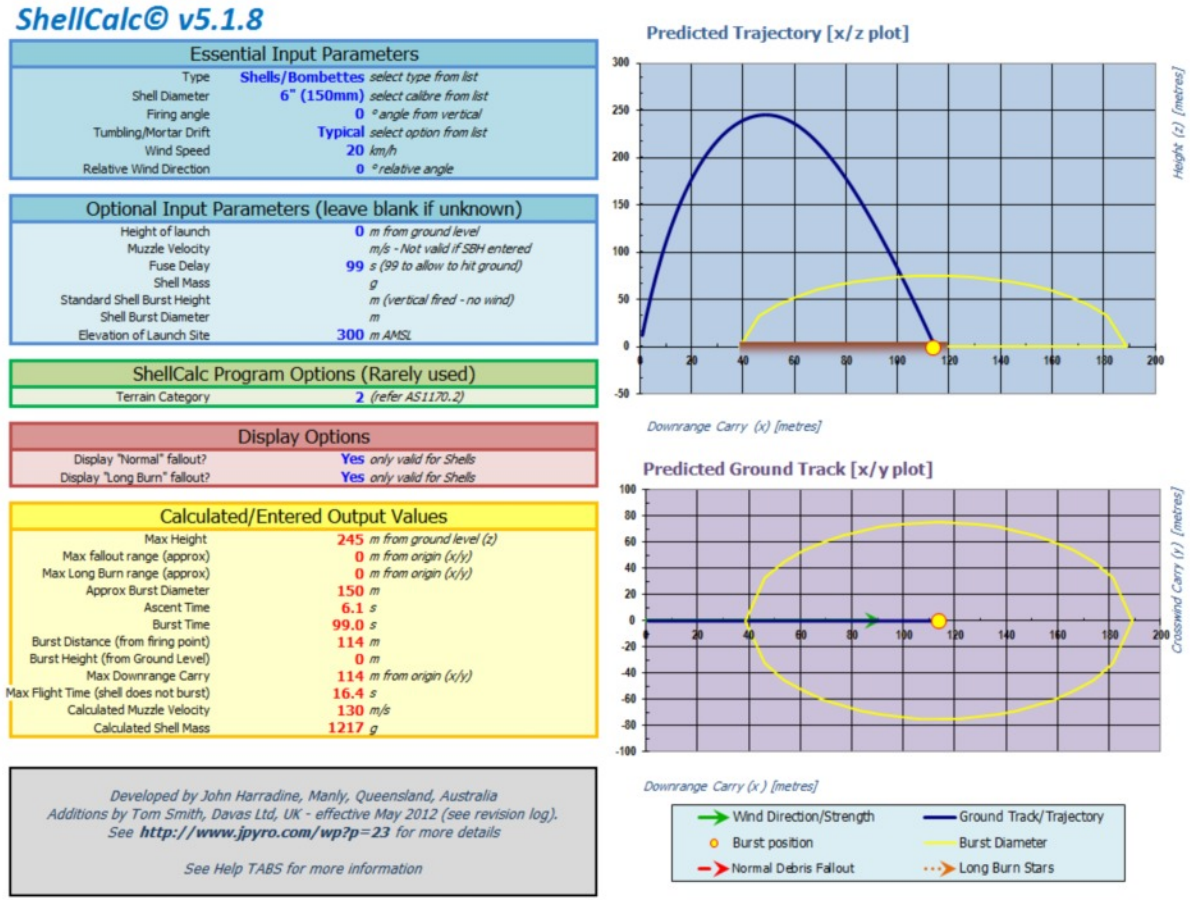

Figure 6. *Ground burst shell simulation.*

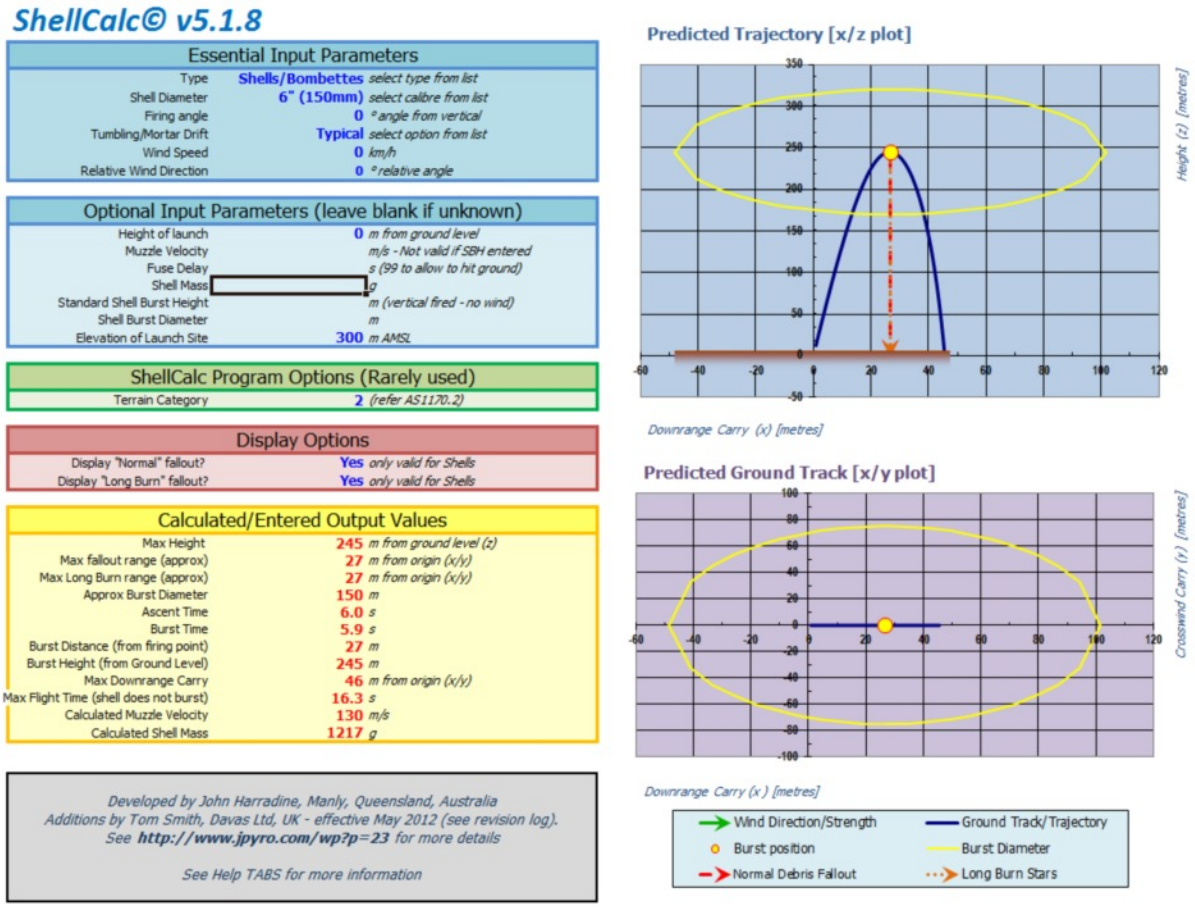

Figure 7. *Typical tumbling/drift illustration for 150 mm shell.*

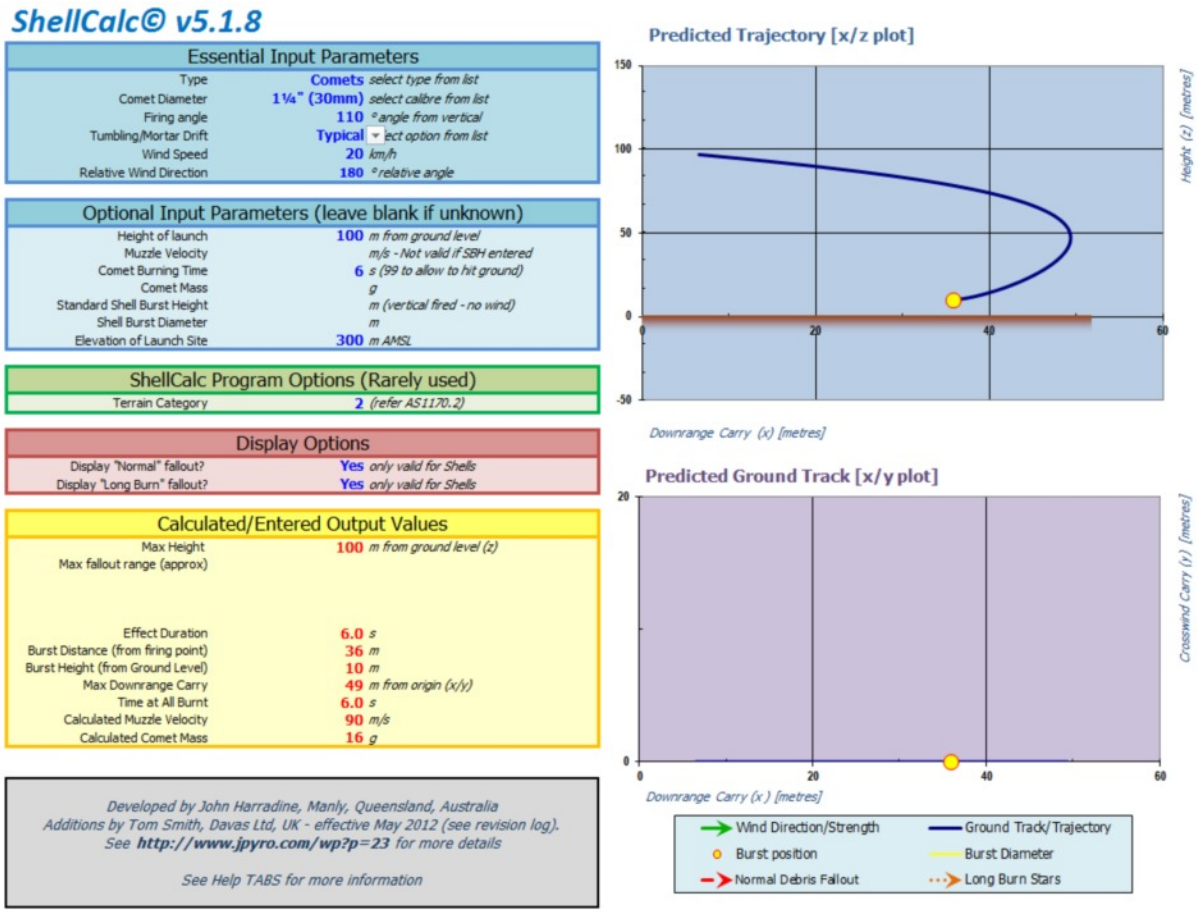

Figure 8. *Effect of wind on long duration comet fired below horizontal and above ground level.*

In this way an estimate of the distance of not only where a shell may land if it fails to function in the air normally, but where the stars may travel to if the shell bursts on the ground may be examined.

Setting the shell delay to a smaller value allows modelling of low burst shells.

The display of the burst of a shell may be distorted owing to the automatic axis scales used by Excel©. Version 5.18 also allows non-automatic scaling of the axes and the use of this for further modelling is described below.

Mortar barrelling and shell tumbling effects

An initial problem identified with the program was the unrealistic modelling of a shell fired vertically upwards in no wind (i.e. the assumption of no wind at all levels). In the original program a shell fired under these conditions would land (assuming it failed to burst) directly down the mortar tube it was fired from.

There are a number of reasons why this is extremely unlikely to occur in practice. These include:

- The effect of zero wind at all levels during the flight of the shell
- Mortar "barrelling" effects – most shells are somewhat slack in the mortar and therefore firing exactly vertically is unlikely
- Shell tumbling effects – shells are subject to the Magnus effect[7] and will move in the air in a direction related to the direction in which it spins

It was considered impossible to quantify these various effects precisely and in a way which had practical use, and hence Shellcalc© allows a Parameter "Tumbling/Mortar Drift" to factor in such effects in terms of an equivalent initial firing angle greater than zero (or entered value) by an amount automatically allocated by the program as shown in Table 2. The user may determine how extreme this effect is by experience and by selecting an appropriate factor.

The program, as it is usually used to model "worst case" fallout, simply add these values to the mortar firing angle. We accept that this is an inelegant and rather inaccurate solution, but there seems to be no point in modelling a shell that tracks into wind when the most significant distance of the major hazard will be from shell failure, fallout and debris in the downwind direction.

Figure 7 shows the use of "Typical" drift on a 150 mm shell fired vertically in no wind

Firing above ground level

The increasing use of fireworks fired from structures necessitated the ability for Shellcalc© to model such situations. In addition the firing of such effects (usually comets) can be at a wide variety of angles, including

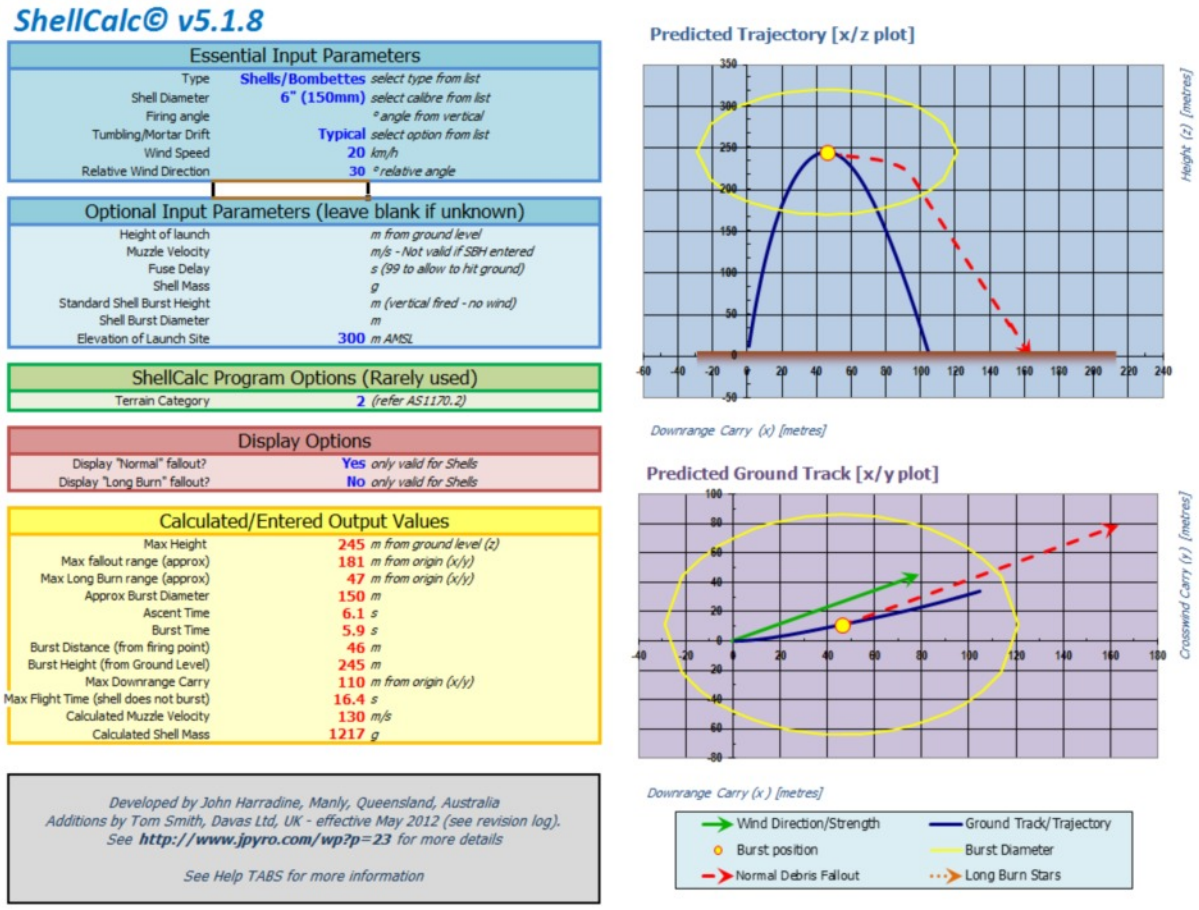

Figure 9. *"Normal" fallout from a shell.*

below horizontal. It is important, when firing from such structures, to model the potential for comet stars to be blown back towards the structure itself. In most cases the comet star will be extinguished before this undesirable event occurs, even in high wind conditions, but it can be useful to artificially increase the "Comet Burning Time" parameter to model a situation of a long burning star. Figure 8 shows all these effects combined with the comet being fired directly into a strong wind (i.e. wind direction of 180 degrees). Note that without manually changing the comet duration to 6 seconds, Shellcalc© calculates the comet burning time to be 3.3 seconds and the resulting "blowback" is reduced.

Shellcalc© can also model shells or bombettes fired in a similar manner.

The brown line in Figure 8 highlights the ground level for such situations. Future versions of Shellcalc© will make the display of this line optional.

Display of "normal fallout"

The modelling of "normal" debris from a shell is complex and depends on many factors. Over the course of many years we have amassed a large amount of data from real displays and from published data from around the world. The major issues in trying to quantify this for incorporation into Shellcalc© were:

- The effect of differing wind speed and direction at different heights
- Local effects, such as funnelling of wind between buildings or down valleys
- The variety of debris formed from the normal functioning of a shell – including internal sub-components and pieces of shell casing
- The effect of wind on these items according to their size, density and shape
- The initial velocity of these items as the shell bursts

We have based the calculation of "normal" debris on shell case fragments of a size, mass and velocity which would do damage to the eyes of a spectator[8] should the debris impact them directly. Figure 9 shows the indication of "normal" fallout from a 150 mm shell.

The fallout of "normal" debris is shown as an arrow indicating the furthest point at which such debris reaches the ground. The trajectory of the debris is not modelled accurately but is merely indicative and shows (and calculates) a likely path dependent on the bursting of the shell. In some cases it is possible for "normal" debris to fall within the predicted range of a "blind" shell as shown in Figure 10. This is not an error and primarily occurs when the mortar is angled significantly and the wind speed is low. It is important, and obvious, therefore that

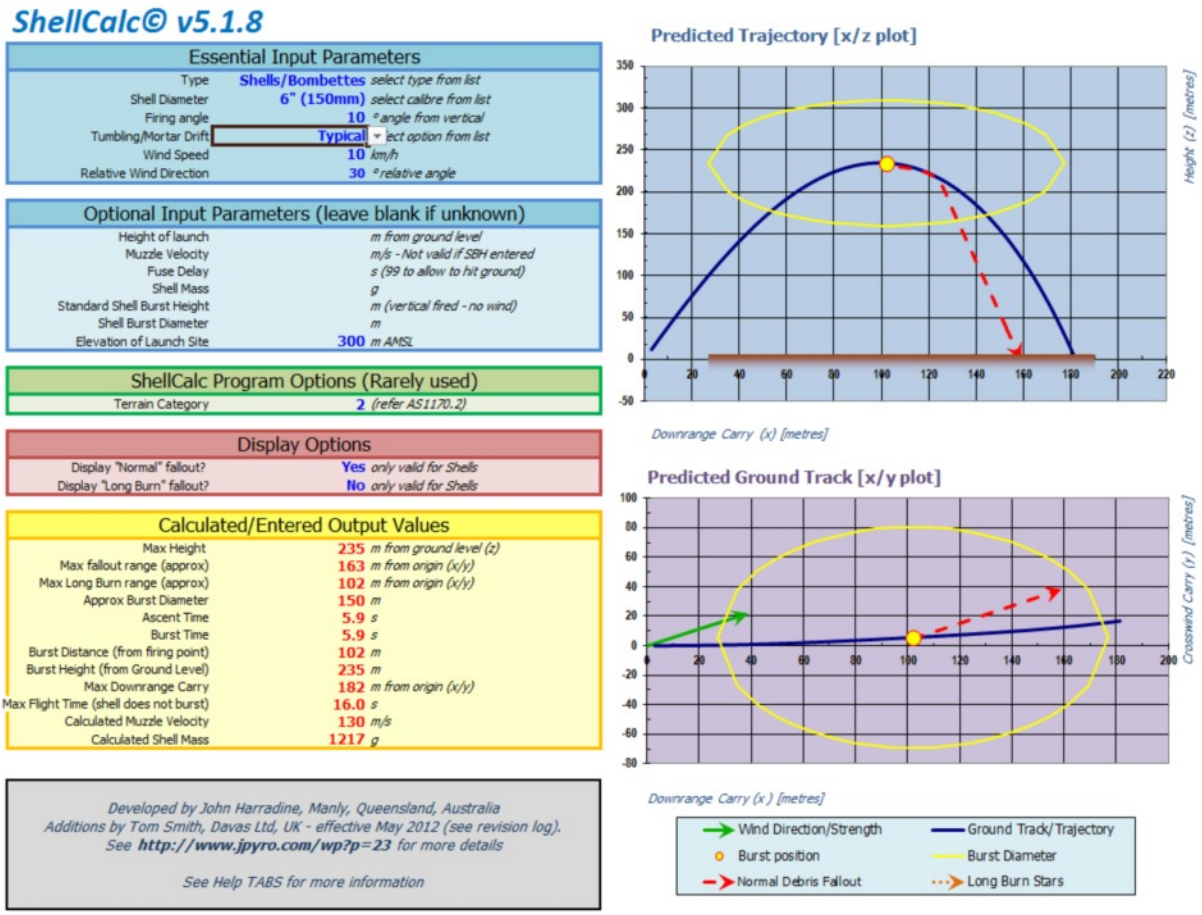

Figure 10. *Angled shells and normal and blind debris effects.*

both "normal" debris and "worst case" blind shell failures are used in order to determine adequate separation distances. The two effects pose different risks, of course, and are of very different likelihoods (frequencies) – but both are relevant and the relative importance may depend on the venue and nature of the display.

Long burn effects

An obvious further extension to modelling "normal" fallout is to try and estimate the debris pattern of long burning effects such as glitter/strobe stars or willow/Kamuro. In glitter/strobe effects the additional deliberate burning duration means that the stars from a shell may travel further downwind and may indeed reach the ground while still alight. In many cases as the stars are similar in density to "normal" debris, the distance travelled will also be similar. Lightweight long burning debris, such as that in willow or Kamuro stars, presents a slightly different problem. Here the falling lit material is of lower temperature and density than "normal" debris and may travel further at the mercy of the prevailing wind. We have modelled the debris of such long burning stars from data from displays and available in the literature. Figure 11 shows the same launch parameters as that in Figure 9 and illustrates Shellcalc© modelling of long burning debris.

Table 2. *Shell tumbling and drift effects*

Parameter value	Effect on shell firing angle
None	0
Minor	2
Typical	4
Major	6
Extreme	8

Again it is important to appreciate that although the final distance reached by such debris is certainly indicative, it is very dependent on local effects and the trajectory of the debris is an approximation. Such debris is usually only considered to be a significant risk when the audience or high hazard areas would be affected by it and in many cases conditions will dictate that it is not appropriate to use such effects. Only by a clear understanding of the performance parameters of the fireworks being fired can a company assess that such long duration debris will be extinguished before it reaches the ground (which is often the case by design) and that under the conditions of firing, using appropriate mortars, that the risks are acceptable.

Manually setting shell burst height

The mortar exit velocities used in Shellcalc© are the primary determinant of how high and far a shell will

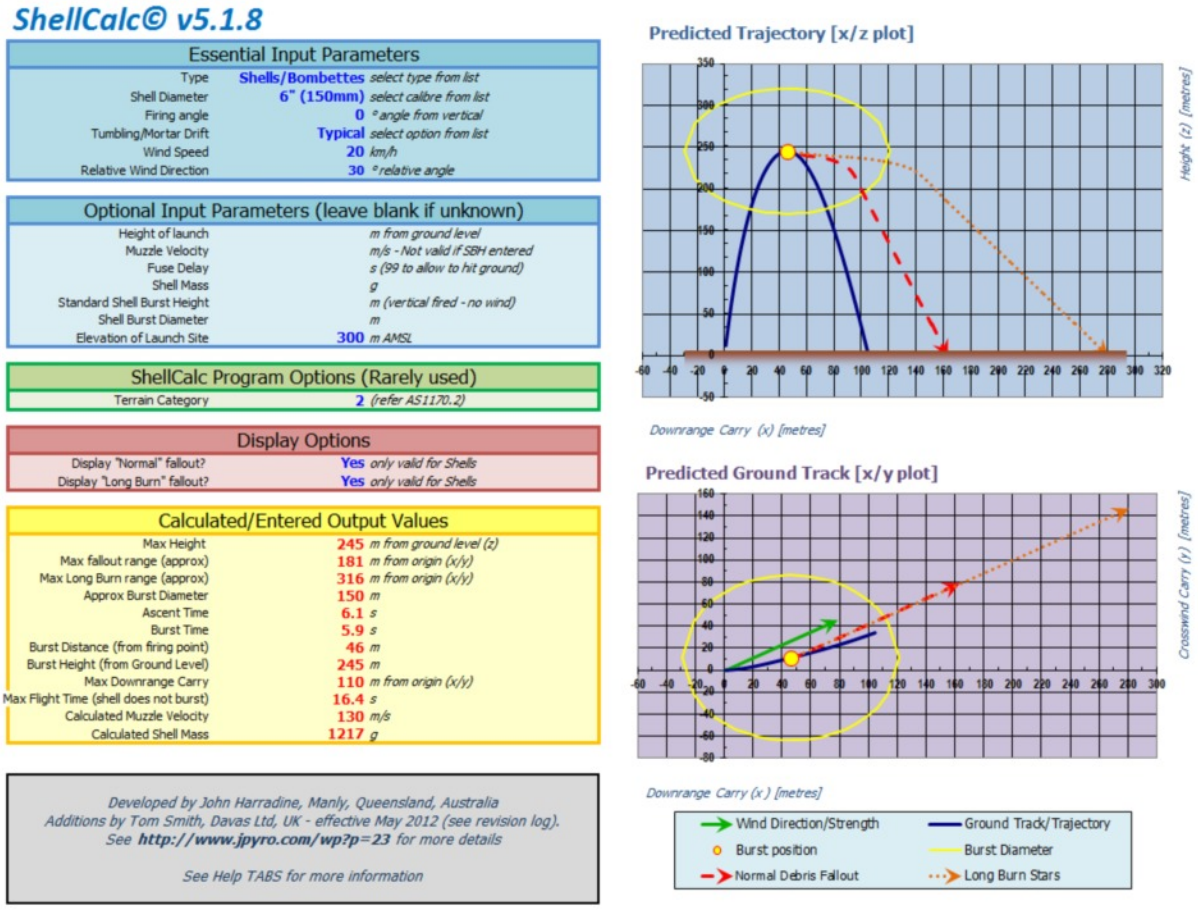

Figure 11. *Long burning debris from shell bursts.*

travel as described in the original Shellcalc© paper. Shellcalc© has always permitted the exit velocity (V0) to be alerted to allow more detailed modelling to be done. However, in practice the determination of V0 is not easy and instead companies may determine the shell burst height for a specific type or manufacturer's shell fired from their own mortars. Work developing the European Standard for Category 4 fireworks done, amongst others, by BAM[9] shows that the burst height of a "standard" shell (i.e. one of standard weight and with standard lifting charge) is dependent on both the mortar length and mortar calibre as would be expected. In addition, of course, in normal manufacturing there will be variations in lifting charge, even amongst a batch of similar shells.

Manually setting the burst height for a shell fired vertically upwards in zero or low wind test conditions allows Shellcalc© to more accurately reflect the actual trajectory of a particular shell. Figure 12 shows the same calculations as Figure 9 but the burst height reduced from a calculated 245 m to 180 m to emphasise the differences obtained.

Future developments of Shellcalc© are planned to allow a range of other parameters to be adjusted manually. These changes will have particular significance to modelling shells supplied under the European Standard[10] where some of the parameters are required to be tested and displays on the shell label for the "professional" user to determine adequate "safety" distances for the particular effect. As a result of the work done in developing the Standards it is obvious that there is some variety in shell burst height, even from a single batch of product, and we recommend that the maximum value obtained (and possibly with an additional height to allow for a suitable margin of error) be used in Shellcalc© calculations so that the user does not under-estimate the trajectories of blind shells and normal debris and as a result under-estimate the distances to the audience or other hazards.

Fixed scale plots

As noted above, the original and current versions of Shellcalc© display shell trajectories on a plot where the axis scales are determined automatically by Excel. This is necessary because of the very wide variety of effect heights and trajectories that may be obtained from modelling effects as diverse as 15 mm comets and 250 mm shells. We do not believe that in most cases the distortion of the shell burst sphere, as in Figure 8 for example, diminishes the usefulness of the program in most cases. However there are occasions where having both the *x*- and *y*-axes to have a common scale is important and useful.

Shellcalc© 5.18 and subsequent versions have an additional tab ("Scaled Plot") to allow the display of such information and adjustment of the axis parameters by the user. Figure 13 shows such a plot.

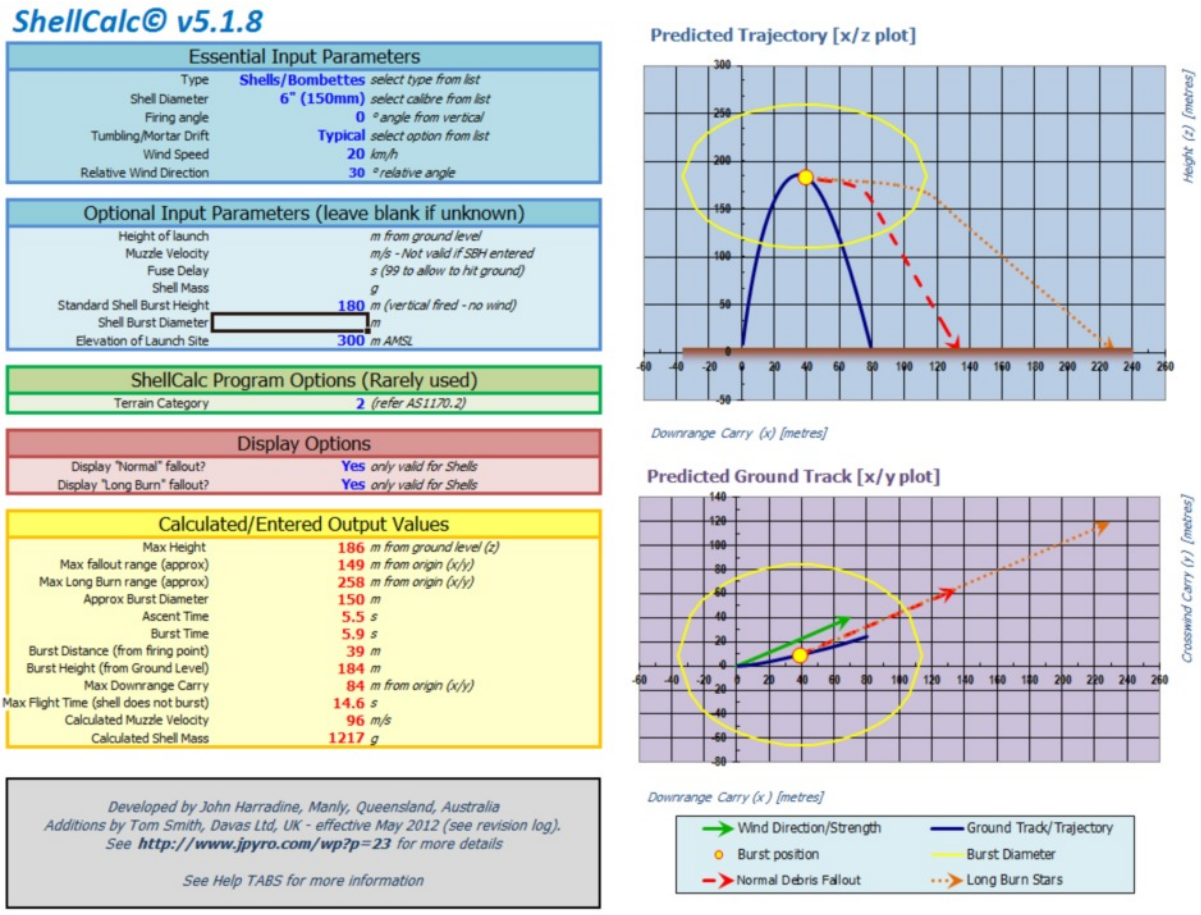

Figure 12. *Manually changing the burst height.*

The combination of several of these plots is useful, particularly for modelling comets fired from structures or for shells fired simultaneously from multiple mortars and the effect of wind on such firings. Combination is best achieved by screen-grabbing the Excel plot with a tool such as the Microsoft "Snipping Tool"[11] included in Windows Vista and above and subsequent superposition in, for instance PowerPoint© or another graphics program. For instance for firing long burning comets from a building with a 30 kph cross wind the effects of "head" and "tail" winds on the trajectories of the comets is obvious as shown in Figure 14.

Limitations of Shellcalc©

Shellcalc© does, of course, have a number of limitations in its use and no user of the program should consider that Shellcalc© gives an absolute indication of the trajectories of comets or shells, or gives an absolute "safety" distance for their use. However the program does provide significantly more information that relates to the specific fireworks chosen for a specific display and allows modelling of the likely display safety parameters under a variety of conditions. In this way it is a simple but much more effective tool than just basing "safety" distances on the calibre of the shell (as is done in effect, in the US[12] amongst others) or on a combination of shell calibre and apogee (as is the case in France[13] and Germany[14]).

In general we find it most efficient to use Shellcalc© to model the "worst case" and "most likely" hazard scenarios for a particular event and venue and to use the information obtained, in conjunction with historical shell failure information, to provide the event organiser with various options for the display and then allow the show designer to work within the agreed constraints. For instance it is normal at many shows to accept that there is a low (but tangible) level of risk to the audience or to structures. Provided the risk is sufficiently low the display can be designed to incorporate a wide variety of firework effects fired at a sensible distances from the identified hazards. In this case, because the number of high calibre shells is low, or because the audience may only be affected by a very low number of shells containing long burning stars if such stars reach ground level, it is acceptable to plan and fire the display with a low (but non-zero) risk.

At very large, highly public events – such as the Olympic opening and closing ceremonies – the event organiser has to weigh the low risk of a "normal" display against the possible adverse impact of such an incident occurring and may decide, quite properly, that a display designed to produce a much lower risk (or even near-zero risk) display is what he or she requires the display company to design.

In addition, of course, the display company should use Shellcalc© to determine the products suitable for meeting the creative and organisational constraints of the event

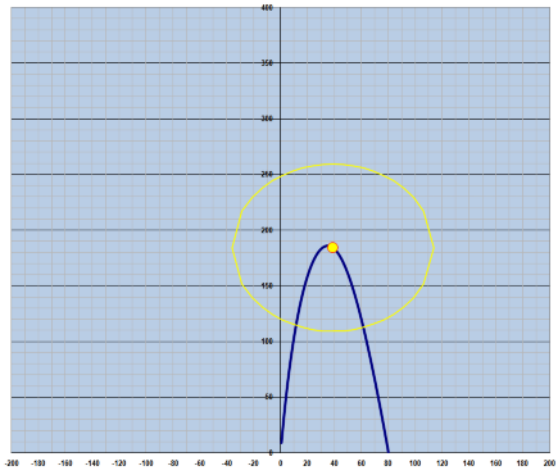

Figure 13. *Scaled plots adjustable by the user.*

organiser under a variety of conditions, and, critically, to determine what material needs to be removed from the display under a variety of other wind conditions. In this way an objective contingency table may be agreed between the display company and the show designer, the event organiser and potentially the broadcast media so that each is clear what show may be fired under specified conditions, and when cancellation is required. The process is more fully explained in the author's recently published book.[15]

Hazard and risk assessment for displays

In a previous paper[16] the author has described the use of Shellcalc© to model shell fallout and failures in order to provide a semi-quantified assessment of risks from firing shells at a display, and to attempt to set a "safety" distance. Shellcalc© can be used by event organisers, event consultants and practitioners of displays to assist in determining appropriate fireworks for displays and for curtailment or cancellation criteria.

In its simplest terms a quantification of risk may be made by evaluating the simple risk equation

$$\text{Risk } (R) = \text{Hazard } (H) \times \text{Frequency } (F) \qquad (1)$$

Or more simply

$$R = HF \qquad (2)$$

and more generally

$$R_{\text{total}} = H_1F_1 + H_2F_2 + \ldots \qquad (3)$$

Shellcalc© predominantly examines the potential hazards arising from shells and comets by modelling where a "blind" shell may land or where debris may fall. It gives realistic maximum distances which can be used to assess the hazards to persons or structures impacted by these fireworks. It does not make any predictions about frequency, and therefore risk. The user must factor in the frequency of a variety of failures to determine an overall risk which is acceptable to the event organisers, their insurers, and the local regulations.

We urge display companies, in particular, to adapt the basic Shellcalc© program to reflect their own firing procedures and techniques both from an artistic and from a practical point of view. For instance, a particular company may have, as a result of previous incidents, developed a range of mortars with set maximum firing angles. Another company may use particularly long mortars, or use a range of shells that has been manufactured with lower than standard lifting charges.

The risks posed by shells and other fireworks at most displays and venues are quantifiable and are generally low – otherwise the display companies using them would have gone out of business a long time ago. However it is important to have a solid understanding of the performance characteristics and possible failure modes of the fireworks that are proposed to be fired, and to

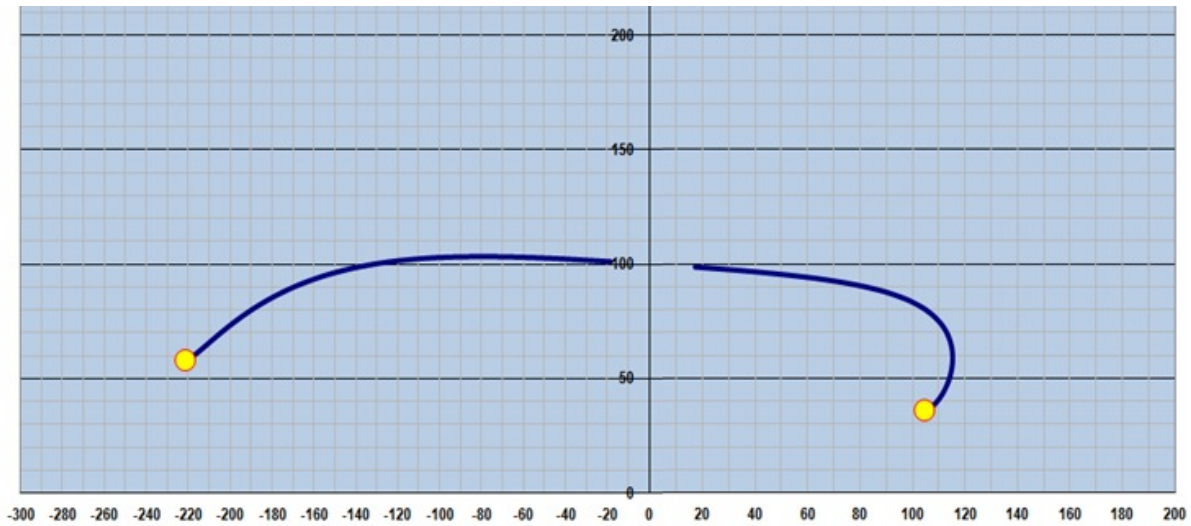

Figure 14. *Combination of two Shellcalc© plots for comets. Wind from right to left.*

develop objective criteria for display design, display curtailment or even cancellation.

Examples of the use of Shellcalc©

The following are illustrations of the use of Shellcalc© in determining the effect of wind in planning the display by superimposing Shellcalc© plots to replicate the multiple firing angles used in the display.

Shellcalc© 5.18 allows screen grabs (using the Snipping Tool in Windows) at a fixed scale (using the "Scaled Plot" tab). We find the most efficient way to superimpose Shellcalc© plots onto a common image is as follows:

- Set up Shellcalc© with the maximum shell or candle calibre and with the wind of typical strength and direction that represents the "worst case" scenario (usually wind towards audience)
- Determine the widest *x*-axis by allowing the trajectory to be calculated for firing the firework "downwind" at the greatest firing angle
- Ensure that the axes on the "Scaled Plot" tab will cover the full range of "blind" shells or fallout. Right-click on the axis and set maximum and minimum values. We find it useful to ensure that the total *y*-axis range is the same as the total *x*-axis range – for instance if the *x*-axis is −200 to +200 then set the *y*-axis to be 0 to +400
- "Snip" the "Scaled Plot" and paste the resulting image into a graphics program. We use Microsoft PowerPoint © but any similar program will work
- Replot the same firework changing only the firing angle each time (in 10 or 20 degree increments is usually sufficient)
- "Snip" the relevant part of the trajectory and paste into PowerPoint. Do not scale the images so that they may be correctly superimposed on each other.
- Align the new pasted image by zooming in and using "Alt" + mouse to prevent the pasted image "snapping" to fixed points in the original image
- Use the Picture Format Tools to either crop the pasted image, or to remove its background so that only the trajectory is displayed
- Repeat as required
- Copy/paste the final image into a report as required (as has been done here).

It is not necessary to model every possible trajectory, we usually model the extremes and a point in between (for instance for a Roman candle battery comprising 5 candles equally spaced we will only model 3).

Determining appropriate shell size for displays

Figure 15 and 17 show the firing of 30 mm Roman candles and 150 mm shells from the Plymouth Mountbatten breakwater by Jubilee fireworks in 2006. It is obvious from the photograph that there is a medium strong wind (approximately 15–20 kph) from left to right as viewed in the picture.

Figures 16 and 18 show Shellcalc© simulations to reproduce the effects seen. Note in particular the displacement downwind of the Roman candle trajectories and a reduction in height on the downwind side. The effect for the shell simulation is similar – the vertical shell busts downwind of the centre line, and the downwind shell bursts further away from the mid-point and at a lower altitude than the shell fired upwind.

These results are, of course, what would be expected by an experienced display designer with experience of firing Roman candles and shells in a variety of conditions, but we believe Shellcalc© allows the effects to be quantified and displayed pictorially for the less experienced designer and as a way of allowing users to plan their display safely by knowing the likely effect of wind on "blind shells" or fallout under a variety of conditions.

Firing Roman candles from structures

Figure 19 shows the firing of single shot 30 mm Roman candles from the London Eye as part of the New Year celebrations. The Roman candles are fixed in firing pods to the structure of the wheel and are fired both radially away from the centre of the structure to produce the greatest effect, and away from the structure to minimise the possibility of debris blowing back on the structure itself. In this image there is a light (5 kph) wind from left to right.

Figure 20 shows the simulation corresponding to Figure 19 and the effect of wind on the comet trajectories can be clearly seen.

These examples effectively validate the Shellcalc© models in accurately predicting the effect of wind on Roman candles and shell trajectories.

Planning a display

The use of Shellcalc© is, of course, most useful in planning a display and allowing contingency tables to be created to inform the display firers which fireworks should be removed from the display under a variety of conditions.

The display site used for the Plymouth Firework competition is shown in Figure 21. The site comprises a >250 m long concrete breakwater which is used to fire three displays on two consecutive nights.

Figure 15. *Shells and candles at Plymouth with strong left to right wind (Photo – Jubilee Fireworks).*

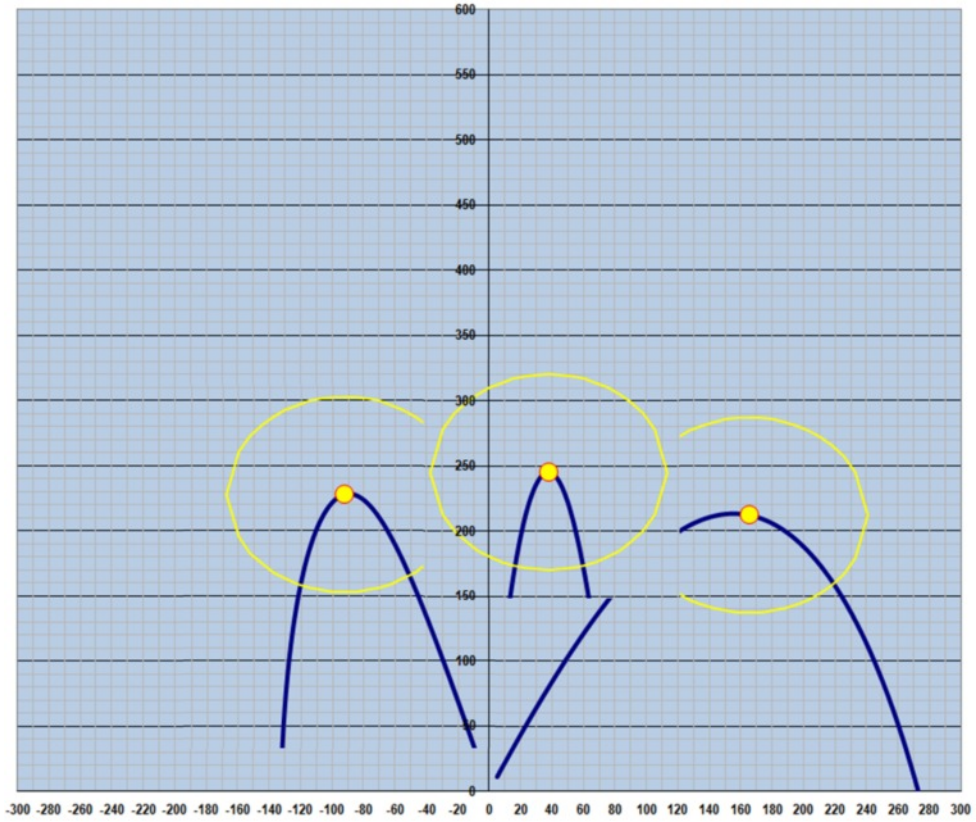

Figure 16. *Superimposed simulations of 150 mm shells corresponding to Figure 15.*

Figure 17. *Shells and Roman candles at Plymouth with strong left to right wind (Photo – Jubilee Fireworks).*

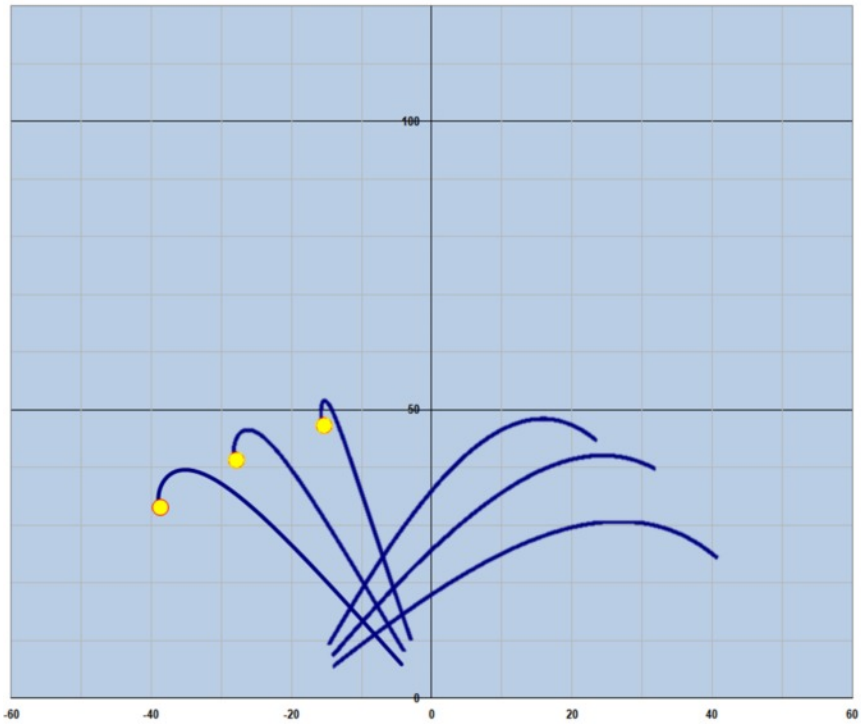

Figure 18. *Superimposed simulations of 30 mm Roman candles corresponding to Figure 17.*

Figure 19. *London Eye at New Year – wind slightly left to right (Photo – Jack Morton).*

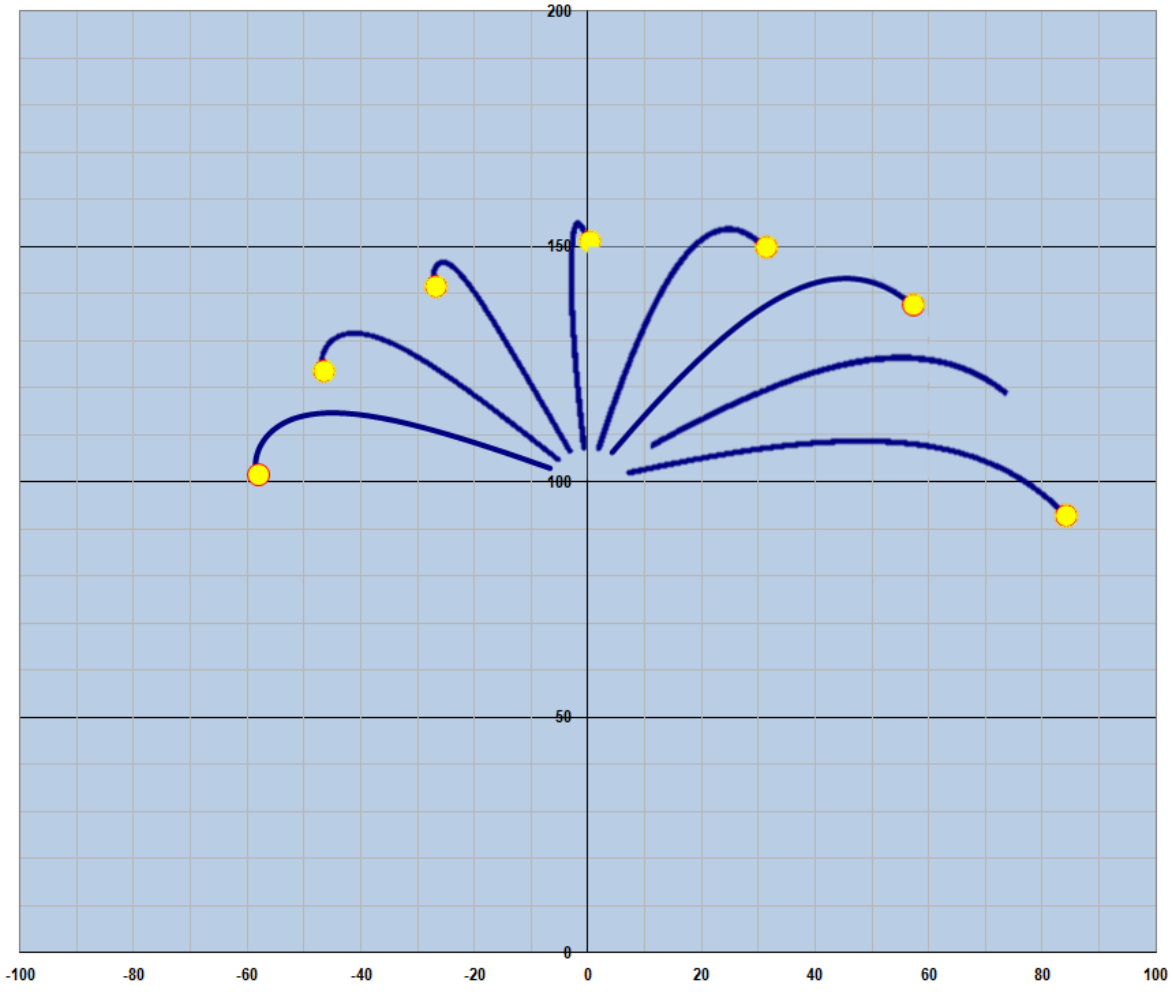

Figure 20. *Superimposed simulations of Roman candles corresponding to Figure 19.*

In 2012 plans were approved by the local Council to redevelop an old building at the eastern end of the breakwater and this necessitated a re-examination of the constraints placed on competitors for subsequent years' displays.

Shellcalc© was used to model the different hazards from shells and large calibre Roman candles fired at various angles under a variety of wind conditions. In Plymouth the prevailing wind is from the south-west (i.e. taking fallout to the north-east of the firing sites).

The distances from each firing site to the new development and the crowd line are shown in Table 3 and the calculated distances from each firework under a maximum wind speed of 21 kph (Beaufort Force 4) which we use as a "standard" maximum for planning displays are shown in Table 4.

The table headings in Table 4 are explained in Table 5.

Several things are apparent from these calculations.

- Firstly, although the distances would be considered adequate for the displays by most display companies in most countries using their existing criteria (for instanced based on shell calibre alone), it is obvious that "blind" shells and debris could reach both the new development and the crowd line if the wind were up to 21 kph and blowing debris towards them. Hence persons at these distances are not "safe".

Table 3. *Distances from displays to hazards at Plymouth*

From	To	Distance (m)
Display A	Development	231
	Crowd Line	320
Display B	Development	170
	Crowd Line	261
Display C	Development	130
	Crowd Line	222

- Secondly, the maximum distance travelled downwind is not necessarily from the largest calibre fireworks if the firing angle is restricted.
- Thirdly, that the maximum permitted firing angles and maximum calibre shells permitted should be reduced in order to minimise the hazard from large calibre fireworks reaching the crowd. The range of permitted fireworks may also be restricted by the event organiser and display adjudicator if the wind is greater than 21 kph or is blowing from an unusual direction.
- Lastly, that under the standard "worst case" conditions (i.e. with the wind blowing directly towards the audience and development) that it is likely that some debris will reach both positions.

The frequency of shell failure leading to shell burst at or near the ground is very low and calculated to be approximately 1 in 10 000 shells fired. It is only the highest calibre shells that would create such a hazard at

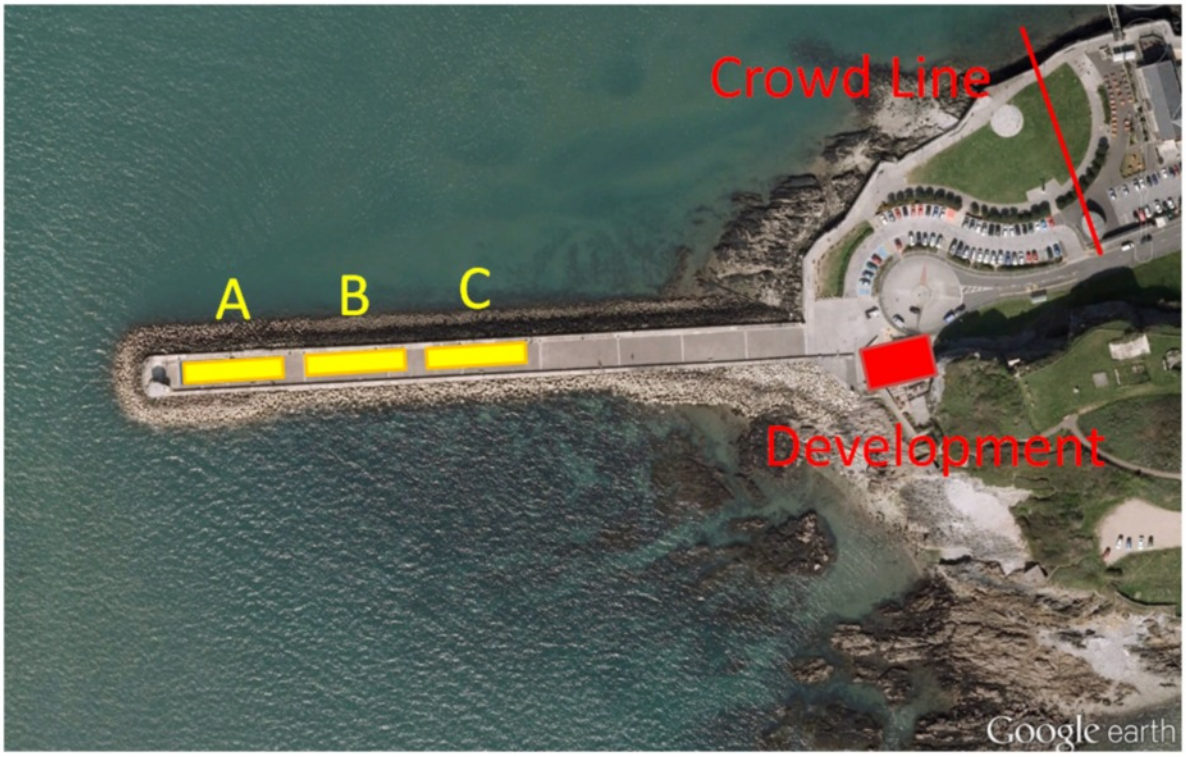

Figure 21. *General layout of the firing site for the British Firework Championship competition held annually in Plymouth, UK*

Table 4. *Calculated distances for a Force 4 wind (20–24 kph)*

Calibre	Max. angle from vertical (degrees)	Burst height (m)	Normal fallout distance (m)	Long burn fallout distance (m)	Shell distance (m)	Max. star distance (m)
≤65 mm	40	121	207	262	212	243
75 mm	35	139	226	293	234	271
100 mm	30	188	276	368	289	339
125 mm	20	219	278	395	279	341
150 mm	10	245	254	393	226	301
175 mm	0	267	207	360	124	211
200 mm	0	299	226	395	134	234
250 mm	0	331	224	388	141	266
300 mm	0	368	249	433	151	301

Note that maximum values in each column are shown in red.

Table 5. *The distances described in Table 4 columns*

Heading	Comments
Burst height	The burst height of the shell – for information
Normal fallout	The distance that shell fragments and unburnt stars may fall
Long burn fallout	The distance lightweight debris and long burning stars (e.g. "Kamuro" or "strobe") may fall – the distance is greater than the "normal" fallout distance because the debris has lower terminal velocities and burns for longer
Shell distance	The distance a shell could reach if the bursting charge failed. This may be shorter or longer than the "normal" debris depending on firing angle and windspeed. The frequency of such an event is very low (*ca.* 1 in 10 000)
Max. star distance	The distance stars could reach if a shell hit the ground and exploded on impact. The frequency of such an event is extremely low (*ca.* 1 in 100 000)

the distances as shown, and hence the risk from a large calibre "blind shell" falling to the ground is extremely low. This is a typical High Hazard/Low Frequency event and the type of event that must always be considered in the planning of a display (but frequently it is ignored).

Normal and "light" debris falling to the ground is, on the other hand, is a Low Hazard/High Frequency event (indeed there is always debris so the frequency is in effect 1) insomuch that no fatality is likely from such debris, but there is a hazard to persons from ignition of flammable material (such as a lightweight nylon coat) or direct impact on the skin or eye. Lit debris could also ignite waste or other flammable material leading to the spread of fire to a structure.

In addition risks to other persons (such as firers) must be considered and both the scenarios outlined above must be considered and used to calculate the overall risk (as outlined in equation 3).

In future years, owing to the development on the site, the range of firing angles and maximum calibres of fireworks will be reduced.

Future developments

It is proposed to make significant changes to future versions of Shellcalc© to allow

- Modelling of a wider variety of effects including mines and aqua shells
- Further work on manual input of a wider variety of parameters such as shell burst height and diameter and in particular to accommodate the parameters specified for mandatory testing and labelling as specified in the European Standard for Category 4 fireworks of various types
- Potentially modelling shell calibre and length effects to allow deviation from "standard" data
- Further modelling of "normal" and long duration debris
- Further development of data entry and output screens
- Make display of features such as ground level optional (as it is with fallout)

Conclusions

Shellcalc© has proved a useful tool in the assessment of risks from firework displays and has found application as a standard method in a wide variety of countries. The program has been significantly developed and enhanced in recent years and provides an easy to use and graphically attractive way of modelling shell and comet trajectories and potential fallout under a wide range of wind conditions and firing variations.

Obtaining Shellcalc©

The most recent version of Shellcalc© is available for download at http://archive.jpyro.com

Acknowledgements

I would like to thank Jubilee Fireworks for supplying photographs of the Plymouth Firework Competition, Jim Donald of Jack Morton Worldwide for supplying photographs of the London New Year display and Christian Lohrer of BAM, Germany and Chris Pearce of Jubilee Fireworks for helpful suggestions on an early draft of this paper.

Unfortunately I have been unable to contact John Harradine in recent years, so if readers could provide current contact details for him I would be very pleased to receive them.

References

1 J. Harradine and T. Smith, *Journal of Pyrotechnics*, Issue 22, 2005, pp. 9–15. Available at http://www.jpyro.com/wp/?p=23

2 Investigation Report – Bray Park Tragedy – 20 May 2000. See http://mines.industry.qld.gov.au/assets/explosives-pdf/coronorrpt_summ.pdf

3 The Carmel Explosions – see http://www.dmp.wa.gov.au/documents/Reports/DGS_IR_CarmelExplosion.pdf

4 "Reducing Risks, Protecting People" – see http://www.hse.gov.uk/risk/theory/r2p2.pdf

5 T. Shimizu, *Selected Pyrotechnic Publications of K.L. and B.J. Kosanke Part 4*, 1995–1997, pp. 78–82 – see http://www.jpyro.com/wp/?p=336

6 Shellcalc© version 5 – see http://www.jpyro.com/wp/?p=1443

7 Aerial Shell Drift Effects, *Selected Pyrotechnic Publications of K.L. and B.J. Kosanke, Part 2*, p. 68; Results and conclusions from the investigation of an accident with a display shell, D. Eckhardt and Andre, 5th International Symposium on Fireworks, Naples, 2000.

8 This work is part of an ongoing project for a major display and will be published by us when complete.

9 Burst Height Measurements of Spherical Shells for Different Calibers and Mortar Lengths, C. Lohrer, A. Kampa, H. Fink, L. Kurth and G.Alef, 13th International Symposium on Fireworks, Malta, 2012; Impacts of Various Conditionings on Performance Parameters of Category 4 Fireworks Shells, K. Stattaus, K. Kurth, A. Dutschke, N. Kästorf and C. Lohrer, 12th International Symposium on Fireworks, Porto 2010

10 The European Standard for Category 4 fireworks EN 16261 will shortly be available from http://www.cen.eu/cen/pages/default.aspx

11 A description of the use of the Snipping tool is available at http://windows.microsoft.com/en-GB/windows7/Use-Snipping-Tool-to-capture-screen-shots

12 The US system (NFPA 1123) is available at http://www.nfpa.org/aboutthecodes/AboutTheCodes.asp?DocNum=1123&cookie_test=1 and http://www.celebratecanada.info/docs/NFPA1123.pdf

13 A brief summary of the French system is available at http://firework.online.fr/legislation/reglementation.php

14 A description of the German system is available at http://www.bam.de/de/service/amtl_mitteilungen/sprengstoffrecht/sprengstoffrecht_medien/leitf_abbrennen_von_feuerwerk_f4.pdf

15 T. Smith, *Firework Displays: Explosive Entertainment*, Chemical Publishing, ISBN: 978-0-8206-0090-1 – see http://www.fd-ee.com

16 T. Smith, *Journal of Pyrotechnics*, Issue 29, 2010, pp. 12–31. Available at http://www.jpyro.com/wp/?p=1164

Encyclopedic Dictionary of Pyrotechnics
(and Related Subjects)

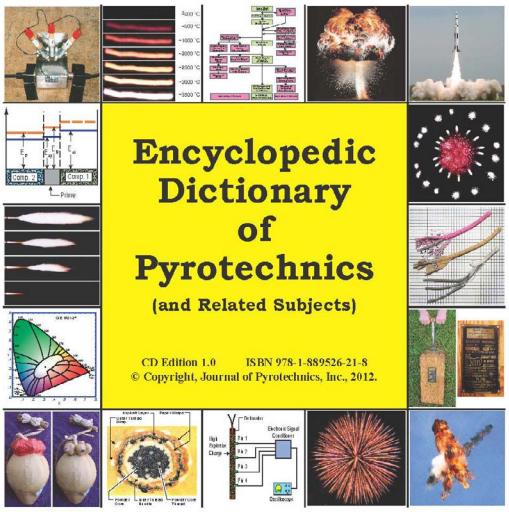

After 7 years of steady work, the first edition of the Encyclopedic Dictionary of Pyrotechnics (and Related Subjects) is finally available. The dictionary is available as a CD (priced very modestly) and as a 3-volume set of books in either color or black and white. For more information visit the JPyro web site (www.jpyro.com) and click on the Encyclopedia link.

The Encyclopedic Dictionary of Pyrotechnics (and related subjects) is an updated and greatly expanded version of the Illustrated Dictionary of Pyrotechnics, published in 1995. The new dictionary consists of more than 4600 entries (not counting cross-references), 1200 large format pages (8.5 x 11 inches), including 3000 photographs and illustrations, 600 pyrotechnic formulations and 500 data tables. In addition to many more entries, much more explanatory information is included, with many entries now ranging from 1/2 to 1 (or even several) pages of text.

The following quotes are extracted from reviews of the Encyclopedic Dictionary of Pyrotechnics (and Related Subjects). Full reviews are on the JPyro website.

John Conkling: "this is a book that everyone working in the broad field of pyrotechnics should have …" and "this is a valuable reference for you to have readily available …"

Paul Cooper: "I recently received a copy of this book and was amazed by its coverage of the title subjects." and "I consider this 1200 page gem a must have reference."

Chris Pierce: "It is without doubt a major work – something of a magnum opus, in fact, and thoroughly comprehensive in its coverage of all aspects of pyrotechnics from both practical and theoretical standpoints. However, it goes beyond that and reaches into historical, legal, and even social areas – creating a final document that is by far the most extensive publication of its type ever to have appeared to date."

John Steinberg: "exhaustively detailed, profusely and well-illustrated, comprehensive in its scope." and "The Journal of Pyrotechnics is to be commended for producing one of the finest reference works I have ever had the pleasure of using."

Robert Winokur: "anyone who finds themselves putting down on paper thoughts about pyrotechnics, will find the dictionary extremely important." and "This dictionary covers most topics that are involved with pyrotechnics and fireworks and includes nearly all aspects of those topics."

Fireworks Business:"It's monumental, it's thorough, and it's impressive." and "Its significance to the pyrotechnic world is past superlatives."

Pricing

CD containing PDF files $39 – shipped anywhere.

3-volume set of B&W hard-bound books $120 (US) or $155 (non-US)

3-volume set of full color hard-bound books $240 (US) or $300 (non-US.

Measurements of Sound Pressure Levels for Aerial Shell Mortar Firings and Star Shell Bursts

K. L. Kosanke and B. J. Kosanke
PyroLabs, Inc., 1775 Blair Rd, Whitewater, CO 81527, USA

***Abstract**: A large number of sound pressure level (SPL) measurements were recorded for the firing and bursting of firework star shells ranging in size from 3 to 6 inch (75 to 150 mm). The results of a series of 400 measurements of SPLs of firework aerial shell mortar firings as a function of distance from the mortars are reported. Also, the results of a series of 200 measurements of SPLs of firework star shell explosions occurring at their normal burst heights are reported.*

***Keywords**: Sound pressure levels, shells,*

Introduction

It is a requirement in many countries that workers must be protected from hearing loss resulting from exposure to loud sounds in their work environment. However, while some data have been published on the sound pressure levels (SPLs) produced by fireworks, those data are far less than exhaustive. This is especially the case for SPL exposures experienced by workers during the course of performing firework displays. To augment the existing data, a large number of measurements of SPLs have been recorded for the impulse sounds produced by firing and functioning of small to medium-size firework star shells.

Fireworks

Only hard-breaking, well-constructed, Chinese-manufactured, spherical, single-break, chrysanthemum and peony star shells were used for these measurements. Principally, those aerial shells were manufactured by Sunny, Lidu and An Ping. Only small to medium-size star shells, 3 to 6 inch (75 to 150 mm), were used. Salute shells and multi-break shells were not used.

Instrumentation

The instrument used to record sound pressure levels was a Quest Technologies 1800 (a type 1 instrument), operated in the 'peak' mode and using 'linear' weighting, with a QE-4110 microphone, and calibrated using a Quest Technologies QC-10 calibrator. When calibrated as normal, the maximum SPL capable of being recorded in this configuration is 170 dB. However, under conditions when a few sound levels slightly exceeded this limit, measurements were made with the instrument gain recalibrated to allow measurements to approximately 174 dB. In all cases, the SPL instrument was positioned 5 ft (1.5 m) above the ground, at the approximate level of the ear of a typical person.

In some cases, when recording SPLs not exceeding 140 dB peak-linear, a calibrated Quest Technologies 2700 (a type 2 instrument) using its standard microphone was also used.

Mortar firing sounds

Sound pressure levels of star shells were recorded at various distances from the firing mortar. Over the range of distances investigated, 12 to 300 ft (3.6 to 90 m), any difference in SPLs for buried mortars versus mortars in above ground racks was insignificant compared with the normal variations in SPL from firing to firing for the same size star shell. Accordingly, to improve the reliability of the data, both data sets (for buried mortars and mortars in racks) were merged.

The data were recorded over an interval of several

Article Details	***Article No: - 0098***
Manuscript Received:-28/05/2013	***Final Revisions:-31/07/2013***
Publication Date:-01/08/2013	***Archive Reference:-1568***

Table 1. *Mortar firing SPL data (peak-linear) for 3 inch (75 mm) star shells.*

Distance[a] (ft)	No. of measurements	Sound pressure level (dB) [b]			
		Min.	Max.	Average	Fitted
12	14	152	166	160	156
25	7	141	153	145	148
50	21	131	148	141	141
75	11	128	140	136	139
100	15	134	142	137	137
150	17	129	137	134	135
200	17	123	138	133	132
300	18	122	139	131	129

[a] To convert feet into SI units (m), divide by 3.28. [b] SPL values are reported to the nearest 1 dB.

years, always in Spring in eastern Tennessee (USA), at an elevation of approximately 1200 feet (470 m) above sea level. On various days, the temperature ranged from approximately 65 to 75 °F (18 to 24 °C). The atmospheric pressure was not recorded, but given the weather conditions was in the normal range.

The mortar firing SPL curves for the different size shells each had the same general shape as a function of distance. This was expected because the physics of sound propagation in this environment changed very little for the different size shells. To improve the statistical reliability of the data, given the wide range in individual test results, the same curve shape was used for all shell sizes. The exception was to adjust the curve slightly up or down for the best fit of the data for each size shell.

Included in the data tables (Tables 1 through 4) that follow are the averaged SPL results along with the minimum and maximum values recorded at each distance. The graphs (Figures 1 through 4) present the averaged SPL results along with the minimum and maximum values recorded at each distance. Also included in the data tables are the curve-fitted SPL results, as a function of distance, taken from the graphs.

Shell bursts at altitude

Sound pressure levels of spherical, single-break star shell explosions occurring at their typical burst altitudes were recorded. The data were taken under the same physical conditions stated above, and within approximately 100 feet (30 m) of the firing mortars. Based on prior measurements and the atmospheric conditions, the average burst heights would have ranged from approximately 400 feet (120 m) for the 3 inch (75 mm) star shells to 780 feet (240 m) for the 6 inch (150 mm) star shells. These data are presented in Figure 5 and Table 5.

Table 2. *Mortar firing SPL data (peak-linear) for 4 inch (100 mm) star shells.*

Distance [a] (ft)	No. of measurements	Sound pressure level (dB) [b]			
		Min.	Max.	Average	Fitted
12	20	155	173	164	160
25	14	143	158	151	152
50	11	137	153	146	145
75	14	137	146	142	143
100	10	137	143	139	140
150	8	130	142	138	138
200	8	133	137	136	136
300	8	130	134	132	132

[a] To convert feet into SI units (m), divide by 3.28. [b] SPL values are reported to the nearest 1 dB.

Table 3. *Mortar firing SPL data (peak-linear) for 5 inch (125 mm) star shells.*

Distance [a] (ft)	No. of measurements	Sound pressure level (dB) [b]			
		Min.	Max.	Average	Fitted
12	15	150	169	163	163
25	12	147	160	154	154
50	12	138	155	148	148
75	13	140	151	146	146
100	11	140	145	143	143
150	9	137	148	141	141
200	12	135	145	140	138
300	8	133	140	135	135

[a] To convert feet into SI units (m), divide by 3.28. [b] SPL values are reported to the nearest 1 dB.

Table 4. *Mortar firing SPL data (peak-linear) for 6 inch (150 mm) star shells.*

Distance [a] (ft)	No. of measurements	Sound pressure level (dB) [b]			
		Min.	Max.	Average	Fitted
12	8	153	174	165	163
25	25	142	160	154	154
50	21	141	155	149	148
75	17	142	151	146	146
100	8	136	147	144	144
150	8	138	145	141	141
200	14	124	146	137	139
300	6	126	137	132	136

[a] To convert feet into SI units (m), divide by 3.28. [b] SPL values are reported to the nearest 1 dB.

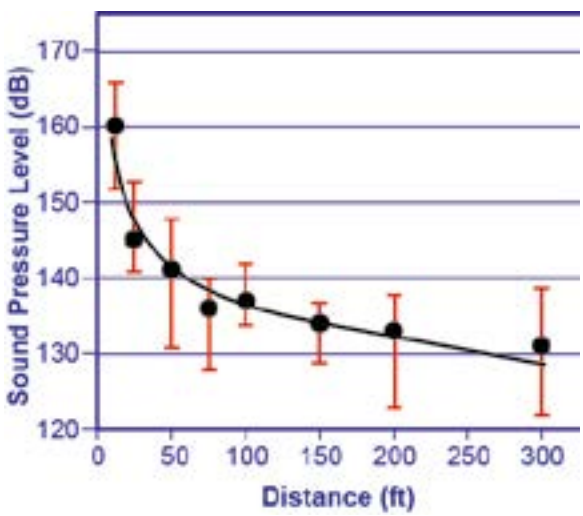

Figure 1. *Mortar firing SPL data (peak-linear) for 3 inch (75 mm) star shells.*

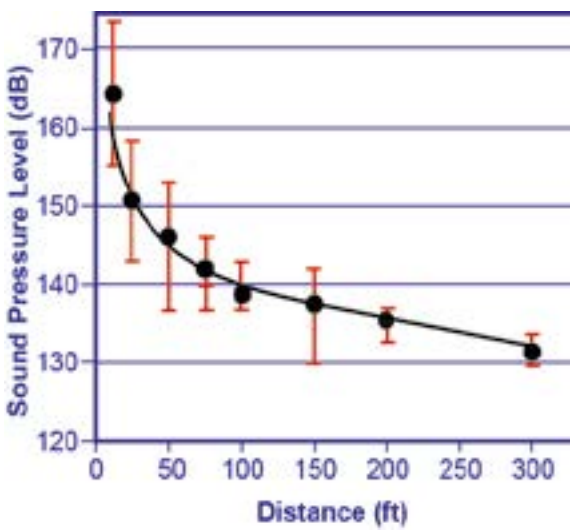

Figure 2. *Mortar firing SPL data (peak-linear) for 4 inch (100 mm) star shells.*

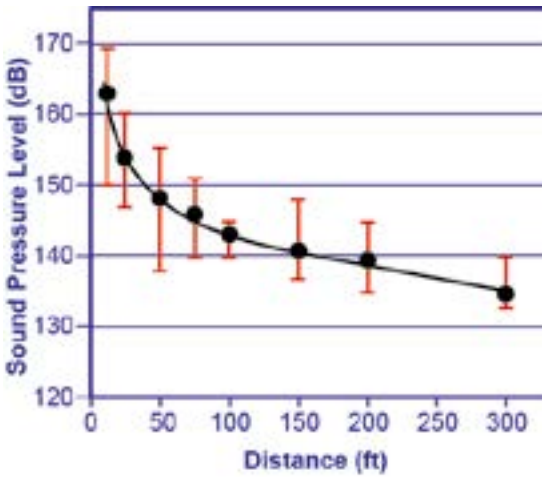

Figure 3. *Mortar firing SPL data (peak-linear) for 5 inch (125 mm) star shells.*

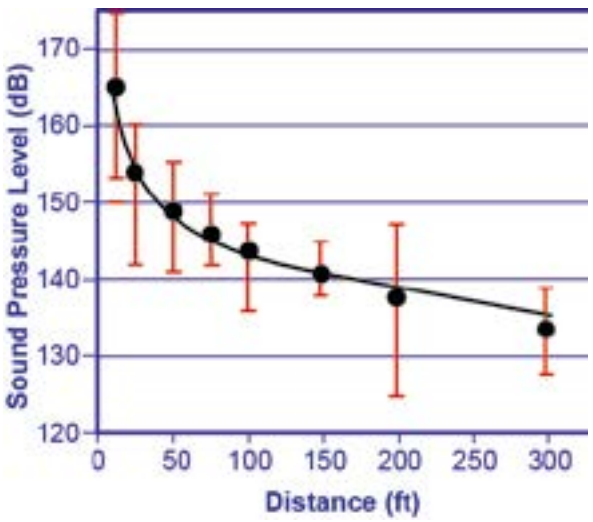

Figure 4. *Mortar firing SPL data (peak-linear) for 6 inch (150 mm) star shells.*

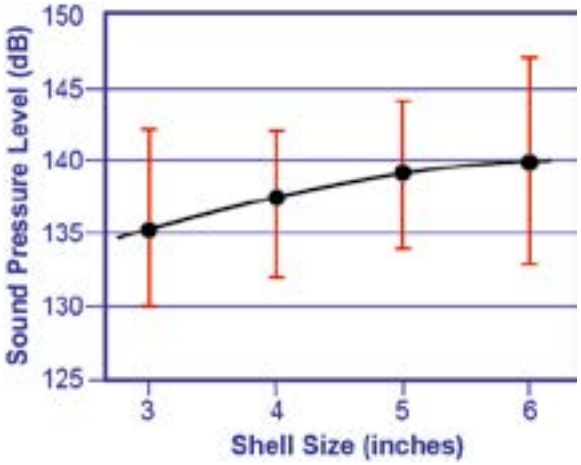

Figure 5. *Shell burst SPL data (peak-linear) for 3 to 6 inch (75 to 150 mm) star shells.*

Table 5. *Shell burst SPL data (peak-linear) for 3 to 6 inch (75 to 150 mm) star shells.*

Size [a] (in.)	No. of meas.	Sound pressure level (dB) [b]		
		Min.	Max.	Ave.
3	56	130	142	135.2
4	32	132	142	137.8
5	49	134	144	138.8
6	58	133	147	139.5

[a] To approximately convert inches into SI units (mm), multiply by 25. [b] Minimum and maximum levels are reported to the nearest 1 dB and average levels are reported to the nearest 0.1 dB.

Acknowledgement

The authors are grateful to Lansden Hill and Pyro Shows, Inc. for allowing access to their yearly live-fire training for the purpose of taking the sound pressure level measurements reported in this paper.

The Senko Hanabi Sparkler:
A Study Of Factors Affecting Construction And Performance

Frederick Van Der Sypt, M.D.
Ghent, Belgium

Abstract: *This article describes the many variables that influence the proper functioning of a senko hanabi sparkler. Standardization of these variables led to the development of a reliable and optimized device. On top of this, two new effects were added to the traditional design, the first being a diversification and maximization of the spark effects by splitting the composition. The second innovation is the addition of pure magnesium that gives the sparkler a spectacular glitter finish. The possibility of producing a significantly colored glitter other than white and yellow, is brought into question by the current experiments.*

Keywords: *Senko hanabi, sparkler, satori effect, glitter*

Preface

This article is the first to emerge from a comprehensive study of the senko hanabi sparkler. The findings of this study are of a practical as well as of a theoretical nature. This first part will deal with all of the practical insights that influence the performance and construction of a senko hanabi sparkler. Also, it will provide the reader with some historical and pyrotechnic background. The second part of the original study will be published as an accompanying article that focuses on the reaction mechanisms that take place inside a senko hanabi droplet.[1] The relevant literature will be reviewed and compared to some new experimental findings.

I hope this first article will be a starting point for other pyrotechnicians to construct this fascinating yet surprisingly challenging pyrotechnic device that combines a high level of safety with enchanting beauty.

Introduction

What is senko hanabi?

Senko hanabi is a traditional Japanese sparkler. It displays one of the most beautiful and intriguing pyrotechnic phenomena: a mesmerizing spectacle of delicate sparks that explode into pompoms of fire. This magnificent display is shot from just one boiling drop of pyrotechnic melt, suspended from a paper string (Figure 1).

Senko Hanabi sparklers originated in Japan in the Edo period (1603–1868). In the pleasure quarters of Osaka, they were burned next to incense sticks that kept track of time while men enjoyed the Geisha delights. After WWII, they were very popular until their labor intensive production shifted to China around 1980. Then, in 2000, several Japanese fireworkers started producing them again. Despite the fact that they are still more expensive than the Chinese ones, the Japanese senko hanabi sparklers are preferred because of their performance and elegant finish. In Japan they typically come last at families' firework parties and because of their relative safety, they can also be enjoyed by children (Figure 2). The sparklers evoke an emotion that the Japanese call "mono no aware", the feeling one gets when confronted with the beauty and transience of life.[2]

What's so special about senko hanabi?

Until now, the senko hanabi sparkler has remained relatively unknown outside of Japan. Yet it has some attractive features for the spectator as well as for the pyrotechnician.

Article Details	***Article No: - 0099a***
Manuscript Received:- 03/06/2013	***Final Revisions:- 17/07/2013***
Publication Date:- 20/10/2013	***Archive Reference:- 1601***

Figure 1. *A collection of split-composition senko hanabi 'Satori' sparklers. The 'Golden series' sparklers on the right contain some sodium bicarbonate to generate a golden-yellow glitter finish. The nine depicted sparklers together weigh less than 1.5 gram.†*

Figure 2. *Children's fireworks – senko hanabi, Miyagawa Shuntei, 1896.*

- Because its performance is influenced by many variables, every single sparkler goes through its own unique life-cycle. This makes every new sparkler potentially the most beautiful one has ever seen. This is opposed to the more uniform and predictable dipped sparklers.
- The different types of sparks can be enjoyed from up close and probably are the most refined in the whole world of pyrotechnics (Figure 3).
- Because of its small size, a senko hanabi sparkler is very safe during production as well as burning. One sparkler contains the same amount of pyrotechnic composition as 5 matches. On top of this, the ingredients are relatively insensitive and non-toxic.
- When compared to other types of firework, a senko hanabi sparkler has a very favorable production-time/effect ratio. It also provides the pyrotechnician with direct insight into the nature of glitter phenomena.
- The possibilities for experimenting with the formulation, the many possible additions and

Figure 3. *Typical display of soot-sparks.*

Figure 4. *Satori-phase, a medusa of other-worldly sparks.*

different methods of production are endless. On top of that, multiple sparklers can be combined to give miniature firework shows.

Why this article?

Although the senko hanabi sparkler has already been enjoyed for many centuries, many variables that affect the performance have even never been described in the literature. Therefore today it is a surprisingly difficult challenge to produce a reliable senko hanabi sparkler, even for an experienced pyrotechnician.

The research behind this article was primarily aimed at defining the many different variables that affect a senko hanabi sparkler's performance and to

Figure 5. *A finished 2-stage senko-hanabi sparkler.*

determine their relative importance. This resulted in a standardised procedure for the production of an efficient and reliable device. Additionally, two newly discovered elements that diversify and enrich the sparkler's traditional design are discussed. These elements are the introduction of a rebirth-phase ('umarekawari' effect) and secondly the incorporation of a pure magnesium glitter ('satori' effect, Figure 4). Also, some attempts to produce colored glitter are discussed.

Construction of a senko hanabi sparkler

What follows is the step-by-step procedure for making a reliable and efficient senko hanabi sparkler (Figure 5). The design was optimized so that the sparkler will function in zero-wind conditions as well as in light winds. Moreover, two new techniques are added to the traditional design. Splitting the composition by carbon-type makes the sparks bigger and more diverse. This

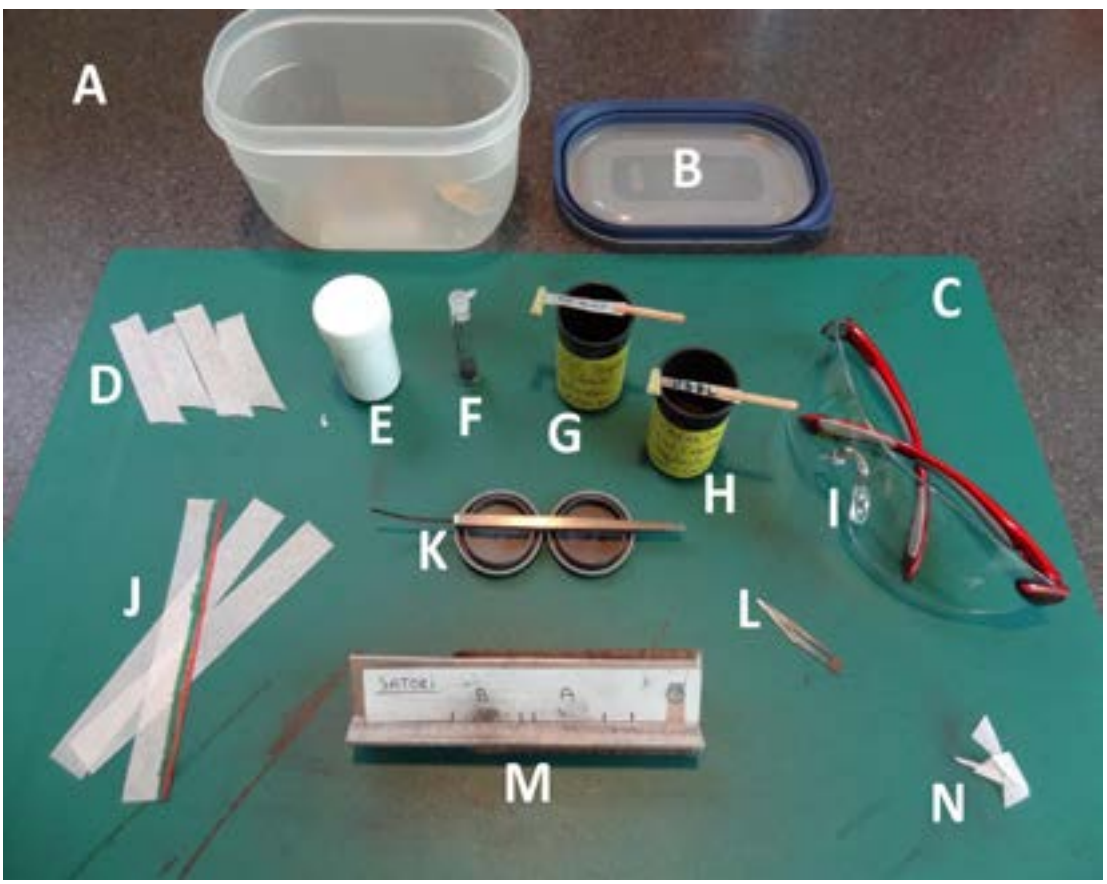

Figure 6. *Overview of working area.*

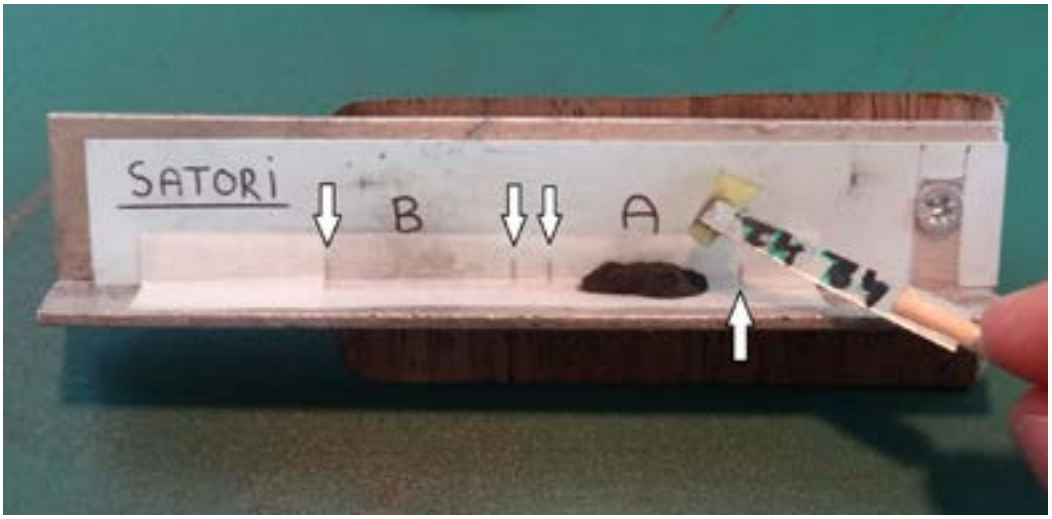

Figure 7. *Close-up of markings and spoon.*

also allows for the addition of pure magnesium to the composition. This second innovation adds a spectacular finish to the end of a senko hanabi sparkler's performance. The sparkler was named after this crackling metal-glitter effect: 'Satori', a zen term that means 'sudden enlightenment'.

Because the ingredients and materials will vary according to local availability, the design will likely have to be fine-tuned. Consulting the methods and results from this study will help in doing these final adjustments.

Overview of the working area and materials (Figure 6)

A: fire-proof working surface

B: hermetically sealing box with lid that easily pops off in case of overpressure

C: cutting mat

D: plain tissue-paper for finishing the sparkler

E: salt used for special effects (e.g. $NaHCO_3$ for yellow satori flashes)

F: magnesium powder treated with linseed oil

G: soot composition with specific spoon

H: charcoal composition with specific spoon

I: polycarbonate safety-glasses

J: Gampi-paper strips

K: small flat spatula with rounded end

L: sharp knife

M: aluminium paper holder on wooden base

N: cut ends of paper

Construction procedure

A strip of Gampi-shi Silk Tissue paper (Awagami-factory, Japan), 16 mm wide and 12 cm long is put on the aluminium holder on a fixed point. At the other side, the strip is folded back upon itself until it reaches the last marking (Figure 7, left arrow). Then, the strip is folded lengthwise in the middle and put back in the holder.

The compositions to be used are prepared in a mini-ball mill in which 20 g of combined ingredients and 40 ml of hexane are mixed for 2 hours. After separating the resulting slurry from the lead balls, it is left to dry and forced through a 100 mesh screen (see also methods and results).

A dedicated spoon that holds a standardised amount of composition A (KNO_3 50/S 35/pine-charcoal 15) is loaded in 3 times and in between the spoon is tapped on the holder so that the composition settles and air-pockets are avoided. The surface of the spoon is leveled with the small spatula and all of the composition, about 42 mg, is poured out on the paper strip in zone A. The same procedure is applied to composition B so that 42 mg are placed in zone B. After this, one uses the rounded tip of the spatula to distribute both compositions evenly between the markings. The spacing between both

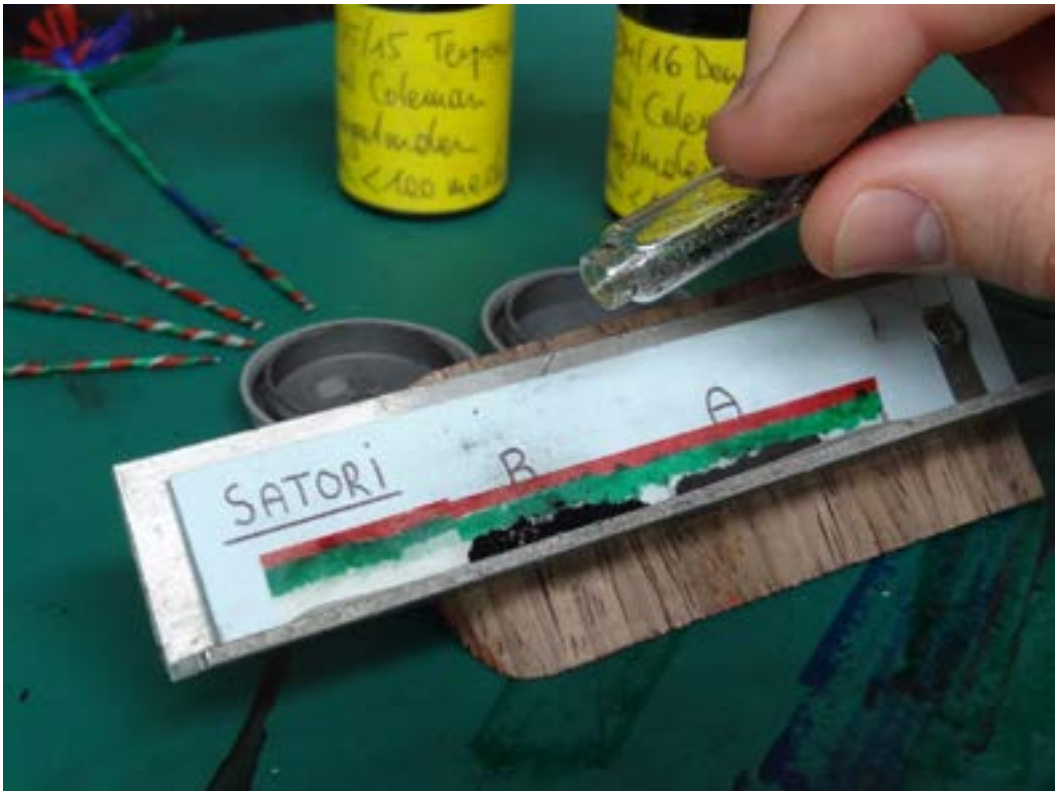

Figure 8. *Compositions in place.*

compositions is about 4 mm. The holder is raised and gently knocked on the working surface so that both compositions can settle out. Finally, a few grains of magnesium are seeded over the last 1 cm of composition B (Figure 8). Optionally, a few mg of a salt can be added to provide an extra effect, e.g. $NaHCO_3$ to color the satori flash yellow.

Now one takes the paper strip from the holder and starts rolling it onto a sparkler. Right-handed people take the folded strip between thumb and index finger of their left hand, while the right thumb and index finger start twisting the end of the strip into a string. The left hand exerts very little pressure while doing this. The angle between the strip and the string is about 45° while rolling the first composition, but when one arrives at the space between compositions, the right hand further increases this angle until it reaches 60–80° (Figure 9).

When rolling the second composition it is even more important not to use too much pressure so that the string isn't twisted too tight. Near the end of the second composition, the angle of rolling is now lowered again to 45° and this angle is maintained for the rest of the sparkler. At this moment, one is left with approximately 1 cm of folded strip. This is cut open with a sharp knife and between the two layers, one inserts a strip of plain tissue paper whose beginning was cut to a 45° angle beforehand (Figure 10).

Now the strip is further rolled into a string and the sparkler is finished by folding back the end of the strip so that the final portion of the string is thicker and the ascending melt-droplet is stopped, protecting the fingers. If price and availability of Gampi-paper is of no concern, then the sparkler's construction can be simplified by starting with a much longer strip of Gampi-paper and to also use it beyond the critical reaction zone.

After rolling, the sparkler should be compressed/tightened over its full length by twisting it firmly between thumb and index fingers of both hands. Only the middle of the second composition should not be compressed to retain its reactivity.

Finally, one cuts the sparkler at the start of the first composition, so that it can be easily lit.

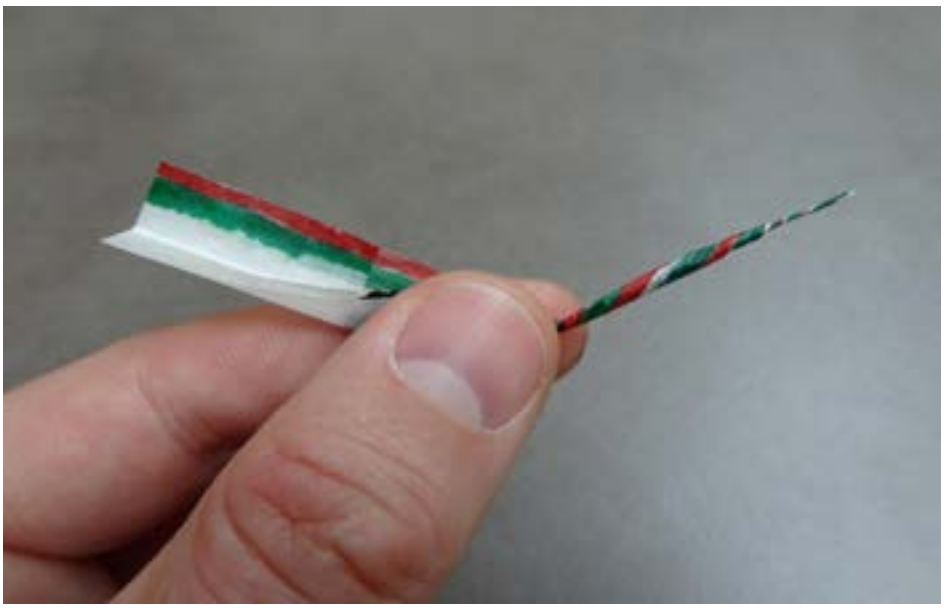

Figure 9. *Twisting the paper strip. Note that the colored lines now create a 2-color spiral.*

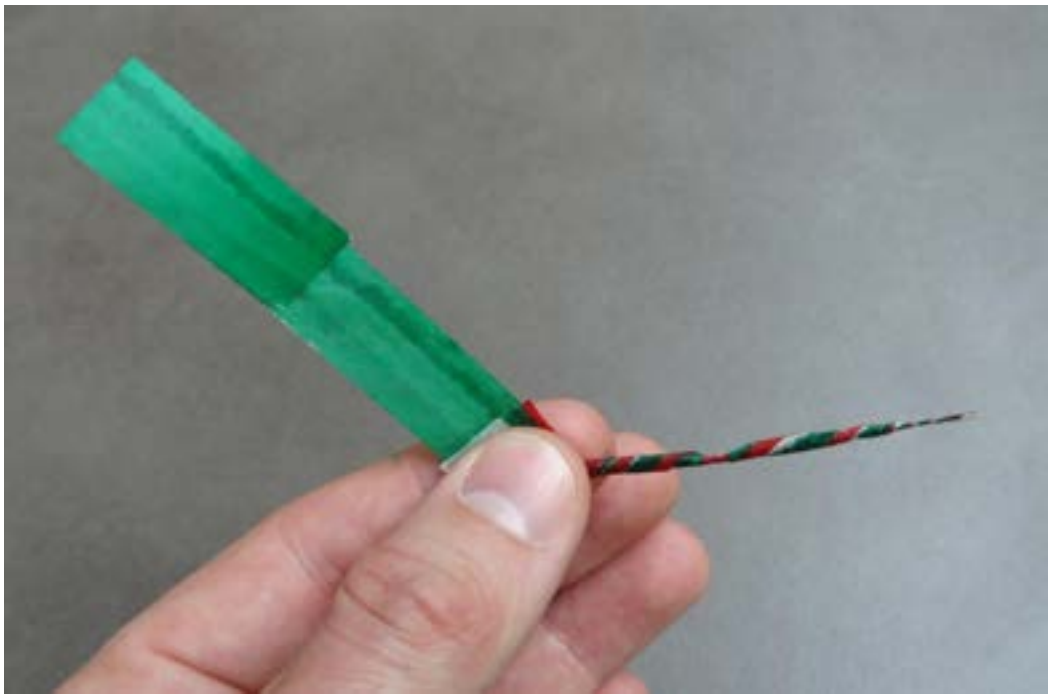

Figure 10. *Adding plain tissue paper.*

Lighting the sparkler

The beauty of the delicate senko hanabi sparks is easily washed away by ambient light. If possible, light the sparkler in absolute darkness. It is amazing how much this adds to the effect.

The boiling of the dross ball and the firing of the charcoal and soot sparks also produce enjoyable sounds that are best appreciated in a quiet environment.

Last but not least, a senko hanabi sparkler is very sensitive to wind. Too much wind simply blows off the droplet. However, in still air there is frequently no satori effect. The full range of effects must therefore be enjoyed in minimal wind conditions, which are in fact more common than zero-wind conditions.

Senko hanabi sparklers should always be lit outside above a fireproof surface. The dross ball can (and will) fall off and is capable of staying hot for a very long time by the very nature of the senko hanabi phenomenon. Occasionally, a falling droplet mildly explodes when it hits the ground.

An alternative way to appreciate a sparkler is to wait for the moment where the sparks start to emerge and then shoot the drop away with a finger. This gives rise to a surprising display of sparkling drops that fill the air in front. Of course, one should always aim towards a fireproof area and well away from other persons (Figure 11).

Troubleshooting

The dross ball doesn't form

- Wrong formulation: try adding more sulphur. Soot-based compositions are less reactive than charcoal-based ones.
- Too much paper: try using thinner paper or using a narrower paper strip.
- High heat dissipation: try rolling the sparkler more perpendicular to the strip so that it gets shorter and more compact.
- Too much salt added.

Figure 11. *Just one drop of polysulfide melt shot with a fingertip.*

The dross ball drops

- Too much composition: gradually lower the amount.
- Too much wind.
- Jet of reaction gases blows off the droplet: try rolling the sparkler more perpendicular to the strip so that the jet is aimed outwards instead of downwards.
- Viscosity too low: lower the amount of soot.
- Paper string above dross ball is burned: use a double layer of paper just behind the composition. Try unwinding the region just behind the composition a little bit.

Sparks are small

- Suboptimal formulation: systematically test compositions around the current one by means of the composition triangle (see methods and results).
- Wrong type of carbon: use soot for larger sparks.
- Dross ball continues to climb, thereby consuming paper and lowering its overall reaction rate and temperature: add more twist to the paper just behind the composition. A tightly wound paper string slows the ascent of the drop.
- Too much wind: wind stimulates the formation of many but shorter sparks.
- Addition of salts: only use the minimal amount necessary.

Dross ball is blown off when arriving at the second composition

- Second composition reacts too fiercely: while rolling, put some more pressure on the starting zone of the second composition so that air pockets are minimized.
- Jet of gases blows off droplet; increase the angle of rolling so that the jet is aimed outwards.

No satori effect

- Magnesium was burnt in the initial phase: only add magnesium to soot-based compositions.
- Not enough magnesium: try adding just a little bit more.
- Still air: light the sparkler outside in very light wind conditions or gently blow on the reacting drop.

Satori effect comes too soon

- Too much magnesium, add less.
- Addition of $NaHCO_3$: lower the amount of this salt.

No old-age phase‡

- Suboptimal formulation: test others.
- Gently unwind the paper string behind the last composition.

Methods and results

For each variable the method used and the observed results are grouped together. As a general methodology it can be stated that when one variable is adjusted, the others are kept as constant as possible. Most of the experiments were video-recorded for better analysis later on.

The paper factor

Paper type

Method: Tissue paper, wrapping paper for shoes, different brands of commonly available tissue paper and a few types of handmade Japanese paper were tested.

Results: Thickness and tear resistance are the main points of interest. Because the polysulfide reactions require atmospheric oxygen, neither the paper nor the residual ash may shield the melt from air. If the paper is too thick, the gases that are evolved may blow off the dangling droplet by creating a tube. On the other hand, the fibres present in the paper keep the drop attached. Standard tissue paper (e.g. 'Canson') works, but is still quite thick (20 g m^{-2}) and tears easily when twisted. 'Gampi-shi Silk Tissue (Awagami-factory, Japan)' is both extremely light (10 g m^{-2}) and surprisingly strong. The fibres come from a bush that has been used by Japanese paper-makers since the 8th century. To date, no other type of paper has been found to be superior for the production of senko hanabi sparklers.

Width and fibre direction of the paper strip

Method: Paper strips were cut along their length

respectively perpendicular to the direction of the fibres. The width of the strips was varied from 12 mm to 30 mm.

Results: Strips that are narrower than 14 mm are difficult to roll and can give leakage of composition. On the other hand, narrow strips seem to promote the start of the secondary polysulfide reactions. This might be explained by the lesser amount of paper that shields the reaction products from the air and by the smaller total amount of ash. On the other hand, broad strips can provide more suspension for the droplet. The thicker the paper, the more important its width. Looking at standard tissue paper, a clear difference in reactivity can be observed between strips of 14 mm and 16 mm. The Gampi-paper is more tolerant, and Ito as well as Saito use strips with widths up to 25 mm.[3,4] After experimental research, the aforementioned factors were found to be well reconciled by choosing a Gampi-paper strip of 16 mm. The direction of the fibres is important because strips that were cut perpendicular to the direction were very prone to tearing while being twisted.

Length of the paper strip

The traditional Japanese sparklers have a length of about 20 cm when finished. In making a sparkler, one can choose to use a very long strip of Gampi-paper or to use a strip of cheaper tissue paper after the critical reaction zone. Audiences seem to appreciate shorter strands of paper, different from the traditional Japanese design, so that the sparks seem to come out of their hands. This design also illustrates the innocent nature of the sparks when they touch the skin. In addition, they are easier to transport this way.

Coloring the paper

Standard tissue paper is available in many colors and this adds to the beauty of the sparkler. Black can be used for its invisibility in darkness, but this makes working with the black compositions harder. Another way of adding color is to color the paper oneself. This opens up many artistic possibilities such as spiralling colors by drawing colored lines lengthwise on the paper. One can choose to use natural dyes (Kimiko Saito uses safflower for pink, kihada for yellow, burdock for purple and a mixture of kihada and Japanese pampas grass for green[4]) or synthetic dyes like alcohol markers. An alternative is to color the sparkler once it has been twisted.

The composition: raw materials

Charcoal types

Method: Shimizu and others make use of both Paulownia-charcoal and pine-charcoal. For these experiments, they were prepared by putting twigs (4 cm diameter) of a young Paulownia-tree and stem-wood from *Pinus sylvestris* in a tin drum sitting on a bed of glowing barbecue charcoal. After cooling down, the charcoal within the tin drum was mechanically ground so that it passed a 100 mesh screen.

Results: Contrary to the findings of Shimizu, the sparks generated by the paulownia-charcoal were smaller and showed less branching than those from the pine-charcoal. The latter shoot approximately 10 cm away from the droplet in the first youth before they explode themselves into dense bushes of sparks a few centimetres in length.

Soot types

Method: Oglesby states that "Lampblack should be made at low temperature and quickly quenched. It consists of bulbous groups of imperfect rings and straggling twisted shreds of crooked chains with many branches coiling back on themselves and each other".[5] Traditionally, soot for senko hanabi sparklers is produced by burning the wood and resin of certain *Pinus* species (e.g. *Pinus densiflora*). In his S*tudies on Senko Hanabi*, Shimizu used soot made from burning anthracene.[6] Saito on the other hand uses soot made from the combustion of the roots of *Pinus* species.[4] The current experiments used pine-soot made by burning just the resin from European *Pinus* species and collecting it on the inside of a metal container. In the article by Ito, soot from burning turpentine was used.[3] This method was tested as well.

Results: The burning of turpentine proved to be the easiest way of producing soot and the quality of the soot did not seem inferior to that of pine resin. In the 'second youth', the sparks produced by these types of soot travelled an average of 20 cm away from the droplet. Sometimes the sparks reached more than 40 cm. In their 'middle age', these sparks still reached 10 cm. After their travel, they exploded into pompoms with sizes

ranging from a plum to an orange.

Sulphur source

Only technically pure sulphur that passed a 100 mesh sieve was used for the experiments. Shimizu also describes finished items containing realgar (arsenic sulfide) as sulfur source for the polysulfide reaction.[8] The highly toxic nature and carcinogenic properties of this material and its reaction products make it unsuitable for use in a hand-held sparkler. Similarly, antimony sulfide, which is commonly used in glitter compositions, poses an unacceptable health risk both in the production and firing of these sparklers.

Potassium nitrate

Technically pure potassium nitrate was used that prior to the processing was sieved to <100 mesh.

Metal powders

For the experiments, pure magnesium powder (100 mesh), magnalium powder 50 : 50 (200 mesh) and atomized aluminium powder (0–325 μm) was used. The magnesium powder was protected from unwanted reactions by treating it with linseed oil in the following manner: 1 ml of boiled linseed oil was added to 25 g of magnesium powder and a sufficient quantity of hexane was added to moisten the powder evenly. Then the powder was allowed to dry for several days.

The composition: formulations

Methods: Many formulations were tested. Building on the research done by Shimizu, a starting ratio of 60 KNO_3//25 S/15 carbon source was used. Throughout the experiments this ratio was systematically changed by placing six points around this point on the composition triangle. The best performing composition (one that easily starts the polysulfide–air reaction and that generates big sparks) was selected and again six points were selected around this composition to further specify the optimal ratio of raw materials. Because the split composition design offers important advantages, few experiments were done to test mixed carbon-source compositions. Shimizu already studied the optimal ratio between charcoal and soot. It turned out to be 4 : 1. This specific ratio was also tested in a composition consisting of 50 KNO_3/35 S/12 charcoal/ 3 turpentine-soot.

Results: The experiments showed that the optimal ratio depends on the desired effect and on the other production variables. Of these, the most important one is the mixing method used. The formulations used by Ito (55/25/15/5)[3,7] and Shimizu (60/25/12/3)[6] are adapted to the mortar and pestle method. When more intimate mixing methods are used (see below), these formulations become too reactive and therefore not usable. After systematic screening of the composition triangle, the optimal ratio when processed by mini-ball mill slurry mixing seems to be 50/35/15, regardless of the carbon source used. Depending upon the direction in the composition triangle that the formulation travels from the reference ratio, specific changes in properties are observed. For example, a soot composition 54/31/15 is less efficient in its youth phase, but gives off more sparks in the old age. A soot composition 54/36/10 is very eager to start the polysulfide–air reaction, but does not give off sparks and gets stuck in phase 2. The description of the properties of all the different compositions tested would take an article by itself. A study of these properties could show trends depending upon the direction the formulation takes in the composition triangle.

The observations made by Shimizu concerning mixed carbon source compositions[6] were confirmed. Sparks travelled about 12 cm from the droplet. The flying range and size of the secondary explosions are however inferior to those generated by split compositions.

Mixing method

Method: A finished sparkler contains less than 90 mg of composition. Taking into account these small quantities used, even small deviations from total homogeneity of the composition can lead to noticeable differences in effect. It is therefore surprising to find that even in recent literature the mortar and pestle method is used.[3,6,7] This manual method however, is very difficult to standardize. Also, the degree of mixing remains inferior compared to automated techniques. For the current experiments, the raw materials were passed through a 100 mesh screen and different mixing methods were successively tested: mortar and pestle (intimate mixing for about 15 minutes), repetitive screening (20 times through a 60 mesh screen), 2 hours of dry ball milling in a mini ball

mill (recipient of 100 ml and lead balls of 5 mm) and slurry ball milling in the same mini ball mill for the same time. The slurry was created by adding 40 ml of hexane to 20 g of composition in the ball mill. It is an adaptation of the Dupont black powder manufacturing technique.[9] After processing, the composition was again passed through a 100 mesh screen.

Results: All dry methods except screening led to caking of the composition. Only the slurry method provided a composition that showed no sparkler-to-sparkler variability. Hence this became the preferred processing technique.

Amount of composition

Method: The use of different amounts of composition was tested. These quantities were originally estimated by the naked eye but were soon weighed on a milligram scale for reasons of standardization. Eventually a measuring spoon was developed that was able to contain reproducible amounts of composition. The properties of this milligram spoon are that it has a smooth surface and very thin surface, so that no powder can stick or rest on it. The arm of the spoon also has to be smooth and very thin for the same reasons. In addition, a rounded end makes it easier to turn the spoon during filling and emptying. Such a spoon was constructed by welding a drinking straw together, gluing a strip of a tin can to it and inserting this into a split bamboo skewer. Many scoops were made this way and each was filled 20 times with composition and the amounts were weighed on a milligram scale. They proved to be reliable and thus the use of the milligram scale became superfluous.

Results: The optimal amount of composition is a trade off between the size of the effect on the one hand and the falling of the polysulfide drop on the other hand. Depending upon the other variables, this amount is between 80 and 90 mg, in accordance with traditional and current literature. In the case of a split composition sparkler, the maximum total amount remains the same.

Addition of metals

Method: Magnesium powder, magnalium powder and aluminium powder (for specifications see 'raw materials') were added to charcoal compositions, soot compositions, mixed compositions and to the soot portion of split compositions. The amount added varied between 1 and 10 mg.

Results: Magnesium can only be added to a soot-based composition. If charcoal is present, the reaction temperature is higher and the magnesium is burnt in the first phase. Magnalium and aluminium are less reactive[10] and can also be added to charcoal-containing compositions. The experiments also showed that only magnesium powder is reactive enough to produce the satori effect in the wind conditions a senko hanabi sparkler can be fired in. So the high reactivity of magnesium is in fact a necessity for it to be used in senko hanabi sparklers. In still air, there frequently is no satori effect. However, the slightest breeze can reliably trigger the effect. Concerning the amount of magnesium to be added, it seems that just a few grains are enough to provide a spectacular finish to the sparkler. Adding more magnesium decreases the time to the satori phase and makes the drop react completely in one flash, like traditional glitter.

Other additions:

The effect of adding different salts to classic glitter compositions has been studied extensively.[11] Now, some of these substances were put to the test in senko hanabi formulations. However, toxic and/or corrosive substances were left out: arsenic sulfide, antimony sulfide, calcium oxalate, sodium oxalate, lithium oxalate and barium nitrate. Only sodium bicarbonate and strontium oxalate have an acceptable health risk for a hand-held device.

$NaHCO_3$:

A small amount (2–5 mg) of sodium bicarbonate was added to the soot composition containing magnesium. This caused significant changes in the melt chemistry and spark effects. Instead of the usual sparks, small droplets were emitted which create a kind of 'rain effect'. Also, the addition of $NaHCO_3$ made the magnesium react earlier. The typical corkscrew sparks were absent and the flash reaction was observed to come only from the surface of the droplet. The flashes clearly emitted a deep yellow color (Figures 12, 13).

Li_2CO_3, $Li_2C_2O_4$, $SrCO_3$ and SrC_2O_4

Method: A few milligrams of lithium carbonate, strontium carbonate, lithium oxalate and strontium

Figure 12. *Indirect light from satori flashes with added salts.*

oxalate were added to the soot composition of split composition sparklers containing magnesium.

Results: The carbonates had a strong inhibiting effect on the reactivity of the polysulfide melt. In a senko hanabi sparkler, they don't seem useful. The oxalates have less of an inhibiting effect, and make the polysulfide melt emit sparks similar to those of $NaHCO_3$. Live sparklers, pictures and stills of video-recordings showed no significant coloration of the flash in comparison to pure magnesium (Figures 12, 13: the indirect photographs show a pinkish hue with strontium oxalate, but to the naked eye the flash remains white).

$Sr(NO_3)_2$

Method: In analogy to Winokur's glitter composition #1, an equal portion of the potassium nitrate was substituted by strontium nitrate. This led to the formula 35 KNO_3/15 $Sr(NO_3)_2$/35 S/15 turpentine soot. The composition was processed like the others i.e. 2 hours of ball milling with added hexane. This composition was used alone and as a second phase in a split composition sparkler.

Results: The presence of $Sr(NO_3)_2$ clearly changed the melt chemistry and led to the emission of many drops which gave the reaction a pronounced 'rain effect'. The magnesium flashes did not change character like with $NaHCO_3$, and there was no significant color change comparing to pure magnesium flashes.

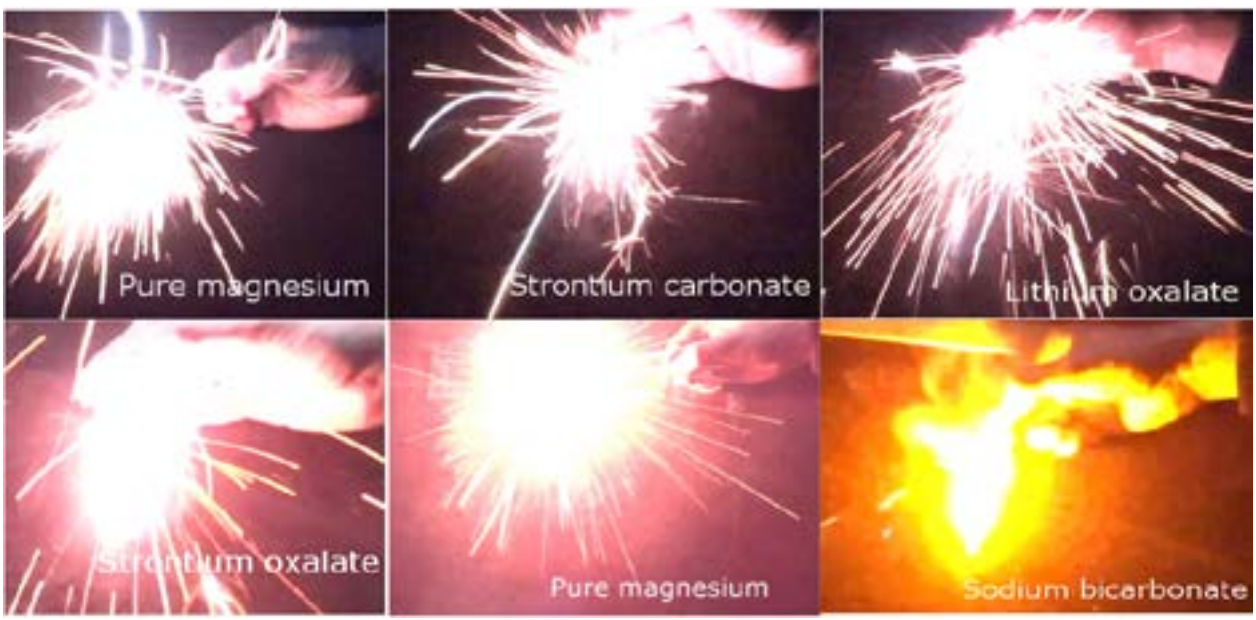

Figure 13. *Satori flashes with added salts.*

Production method

Placement of the composition on the paper strip

Method: the composition is put in the middle of the paper strip over a distance that ranges from 2–4 cm. Both single composition and split composition sparklers were thus tested.

Results: the optimal length of composition on the paper also depends upon the way the strip is wound up. In general, the composition is best placed over a length of 2.5–3.5 cm. Spreading the composition over shorter distances leads to faster and more violent burning which makes the reaction products less likely to form a reactive melt. In split composition sparklers however, the second one can be spread over a shorter distance, because the first one has already started the polysulfide–air reaction. This makes it easier for the reaction products of the second composition to start reacting themselves. In addition, because the second composition is frequently soot-based, the faster and hotter consumption can be an advantage.

Multiple compositions and spacing

Method: Two or more quantities of composition are put in sequence upon the paper strip. Experiments were done with sequential charcoal compositions, sequential soot compositions and soot compositions following a charcoal composition. The gap between these compositions was varied from 2 to 20 mm.

Results: Charcoal compositions reliably pass on to the middle-age and old-age stages. This way, the paper gets consumed while the polysulfide drop climbs up on the string and can ignite a following composition. It was found that using a 50/35/15 pine-charcoal composition, it is possible to create a string of consecutive reaction zones. Polysulfide drops from soot-based compositions on the other hand have a tendency to remain stationary and die out. Therefore it is better to let a soot-based composition follow a charcoal-based one. Moreover, this way the sparks get larger in consecutive phases.

The spacing between compositions determines when the reacting polysulfide drop makes contact with the next composition. If one increases this length, the drop will have had more time to show its typical display of sparks. On the other hand, when the distance between compositions is kept short, the second composition is consumed while the first is fiercely reacting. This in turn promotes the reaction of the second polysulfide drop. Especially for soot-based compositions, this stimulation is beneficial. So the spacing is a trade-off between viewing the spark display of the first composition and the reactivity of the second. It was found that the optimal spacing distance is 2–6 mm, depending upon the angle the paper makes while rolling the sparkler.

Folding back the strip

Method: Before folding the strip lengthwise, it is folded back over itself so that the final portion is double-layered. The length of this overlap is varied.

R**esults**: The greater the overlap, the more the reactivity of the second composition is tempered to the point where it is not capable anymore of starting the polysulfide–air reaction. If the overlap is made shorter however, the polysulfide drop is less suspended and therefore more prone to falling. In the current experiments, an optimum was reached by folding the strip back to the end of the second composition, or a few millimetres further towards the beginning.

Angle of rolling

The angle at which the paper strip is rolled was varied from almost parallel to the length of the paper to perpendicular to it.

Results: Depending upon this angle, the composition shows differences in burning rate (the more perpendicular, the faster it burns), the direction of the flow of the combustion gases (the more perpendicular, the more the flow is directed sideways), the reactivity of the polysulfide melt (the more perpendicular, the faster the polysulfide reaction will take place) and adhesion of the drop to the paper string (the bigger the angle, the better the adhesion). The following procedure has shown to best take into account all of these elements. One starts with a paper strip folded lengthwise with two compositions spaced 5 mm apart. If one starts rolling at the firing end, the left hand holds the strip between thumb and index, while the same fingers from the right hand start twisting the paper at an angle of 45°. If one starts with a paper strip of 16–20 mm wide, one can observe in the

finished sparkler two zones that spiral around each other. The darker zone is where the composition is covered by only one layer of paper, the lighter zone is where three layers of paper cover the composition. This way, the reaction products have a zone in which they can easily react with the atmospheric oxygen and another one that helps in suspending the drop. After rolling the first composition in a 45° angle, the angle is increased to 60–80° when arriving at the intermediate zone. This ensures that the paper string gets slightly thicker to prevent the reacting first drop to fall. The second composition is rolled up in the same angle. This way, the soot-based composition is consumed faster (promotes reactivity) and the reaction gases are directed sideways, preventing the drop from being blown off. Arriving at the end of the second composition, the angle is again lowered to 45°.

Compacting the composition and winding the paper string tight

M**ethod**: After rolling, the sparkler is twisted with extra force so that some regions are more compacted than others.

R**esults**: The compaction of a certain region of the sparkler tempers the burn rate of the composition, probably because air pockets are squeezed out of it. The experiments show that charcoal-based compositions are best compacted. Soot-based compositions on the other hand seem to gain reactivity when they are kept somewhat loose. If the paper string just behind a composition is more firmly twisted, the tendency of the resulting polysulfide drop to climb up the string is lowered. The drop stays stationary, and this enhances the display of sparks because less non-reactive material is added to the melt. Further on the string, providing less twist can stimulate a prolonged 'old age' phase. So for best results in a typical split composition sparkler, one compacts the charcoal-based composition (to temper the very reactive composition), the string between first and second composition (to give the first polysulfide drop the opportunity to display its typical sparks), the first millimetres of the second composition (to prevent a fierce reaction that blows off the first droplet) and the string just behind the second composition (to let it display its characteristic sparks). Practically, the extent to which the paper can be extra tightened is largely determined by the type of paper used. The aforementioned Gampi-paper is much more tear-resistant than standard tissue paper.

Applying a coating

Applying a coating to a sparkler can make it more water-resistant and can keep it from unwinding during transport.

M**ethod**: After rolling, sparklers were immersed in different solutions: 10% celluloid (ping-pong ball) in acetone, 10% shellac in ethanol and collodion.

R**esults**: Coating the sparkler with shellac leads to the composition reacting very slowly and the coating catching fire. Celluloid dissolved in acetone inhibits the reactions less but the coating still occasionally catches fire. The polysulfide reactions still start, although less vigorous. Collodion puts a thin cellulose nitrate coating around the sparkler. This treatment seems to influence the normal reactions least of all. In general however, coating a senko hanabi sparkler reduces its performance.

Firing conditions: wind speed

Method: Senko hanabi sparklers were burned in still air and in very light winds. The wind speed during the experiments was standardized using a small fan that was aimed at the sparkler.

Results: Wind speed proved to be a crucial factor affecting performance. More wind makes the sparkler react faster and more vigorously. The largest sparks however are observed during low to zero wind conditions. It was observed that the satori effect frequently failed to show in zero wind conditions. So a little wind gives optimum overall performance. The ideal wind speed lies therefore between the one that just causes the magnesium to react and the one at which the drop falls.

Conclusion

This article is probably the first to describe the many variables that influence the proper functioning of a senko hanabi sparkler. Standardization of these variables led to the development of a reliable and optimized device. On top of this, two new effects were added to the traditional design, the first being a diversification and maximization of the spark effects by splitting the composition. The second innovation is the addition of pure magnesium that

gives the sparkler a spectacular glitter finish. The possibility of producing a significantly colored glitter other than white and yellow, is brought into question by the current experiments.

Acknowledgements

I would like to thank my wife for being supportive while the research and writing of this article was being conducted. Also I would like to thank my close friends for helping me with the translation of this document. Thirdly, I would like to thank this journal for giving me the opportunity to share my work and knowledge with fellow pyrotechnicians.

Notes and references

† All figures are made by the author except for Figure 2, source: Japanese art open database.

‡ Traditionally, the different burning stages of a senko hanabi sparkler are seen as phases in the sparkler's life. In the described satori design, these stages are: 'birth': fuse like burning; 'infancy': formation of a dross ball; 'youth' and 'middle age': emission of charcoal sparks; 'rebirth' and 'second infancy': consumption of the second composition; 'second youth' and 'second middle age': emission of soot sparks; 'old age': silent emission of long streaky sparks; 'satori' crackling glitter flashes. For an in-depth description of these phases, see reference 1.

1 F. Van Der Sypt, 'The Senko Hanabi Sparkler: a Study of its Reaction Mechanisms', Journal of Pyrotechnics, Issue 32, 2013, following paper.

2 T. Dillon, 'The Littlest Firework', *Wingspan*, July 2006, pp. 27–31.

3 H. Ito, 'Simple Preparation of Japanese Toy Firework', *Kagaku to Kyoiku* (Chemical Society of Japan), Vol. 39, Issue 2, 1991, p. 130.

4 K. Saito, Senko Hanabi, *8th International Symposium on Fireworks*, 2005.

5 L. S. Oglesby, *Glitter, The Chemistry and Techniques*, 2nd edn, American Fireworks News, 1989.

6 T. Shimizu, 'Studies on Senko Hanabi', *5th International Symposium on Fireworks*, 2000.

7 H. Ito, 'The mechanism of spark generation from Japanese Toy Firework', *Kagaku to Kyoiku* (Chemical Society of Japan), Vol. 39, Issue 6, 1991, p. 682.

8 T. Shimizu, *Fireworks, the Art, Science and Technique*, Pyrotechnica Publications, 1981.

9 I. Von Maltitz, *Black powder manufacturing, testing and optimising*, American Fireworks News, 2003.

10 M. Oguchi and H. Nakamura, The reactivity of magnesium, magnalium and aluminium powder, *8th International Symposium on Fireworks*, 2005.

11 C. Jennings-White, 'Glitter Chemistry', *Journal of Pyrotechnics*, Issue 8, Winter 1998, p. 53.

The Senko Hanabi Sparkler:
A Study Of Its Reaction Mechanisms

Frederick Van Der Sypt, M.D.
Ghent, Belgium

Abstract: *The senko hanabi sparkler was found to be a very useful tool to study glitter phenomena. It was shown that current theoretical frameworks are incapable of explaining all observations. New elements were added to the discussion about the role of critical temperature and potassium sulfate concentration on the glitter flash. Also, the role of sodium bicarbonate as glitter enhancer and coloring agent was demonstrated in the senko hanabi sparkler.*

Keywords: *Senko hanabi, sparkler, satori effect, glitter*

Preface

This article is the second to emerge from a comprehensive study of the senko hanabi sparkler. A first article[1] gave some historical and practical background and discussed the variables that affect the performance and construction of a finished device. This second article will focus on the underlying reaction mechanisms inside a senko hanabi droplet. Insights from recent experiments are compared to data from relevant literature. I hope this review will be a starting point for other pyrotechnicians to do further studies on the fascinating senko hanabi phenomenon.

Life of a senko hanabi sparkler

The sequential chemical reactions and related effects can be seen as stages in the 'life' of a senko hanabi sparkler. These stages were already defined by Maeda for the sparkler's traditional design.[2] This article proposes an updated design that adds new stages (4,5,6 and 8) to the sparkler's life course while leaving the traditional effects untouched.

For each phase, the relevant theoretical frameworks will be discussed. Although many authors agree upon the main chemical reactions that take place inside the reacting melt,[2–4] different views are held about specific theoretical aspects. Currently, there does not seem to be one model that explains all observations.

(1) Birth (8–10 seconds)

A fuse-like burning of the composition that leaves a thread-like melt of reaction products (Figure 1)

In this phase, all of the potassium nitrate reacts.

Figure 1. *Birth.*

Article Details	***Article No: - 0099b***
Manuscript Received:- 03/06/2013	***Final Revisions:- 17/10/2013***
Publication Date:- 20/10/2013	***Archive Reference:- 1607***

The following reaction mechanisms are proposed by different authors:

$2\ KNO_3 + 2\ S + 3\ C \rightarrow K_2S_2 + 3\ CO_2 + N_2$
(Shimizu,[10] Oglesby[5])

$4\ KNO_3 + 2\ C \rightarrow 2\ K_2CO_3 + 2\ N_2 + O_2$

$8\ K_2CO_3 + (3n + 1)\ S_2 \rightarrow 6\ K_2S_n + 2\ K_2SO_4 + 8\ CO_2$

$4\ K_2SO_4 + 7\ C \rightarrow 2\ K_2CO_3 + 2\ K_2S_2 + 5\ CO_2$
(Ito[3])

Measurements show that besides CO_2 and N_2, CO is also generated.[10] Therefore both reaction mechanisms are but approximations of the real reactions going on. Maeda has studied the concentration of different reaction products during the lifespan of a senko hanabi droplet. He showed that in this first stage, much potassium carbonate is present. When the reaction continues, this amount decreases and the concentration of potassium sulfate gradually begins to rise.[2]

From the above equation, Oglesby defines the optimal theoretical formulation as being (KNO_3 67/ S 21/ C 12).[5] Shimizu found through empirical research that the optimal formulation is closer to (KNO_3 60/ S 25/ C 15). He uses a mortar and pestle as the mixing method.[6] Ito also uses this method and formulates his composition as (KNO_3 55/ S 25/ C 15–5).[7] However, when more intimate mixing methods are used, like the slurry ball mill that was used for the current experiments, the optimal formulation now shifts towards (KNO_3 50/ S 35/ C 15). This ratio of ingredients seems independent of the type of carbon used, an observation that Shimizu also made concerning his formulations.[2] This shift of the optimal formulation is analogous to the history of black powder, where the ideal ratio of raw materials changed together with the different mixing methods that were used throughout the ages.[5] This 50/35/15 formula gives the following gross starting ratio of reactants (after minimal correction for sulfur loss by evaporation and without correcting for the ash/volatile content nor for the small amount of carbon that is used during spark generation):

$2\ KNO_3 + 4\ S + 5\ C \rightarrow ...$

Analogous to the theory of black powder, the search for an all-explaining equation is extremely complex. Also, this is by no means the aim of this article. However, it is clear that the proposed ratio of ingredients according to current theoretical models is too far removed from this 50/35/15 formulation to allow any of these equations to account for its high performance.

The melting temperature of K_2S_2 is 470 °C. The reaction temperature is high enough to keep it in a molten state. The surface tension then makes the worm-like melt contract into a drop that soon afterwards begins to boil.

(2) Infancy (3–4 seconds)

The melt contracts to a droplet that boils and sizzles (Figure 2)

This is the moment where the magic of the senko hanabi phenomenon starts. The following reactions are also responsible for the persistent and potentially dangerous afterglow of reaction products after the burning of black powder-type compositions, e.g. in a mortar.

$K_2S_2 + O_2 \rightarrow K_2S + SO_2$
(Oglesby[5])

The temperature of the drop now rises to about 860 °C,[2,8] a temperature where potassium disulfide as well as potassium monosulfide (melting point

Figure 2. *Infancy.*

840 °C) are in a liquid state.

The fact that atmospheric oxygen is essential for the senko hanabi phenomenon to occur can be illustrated by holding a sparkler in pure oxygen and pure carbon dioxide respectively. In the oxygen rich atmosphere, the sparkler starts reacting fiercely and even ignites the paper string. The inert atmosphere immediately stops the reaction. One can also stimulate this polysulfide oxidation by blowing on the drop or holding the sparkler in a light breeze. In still air, fresh oxygen is provided solely by convection around the drop. It was observed that a senko hanabi sparkler ignited in micro-gravity performed poorly. In this study, convection processes inside the droplet were of course inhibited as well.[9]

In designing a senko hanabi sparkler, it is therefore necessary to allow plenty of oxygen to reach the reacting melt but also to provide enough support (paper) to keep the drop suspended. These 2 opposing conditions are met in the current 'satori' design as discussed in the previous article.[1] Folding back the end of the gampi-paper strip to where the soot composition ends, leads to regions where the composition (and afterwards also the melt) is covered by only one layer of paper and other regions where multiple layers can provide support for the drop to hang on. It was observed that this design also allowed the jet of reaction gases to be pointed sideways. In contrast, if one just used a wider paper strip, a tube is created that would direct the exhaust gases towards the drop with the risk of blowing it off.

(3) The first phase where sparks are generated

Maeda[2] divides this phase into:

(3a) First youth

(This phase lasts for 8–11 seconds in a traditional sparkler, 2–10 seconds in a split-composition sparkler, depending upon the moment of rebirth): sparks shoot approximately 10 cm away from the fireball and explode into small densely branched 'bushes' (Figure 3). The effect produces a puffing sound.

(3b) First middle age

(9–10 seconds in a traditional sparkler, 0–3 seconds in a split-composition sparkler, depending upon the moment of rebirth): shorter sparks with smaller bushes are ejected at a higher frequency (Figure 4).

Until now, part of the original amount of carbon

Figure 3. *First youth.*

Figure 4. *First middle age.*

(and any metal present) was latent. These particles were shielded from atmospheric oxygen by a layer of polysulfide melt. When the reaction is stopped at this time, these particles can be observed microscopically.[5] In this phase, the particles react.

$2\ K_2S + 2\ O_2(g) + \text{carbon} \rightarrow \text{explosive burning} + CO_2(g) + K_2S$

(Oglesby) [*sic*]

Ito also states that in this phase the polysulfide melt makes the carbon react with oxygen to form carbon dioxide. According to him, the potassium ion is capable of splitting adjacent carbon grids. He used X-ray diffraction to show that their interatomic distance is increased from 3.35 angstrom to 8.5 angstrom. This way, their susceptibility to oxygen is increased and the carbon dioxide that is evolved shoots away fragments of the polysulfide drop. It was shown that for classic metal glitter compositions, the potassium ion seems to be crucial. This finding is similar for senko hanabi compositions. In a recent review however,[4] Jennings-White showed that beryllium nitrate is also capable of producing an effective glitter. Because of the toxic nature of beryllium salts, they were not tested in the current experiments. For theoretical reasons, it might however be interesting to substitute potassium nitrate for beryllium nitrate in senko hanabi compositions and to see if the sparks have the same appearance. The current observations show that increasing the airflow around the droplet makes phase 3 start earlier. In still air, charcoal-based compositions almost always proceed to phase 3, while soot-based compositions are more inclined to stop at phase 2. Since the reaction temperature of soot-based compositions is lower than that of charcoal-based compositions,[3] it seems that the temperature of the melt influences the occurrence of phase 3. When the airflow increases, the reaction temperature increases, hereby allowing even soot-based compositions to react properly. In analogy, it was shown for classic metal glitter formulations that the light intensity and therefore temperature of the spritzel rises just before the flash reaction.[4] (Analogous to its definition by Oglesby,[5] a spritzel is a burning drop consisting of polysulfide melt ejected by a glitter star or, in the case of a senko hanabi sparkler, suspended on a paper string. It burns at low luminosity in the air at temperatures around 850 °C.)

Reactions 3a and 3b most likely have similar reaction mechanisms. The reason for the differences in length and size of the sparks may be caused by the fact that during this phase, the dross ball gets smaller. Because of this, the generated gases have less distance to travel before reaching the surface of the drop and therefore have less time to expand and accelerate. That evolved gases

Figure 5. *Rebirth – umarekawari.*

are responsible for the emission of the sparks was proven by the observation that senko hanabi sparks shoot less far when atmospheric pressure is increased.[8] The place where the gases are evolved seems equally important. Given the need for atmospheric oxygen, their formation most likely takes place in the outer layer of the droplet. The deeper the gases are formed, the longer they can expand. In windy conditions it is observed that phase 3a very quickly gives way to 3b. Possibly, the airflow makes the most superficial layer of the dross ball heat up quickly, thereby ejecting numerous but smaller sparks.

Both Oglesby's and Ito's equations describe the regeneration of reactants. According to Oglesby, this explains the long duration of the senko hanabi phenomenon. He also describes two reaction mechanisms that compete for the available K_2S and eventually end the reaction:

$2\ K_2S + 3\ O_2 \rightarrow 2\ K_2O + 2\ SO_2$ and

$K_2S + 2\ O_2 \rightarrow K_2SO_4$

Although Oglesby states that K_2SO_4 is a reactant for the metal flash reaction in classic glitter compositions, he does not propose a similar reaction mechanism for the reaction of the carbon source. Ito, however, explicitly describes K_2SO_4 as a crucial reactant. During this second oxidation phase, the temperature of the dross ball rises to about 940 °C.[2,8] At this temperature however, potassium sulfate is still solid (melting point 1069 °C). This would plead against a major role for K_2SO_4 in this phase. Further research will hopefully shed more light on the relative importance of melt temperature and potassium sulfate concentration.

On the pictures that were made during this phase, the light trails of the sparks exhibit a peculiar tube-in-tube appearance. This will be discussed more in detail in phase 6.

(4) Rebirth, 'umarekawari' (4–5 seconds)

The second composition is consumed by the reacting droplet and no more sparks are generated.

A difficult point in creating an effective composition for a senko hanabi sparkler is the charcoal/soot ratio. Charcoal is needed for its reactivity in the polysulfide reaction. Soot on the other hand gives the largest and most beautiful sparks. There exists an optimal ratio that Shimizu experimentally defined to be 4 : 1 for a Paulownia charcoal : anthracene soot composition.[6] This ratio is the best compromise between reactivity and aesthetics. However, this article introduces a new production method that splits the total amount of composition (typically 85 mg) into two separate and sequential compositions: the first one only contains charcoal, the second one only soot. The

Figure 6. *A horizontal >40 cm spark.*

soot composition is put at a short distance from the charcoal composition, so that the latter reacts first. What happens now is that the soot composition is consumed at the moment the first polysulfide drop is in phase 2 or 3. This way, the less reactive soot composition is given a boost by the vigorous charcoal melt. By carefully choosing the spacing between compositions and the way the sparkler is rolled, one can define the moment at which the soot composition is reached by the ascending fireball. The combined polysulfide melt then uses the soot as the spark-forming carbon source. The sparks that are generated this way are far larger and more beautiful than sparks generated by a mixed carbon-source composition. To illustrate this, I refer to Shimizu's 'studies on senko hanabi',[6] where his optimal composition emitted sparks a little more than 12 cm in length. Nakaya and Sekiguti say their sparks travel 10 cm.[8] By splitting the composition, the author succeeds in creating sparklers that throw out sparks 15–40 cm in length, even horizontally (Figure 6).

Another benefit of using this split composition technique is that it brings diversity to the spark effects of a senko hanabi sparkler. The sparks typical for the type of charcoal used as well as those typical for the type of soot are emitted separately. I named the effect 'umarekawari', Japanese for rebirth. Because spectators appreciate this effect and because it also makes the integration of pure magnesium possible (see below, 'satori' effect), the author now produces all senko hanabi sparklers this way.

The optimal formulation for a single-composition sparkler (50/35/15) seems to lend itself very well for split composition sparklers as well. However, further experimentation may even generate better formulations that take into account that the first composition already lived through some phases.

(5) Second infancy (2–3 seconds)

The combined melt continues to boil and sizzle (Figure 2).

Analogous to the first infancy, the dross ball boils and sizzles. This phase is a little bit shorter than the first, because the temperature of the combined melt is already higher from the start.

(6) The second phase where sparks are generated

Analogous to the first spark phase, one can distinguish two sub-phases:

(6a) Second youth (8–11 seconds)

Sparks shoot approximately 20 cm away and explode into large fire pompoms. The effect

Figure 7. *Second youth.*

Figure 8. *Second middle age.*

Figure 9. *Tube-in-tube appearance of light trails.*

produces more of a gushing sound (Figure 7).

(6b) Second middle age (9–10 seconds):

Shorter sparks with smaller pompoms are ejected at a higher frequency (Figure 8).

In this phase, the sparks shoot much farther away from the melt (on average 20 cm in the youth phase, occasionally up to 40 cm) and explode to give much bigger 'fire pompoms' than the charcoal sparks. They also make more of a 'rustling' sound where the charcoal sparks tended to produce small 'puffs'. Upon analysing pictures taken from this phase, it is seen that the sparks share their anatomy with the charcoal sparks: their light trail also has a

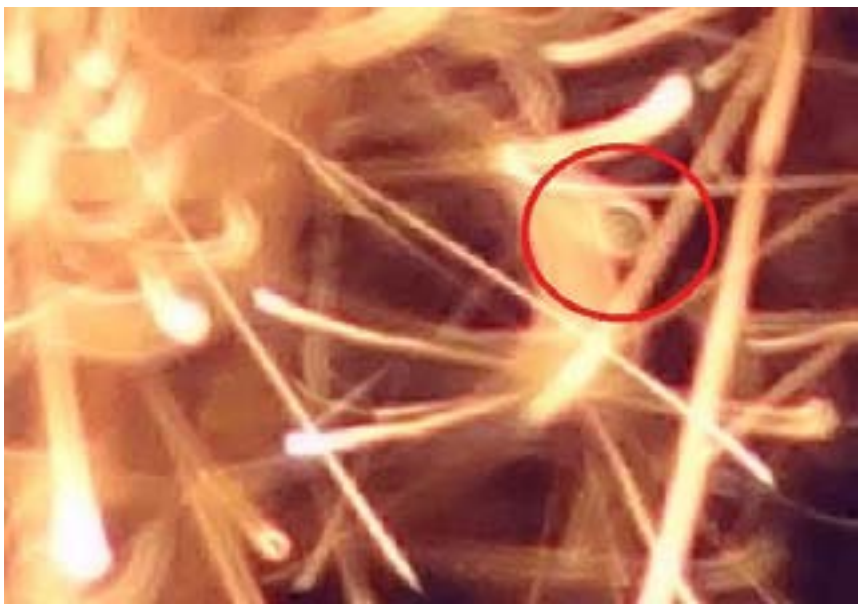

Figure 10. *Dot-in-tube-in-tube appearance of a light trail.*

tube-in-tube appearance (Figures 9 and 10).

So the type of carbon used does not seem to alter the microscopic structure of the senko hanabi sparks. A possible explanation for their different macroscopic appearance might be that soot has the ability to lower the viscosity of the polysulfide melt.[3,7] This would make the evolved gases move more freely and possibly eject the polysulfide fragment further away. The lower reactivity of soot compositions may in turn explain why these fragments can travel further before exploding themselves into pompoms. In summary, the type of carbon used changes the physical properties of the melt which in turn determines the appearance of the sparks. The explanation for the tube-in-tube form of the light trails may be found in theories of fluid dynamics. At first glance, there are striking similarities with the trail of what is called a 'toroidal vortex'. Perhaps the sudden release of gases under the surface of the polysulfide melt makes 'rings' of melt shoot away. More specific research can hopefully shed more light on this in the future.

(7) Old age (8–20 seconds)

The droplet gets smaller and silently, long streaky sparks are ejected (Figure 12).

In this phase the drop, which has shrunken substantially, loses its vivacity. The shape of the sparks changes: now they draw long narrow lines in the air. No sound is emitted any more. The temperature of the melt drops to 850 °C.[2,8]

(8) Metal glitter phase, 'satori' (fractions of a second)

One or more crackling flashes are observed and ejected melt material explodes at a distance. The magnesium sparks have a peculiar corkscrew appearance. The flashes are occasionally accompanied by a metallic whipping sound (Figure 13).

During the 'old age' phase, one or more crackling flashes are suddenly observed. There are little drops of polysulfide melt ejected from the mother drop that explode themselves into more sparks. Also, from the micro-droplets as well as from the mother drop, sparks are emitted that have a typical corkscrew appearance. This reaction does not interfere with the traditional effects and adds diversity to the sparkler. It even adds an element

Figure 11. *Tube-in-tube appearance of light trails.*

Figure 12. *Old age.*

of excitement during the burn and it makes for a spectacular finish. Because it is frequently absent in still air but always present in the slightest breeze, it seems to adapt itself to the setting.

In this phase the magnesium reacts. Until now it has been present in the melt as liquid drops (melting point 600 °C) covered by a layer of polysulfide melt that shields it from atmospheric oxygen.

Analogous to Shimizu's proposed flash reaction of aluminium,[10] we could write the satori reaction as:

$K_2S_2 + Mg \rightarrow K_2S + MgS$

Or, in accordance with Oglesby's theory,[5] this would be:

$K_2SO_4 + 4\ Mg \rightarrow K_2S + 4\ MgO$

Even though no gases are evolved, the sparks are fiercely blown away. This might be caused by the extreme heat evolved by the oxidation of the magnesium. The spritzel heats up and the remaining carbon is oxidised to produce carbon dioxide which divides the mother drop and propels fragments away. If at this stage, the droplet falls to the ground, a single explosive flash is seen which generates a perfect smoke ring in the air. This might be caused by the instantaneous division and thereby flash heating of the total mass of melt. The same effect is observed when one shoots the drop from the string with one's finger. Also, if the air flow is suddenly increased just after the rebirth phase, satori flashes can be provoked. On the other hand, in still air the satori phase often does not appear, even though the sparkler goes through all stages of its life, all the time building up potassium sulfate. These observations indicate that temperature rise, more than a critical build-up of potassium sulfate, seems to be the necessary factor for initiating the flash reaction, much like Shimizu stated for classic glitter effects: "when small particles of molten residue pass through the air, they increase in temperature while being oxidized by atmospheric oxygen. If they achieve a sufficiently high temperature, then blooms are produced".[4] Another theoretical objection to the potassium sulfate theory is that it would still be solid at the temperatures that were measured on the surface of a reacting senko hanabi droplet. However, it might be that sudden local heating liquefies the potassium sulfate and starts the reaction. Further research measuring surface temperatures at the moment of the satori effect may prove useful in clarifying this point. As a side note, these experiments do show that a true glitter effect is possible by only using potassium nitrate, sulfur, charcoal and metal.[4]

If pure magnesium powder is burned in a Bunsen flame, a typical corkscrew appearance of the sparks is observed (Figure 14).

The corkscrew sparks ejected from the melt are larger but have the same appearance (Figures 15 and 16). This observation is concordant with theories that postulate that the metal itself is the fuel for the reaction, and not some reaction product.[4] The sparks are sometimes bright white, other times orange. Other sparks start off as white–yellow corkscrews and then explode

Figure 13. *Enlightenment – satori.*

themselves into a very bright white corkscrew and a few straight orange sparks. It thus seems that even droplets containing both magnesium and polysulfide melt are capable of spiraling away from the droplet. Like the peculiar shape of the charcoal and soot sparks, these spiral sparks show similarities with the appearance of what is in fluid mechanics called a positively buoyant jet.

Pure magnesium powder also gives off a typical sound while burning freely, kind of like a very high 'zing'. This sound is sometimes heard in the course of a satori reaction but then it sounds more like a metallic whip.

The experiments have shown that only magnesium is reactive enough to cause a glitter effect in windspeeds that senko hanabi sparklers can be fired in. Until now, the integration of pure magnesium in glitter formulations was thought to be impossible, because it immediately reacts away in the birth phase.[4,5] Indeed, this also seems true if magnesium is added to a composition that contains charcoal or mixed carbon sources (charcoal/soot). However, now that the total amount of composition is split according to the type of carbon, magnesium can selectively be added to the soot composition. Because soot lowers the reaction temperature,[3] the magnesium is allowed to integrate into the melt without reacting. From the experiments it is seen that this is the case even if a hotter-burning charcoal composition follows the soot composition. This can be explained by the fact that the magnesium is protected from the fresh reactants and the atmospheric oxygen by a layer of soot melt. Whether this protective effect of soot would also apply in stars and fountains has yet to be tested. In these devices, wind speeds are of course much higher.

The current experiments show that the satori effect consequently comes behind the spark phase of the

Figure 14. *Magnesium powder in Bunsen flame.*

carbon source. Between these two phenomena, the temperature of the polysulfide melt drops from 940 °C to 850 °C.[2,8] A few explanations for the higher reactivity of carbon are possible. Carbon could be more reactive because of the special ability of potassium to separate its layers. Or carbon reacts using another reactant than magnesium (K_2S_n *vs.* K_2SO_4) or needs a lower concentration of potassium sulfate to react. However, the critical role of potassium sulfate was already questioned in a previous paragraph. Another explanation could be that when the polysulfide drop gets smaller, the chance of magnesium metal touching the outer surface of the drop gets bigger. This theory is supported by the observation that the quantity of magnesium added determines the nature of the satori effect. The addition of just a few specks of magnesium makes the fireball give off separate sparks that after a short distance explode themselves. This reaction tends to happen in the old age phase and perfectly lends itself for integration in a finished sparkler. When more magnesium is added however, the satori phase tends to start earlier and the polysulfide drop reacts totally, more like a classic glitter flash in stars or fountains. Jennings-White also showed that the delay of the flash reaction in classic glitter

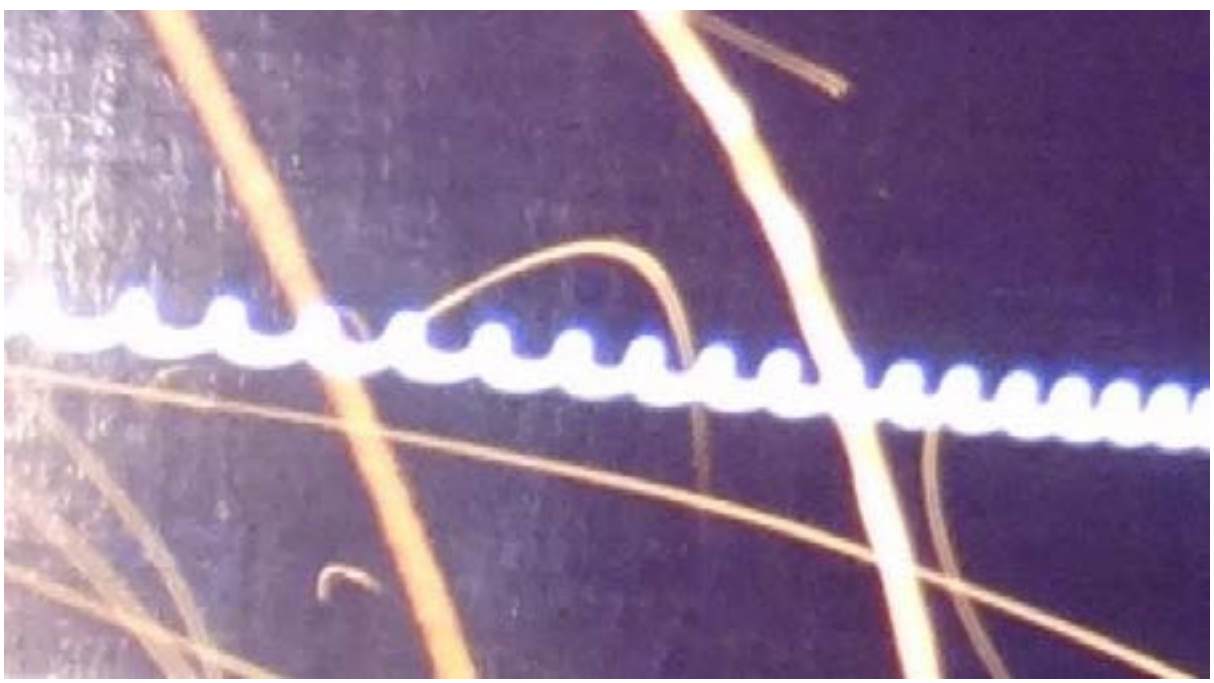

Figure 15. *Corkscrew appearance of satori spark.*

Figure 16. *'Sinusoidal' satori spark.*

formulations is shortened by the addition of more metal.[4]

Because a reacting senko hanabi sparkler containing magnesium can be seen as a stationary 'spritzel', experiments were done to see if flash coloration is possible by using pure magnesium. Although some authors claim to have made non-yellow colored glitter using salts such as strontium nitrate, strontium carbonate, strontium oxalate and lithium salts, these findings could not be reproduced by Jennings-White who studied the subject extensively.[4] The results from the current experiments with a soot based and therefore sodium-free senko hanabi formulation with pure magnesium as the metal show identical results. Pure magnesium gives a bright white flash. Addition of just a little sodium bicarbonate colors the flash vividly yellow and doesn't influence the spark generation too much. Lithium carbonate, strontium carbonate, strontium oxalate and strontium nitrate do not significantly color the flash. Strontium oxalate perhaps gives off a slightly pinkish light but in live sparklers, the flash is observed as being white[1] (Figure 17). These salts also dramatically change the polysulfide chemistry so that the spark effects are ruined. Therefore they seem useless in senko hanabi formulations.

Interestingly, the addition of sodium bicarbonate to a senko hanabi formulation with added magnesium makes the magnesium much more reactive. Classic spark effects are absent, and even in still air, the magnesium very quickly reacts to produce yellow flashes. This observation further questions the role of a critical potassium sulfate concentration to be reached before the flash reaction can occur. Seemingly, the protective nature of the polysulfide melt can be influenced and this makes the metal react easier. This might also explain the role of sodium bicarbonate as a glitter enhancer in classic glitter compositions.

Conclusion

The senko hanabi sparkler was found to be a very useful tool to study glitter phenomena. It was shown that current theoretical frameworks are incapable of explaining all observations. New

Figure 17. *Indirect light from satori flashes with added salts.*

elements were added to the discussion about the role of critical temperature and potassium sulfate concentration on the glitter flash. Also, the role of sodium bicarbonate as glitter enhancer and coloring agent was demonstrated in the senko hanabi sparkler.

The remarkable microscopic appearance of classic senko hanabi sparks was documented and raises further questions about the nature of the polysulfide melt and the mechanism of spark generation.

The possibilities for further research are many. Other salts might be introduced into the composition, influencing melt properties and flash coloration. Different sources of carbon may be tested for their spark-forming abilities. Also, the specific properties of soot in senko hanabi glitter phenomena might prove useful in larger pyrotechnic devices.

Acknowledgements

I would like to thank my wife for being extraordinary patient and supportive while the research and writing of this article was being conducted. Also I would like to thank my close friends for helping me with the translation of this document. Thirdly, I would like to thank this journal for giving me the opportunity to share my work and knowledge with fellow pyrotechnicians.

References

All pictures were taken by the author except Figure 14, 'Magnesium powder in Bunsen flame', which was taken by Ken Kohl.

1 F. Van Der Sypt, 'Senko hanabi: a study of factors affecting construction and performance', *Journal of Pyrotechnics*, Issue 32, 2013, preceding paper.

2 T. Shimizu, *Fireworks, the Art, Science and Technique*, Pyrotechnica Publications, 1981.

3 H. Ito, 'The mechanism of spark generation from Japanese Toy Firework', *Kagaku to Kyoiku* (Chemical Society of Japan), Vol. 39, Issue 6, 1991, p. 682.

4 C. Jennings-White, 'Glitter Chemistry', *Journal of Pyrotechnics*, Issue 8, Winter 1998, p. 53.

5 L. S. Oglesby, *Glitter, The Chemistry and Techniques*, 2nd edn, American Fireworks News.

6 T. Shimizu, 'Studies on Senko Hanabi', *5th international symposium on fireworks*, 2000.

7 H. Ito, 'Simple Preparation of Japanese Toy Firework', *Kagaku to Kyoiku* (Chemical Society of Japan), Vol. 39, Issue 2, 1991, p. 130.

8 U. Nakaya and Y. Sekiguti, 'A physical investigation on sparks of senko hanabi, a miniature firework', Institute of Physical and Chemical Research, Tokyo, 1927.

9 T. Hashimoto and H. Kobayashi, 'Progress of Balloon-based Micro-gravity Experiment System', *ISTS*, 2008, 60th International Astronautical Congress, Daejeon, 2009.

10 T. Shimizu, "Investigation of the Pyrotechnic Glitter Phenomenon, Parts (I) and (II)", *Pyrotechnica* XIV, 1992.

Assessment of Explosives in Squibs

Lutz Kurth,* Holger Krebs, Benjamin Theil, Olaf Mücke, Christian Lohrer

Federal Institute for Materials Research and Testing (BAM) - Unter den Eichen 87, 12205 Berlin, Germany.
Email: lutz.kurth@bam.de

Abstract: *Experiments in this study reveal that the initiating capability of commonly used squibs is not high enough to initiate PETN in all cases. The fulfilment of the 'new' essential safety requirement 4 as set out in the European directive 2013/29/EU and the categorization of squibs as theatrical pyrotechnic articles (T2) can therefore be justified, as the explosive investigated belongs to quite a sensitive type (initiation with low impulse energies possible). Underwater initiating capability tests according to EN 13763-15 led to meaningful results, showing that squibs are usually unable to initiate a secondary explosive. For a general assessment of the initiating capability of squibs and comparable (theatrical) pyrotechnic articles a threshold range of an equivalent initiation capability in grams of PETN on the basis of the performed underwater initiating capability tests was determined. It was found that squibs are generally not capable of initiating secondary explosives if the underwater initiating capability test showed an equivalent initiation capability below 0.25 g PETN. As a consequence of this result, the underwater initiating capability test gives an effective and safer alternative to the experimental confirmation of the 'new' ESR 4 by direct contact of the article with the secondary explosive and should then be preferred to it.*

Keywords: *Squibs, ESR 4, PETN, underwater initiating capability, EN 13763-15*

Introduction and background

The essential safety requirement (ESR) number 4 of the current European Directive 2007/23/EC[1] on the placing on the market of pyrotechnic articles requires the absence of all commercial blasting explosives (except for black powder or flash composition) and military explosives in pyrotechnic articles. However, some existing articles have contained commercial blasting explosives for many years now and where approved by the Member States on a national basis. Well known examples of these types are airbags and squibs to mimic bullet impacts for theatrical or television purposes. The recast of the above mentioned European Directive (2013/29/EU[2]) acknowledges this issue by changing the relevant ESR 4 to the following formulation:

'Pyrotechnic articles must not contain detonative explosives other than black powder and flash composition, except for pyrotechnic articles of categories P1, P2, T2 and fireworks of category F4 meeting the following conditions:

(a) the detonative explosive cannot be easily extracted from the pyrotechnic article;

(b) for category P1, the pyrotechnic article cannot function in a detonative manner, or cannot, as designed and manufactured, initiate secondary explosives;

(c) for categories F4, T2 and P2, the pyrotechnic article is designed and intended not to function in a detonative manner, or, if designed to detonate, it cannot as designed and manufactured initiate secondary explosives.'

Following this approach, an experimental proof of the non-initiation of secondary explosives is mandatory if the pyrotechnic article is designed and manufactured to detonate. An official harmonized

Article Details	***Article No: - 0100***
Manuscript Received:- 01/08/2013	***Final Revisions:-28/08/2013***
Publication Date:- 09/11/2013	***Archive Reference:-1619***

test method for this investigation currently does not exist.

The main aim of this work was to investigate whether common squibs as theatrical pyrotechnic articles would generally fulfil the new 'ESR 4' for the European Directive (2013/29/EU[2]) as stated above.

For the investigations of this work common squibs available on the German market (under the national approval system valid until 2017) were used, as a comparable impact with regard to detonators for explosives was expected. Squibs were chosen as an appropriate representative of pyrotechnic articles where an initiation of secondary explosives cannot be excluded.

Reasons for the direct comparison of squibs with detonators were mainly twofold:

- Squibs contain comparable explosive substances to detonators, and
- Approved test methods for detonators exist for the determination of their performance characteristics.

The squibs of different intensities used in this study (manufacturer Josef Köhler Pyrotechnik; including the net explosive contents [NEC]) are listed in Table 1.

The reference detonators for explosives used for comparison (manufacturer Austin Detonator) are given in Table 2.

Table 1. *Squibs used in this study.*

Type of squib		NEC/g
Squib (Bullet hit)	'HE 1'	0.078
Squib (Bullet hit)	'HE 4'	0.302
Squib free of heavy metals	'Cl-1/4G'	0.008
Squib free of heavy metals	'Cl-1/2G'	0.018
Squib free of heavy metals	'Cl-1G'	0.028
Squib free of heavy metals	'Cl-2G'	0.060
Squib free of heavy metals	'Cl-6G'	0.205
Squib free of heavy metals	'FL-1/8G'	0.006
Squib free of heavy metals	'FL-1/4G'	0.010
Squib free of heavy metals	'FL-1/2G'	0.020
Squib free of heavy metals	'FL1G'	0.028
Squib free of heavy metals	'FL-2G'	0.060

Table 2. *Reference detonators used.*

Copper REF DET 1	0.25 g PETN
Copper REF DET 3	0.60 g PETN

Experiments – comparison of shock energies and maximum pressures of squibs and detonators for explosives

The underwater initiating capability test according to EN 13763-15[3] was applied for the determination of the shock energies and maximum pressures. For every type of squib 3 items and for every reference detonator 5 items were used for reproducibility. The pressure time dependencies were detected with the piezoelectric sensor PCB-W138A05.

This test is based on the principle that the detonation of an explosive charge under water generates a spherical shock-wave and a volume of gas, which expands and then collapses as the bubble rises through the water. The shock-wave and the volume of gas bear a finite relationship to the energy released. By measuring the shock-wave pressure and the time interval between the shock-wave pressure peak and the first collapse of the gas bubble, the equivalent shock and bubble energies can be calculated.[3] Both parameters were determined for the investigated squibs and reference detonators and compared against each other.

The experimental setup in accordance with EN 13763-15[3] is illustrated in Figure 1.

The water tank made of hard plastic had a volume of about 1.4 m^3 with the following dimensions: height 1.2 m, width 1 m, depth 1.16 m.

A typical pressure time dependency including the collapse of the gas bubble is given in Figure 2.

The area in grey is the integral of the shock-wave with the pressure maximum (P_{max}) and $t = t(P_{max}/e)$, where t_b is the time interval from P_{max} to the collapse of the gas bubble.

The following definitions for the equivalent shock and bubble apply (formulas 1 and 2):

Equivalent shock energy

$$E_s = k_s \int_{t=0}^{t=t\left(\frac{P_{max}}{e}\right)} P^2 \mathrm{d}t \qquad (1)$$

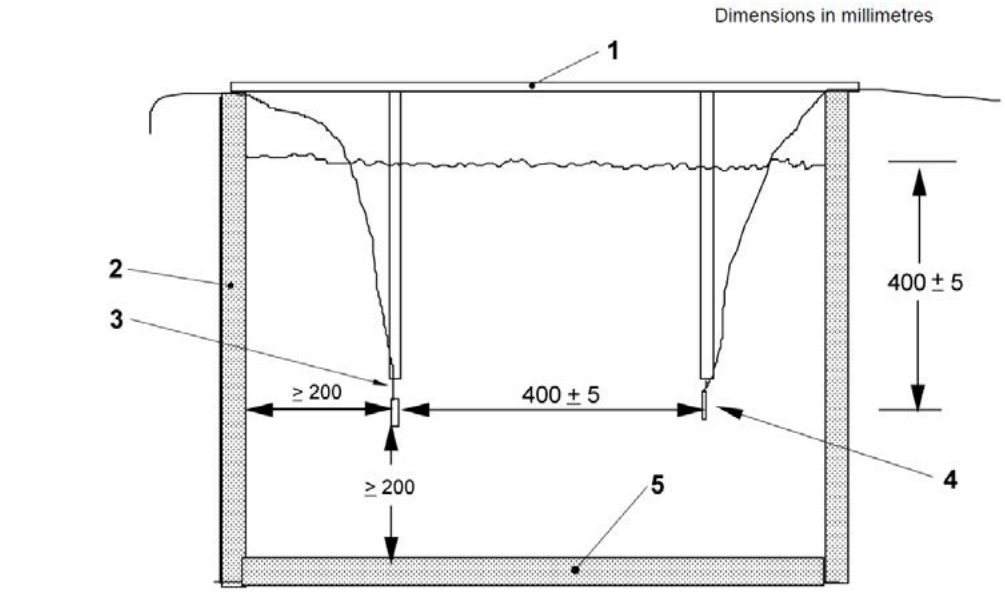

Key

1 Positioning arrangement
2 Water tank
3 Detonator
4 Pressure sensor
5 Non-reflecting, energy-absorbing material

Figure 1. *Scheme of the water tank used with positioning system for sensor and detonator/squib (source: EN 13763-15[3]).*

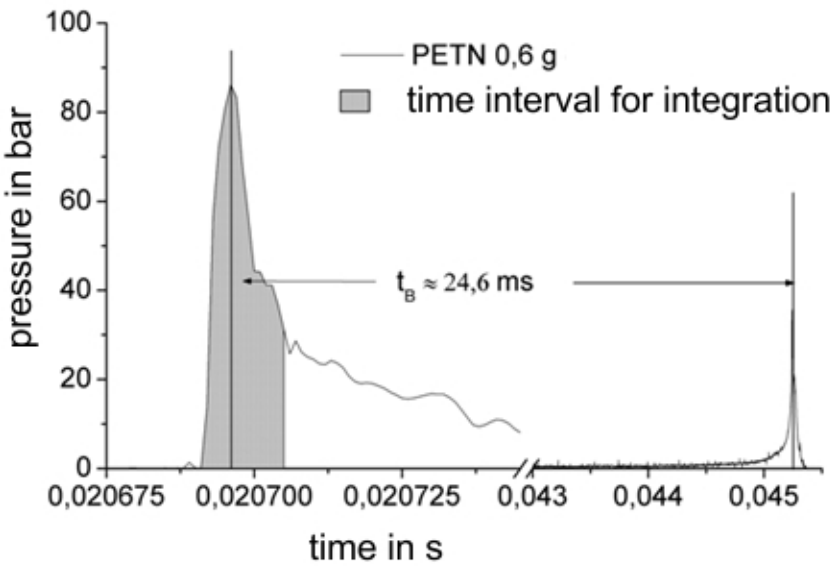

Figure 2. *Typical pressure–time dependence during the underwater initiating capability tests according*

where E_S = shock energy, P = pressure, t = time, e = Euler number, k_s = constant.

Equivalent bubble energy

$$E_B = k_B(t_B)^3 \qquad (2)$$

where E_B = bubble energy, t_B = time interval from P_{max} to the collapse of the gas bubble, k_B = constant.

Results and discussion

The results of the calculated shock energies of the investigated squibs based on the performed pressure time tests are displayed in Figure 3.

All displayed data are averaged values, based on 3 measurements per squib type. The maximum shock energy displayed in Figure 3 was calculated by integration below the pressure curve from the beginning until the culmination of zero over-pressure.

The results reveal that only the squib type 'HE 4' developed comparable shock energies to the reference detonator '0.25 PETN'. All other squibs showed significantly smaller shock energies. The levels of the shock energies thereby correlate with the NECs of the squibs.

The corresponding maximum pressure values are illustrated in Figure 4.

The averaged values of the maximum pressures observed for the squibs were in all cases smaller than the values for the detonators. As for the shock energies, the squib type 'HE 4' was found to have the highest maximum pressure, followed by 'Cl-6G' and 'HE 1'. The differences between the maximum pressures of the squibs and the reference detonators were not as distinct as with the observed shock energies.

The assessment of the bubble energies was abandoned, as the results revealed that no significant comparison between the squibs and the reference detonators with regard to the initiation

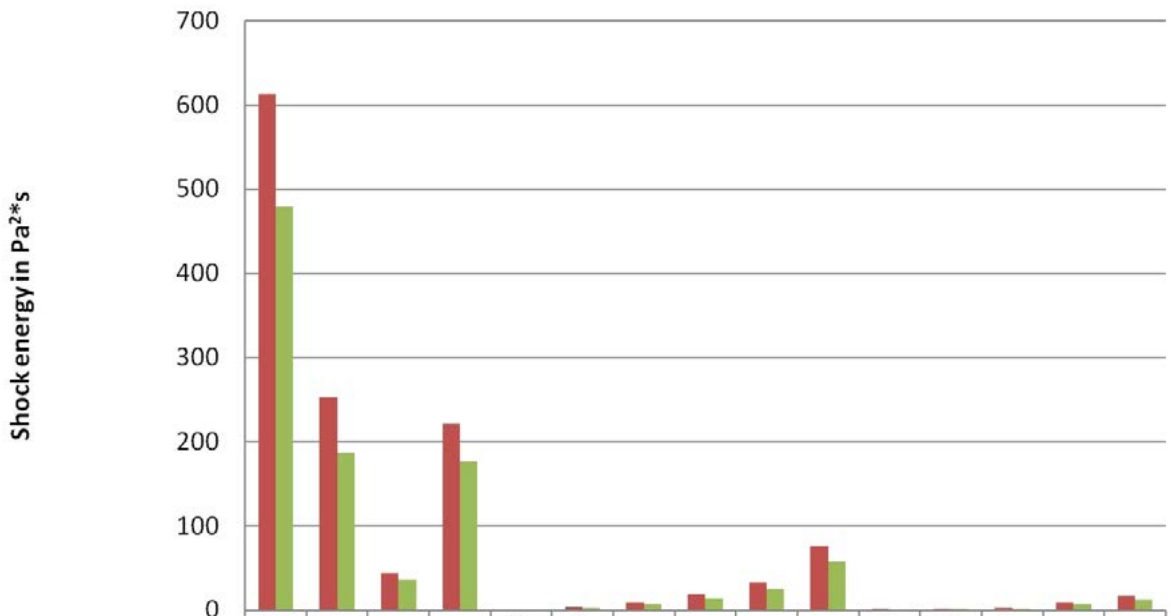

	PETN o,6	PETN 0,25	HE 1	HE 4	Cl-1/4 G	Cl-1/2 G	Cl-1 G	Cl-2 G	Cl-3 G	Cl-6 G	Fl-1/8 G	Fl-1/4 G	Fl-1/2 G	Fl-1 G	Fl-2 G
Shock energy max	613	253	44	222	1	3,8	10	18,8	33	76	1,8	2,2	3,4	10	17
Shock energy	479	187	36	176	0,8	2,9	7,6	14,3	25,5	58	1,4	1,6	2,4	7,5	13

Figure 3. *Shock energies of the investigated squibs and the two reference detonators.*

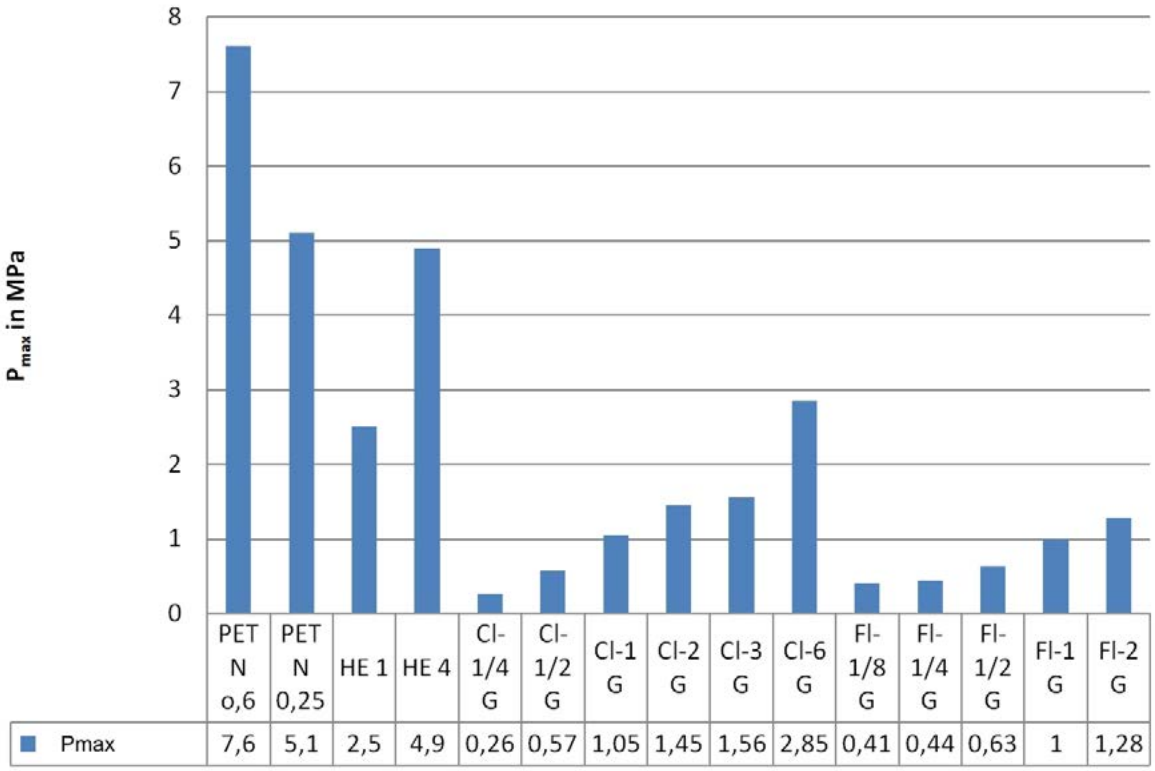

Figure 4. *Maximum pressures of the squibs investigated and the two reference detonators.*

capability was possible.

Figure 5 and Figure 6 illustrate exemplary time–pressure dependences for the reference detonators and some investigate squibs.

The influence of casing material on the detonation characteristics was not further investigated due to the insignificant impact during the underwater initiating capability tests based on the experiences of BAM.

In order to find a better comparison between the investigated squibs and the reference detonators a specific scaling was performed. This scaling reveals for different explosives the required equivalent initiation capability in grams PETN. The shock-wave parameters peak pressure and energy were taken as the basis for characterization, as the initiation is purely due to shock–detonation transition (SDT) in this case.

In direct comparison of the investigated squibs and the reference detonators only the squib 'HE 4' revealed a comparable outcome with the reference detonator 0.25 g PETN. All other investigated squibs showed a significantly lower energy level during the underwater test. Due to this finding, the detonator 0.25 g PETN was chosen for reference in this work. The combination of this reference detonator and the sensitive explosive corresponds to a worst-case-assessment with regard to the capability of initiating secondary explosives.

The calculation of the equivalent initiation capability of the squibs was performed with the following formulas 3 and 4:

$$\frac{p_T}{p_R} \approx \left(\frac{M_T^{1/3}}{M_R^{1/3}} \right)^{1,2} \qquad (3)$$

$$\frac{E_T}{E_R} \approx \frac{M_T}{M_R} \qquad (4)$$

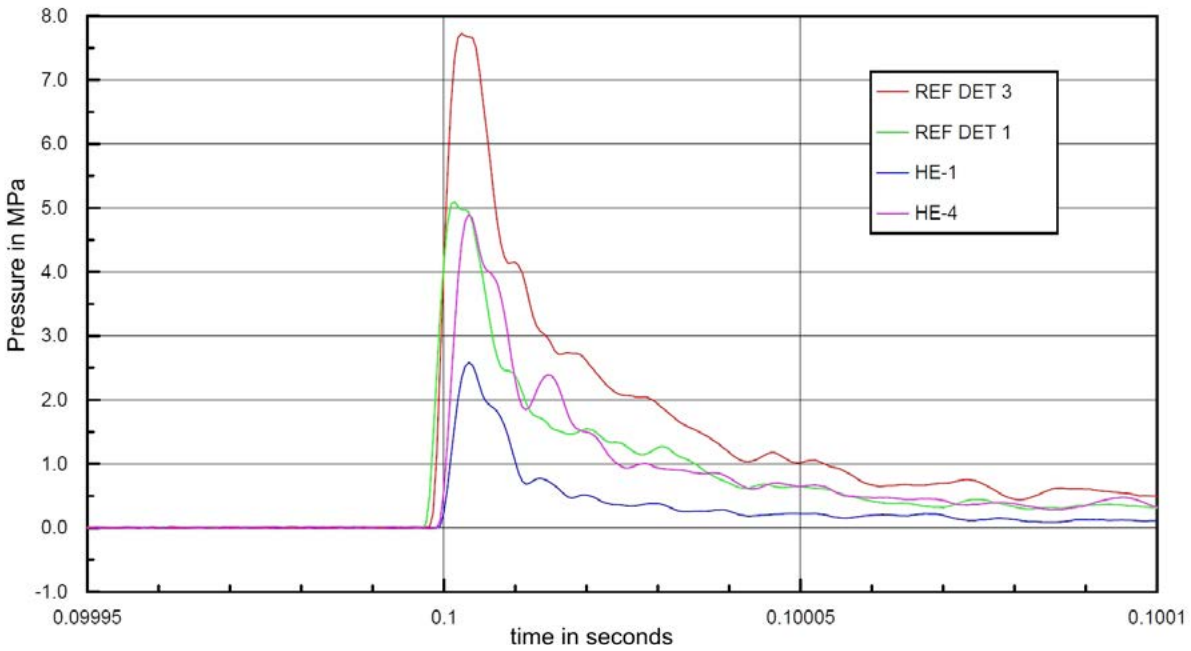

Figure 5. *Time–pressure curves of the investigated squibs 'HE 1' and 'HE 4'and the two reference detonators.*

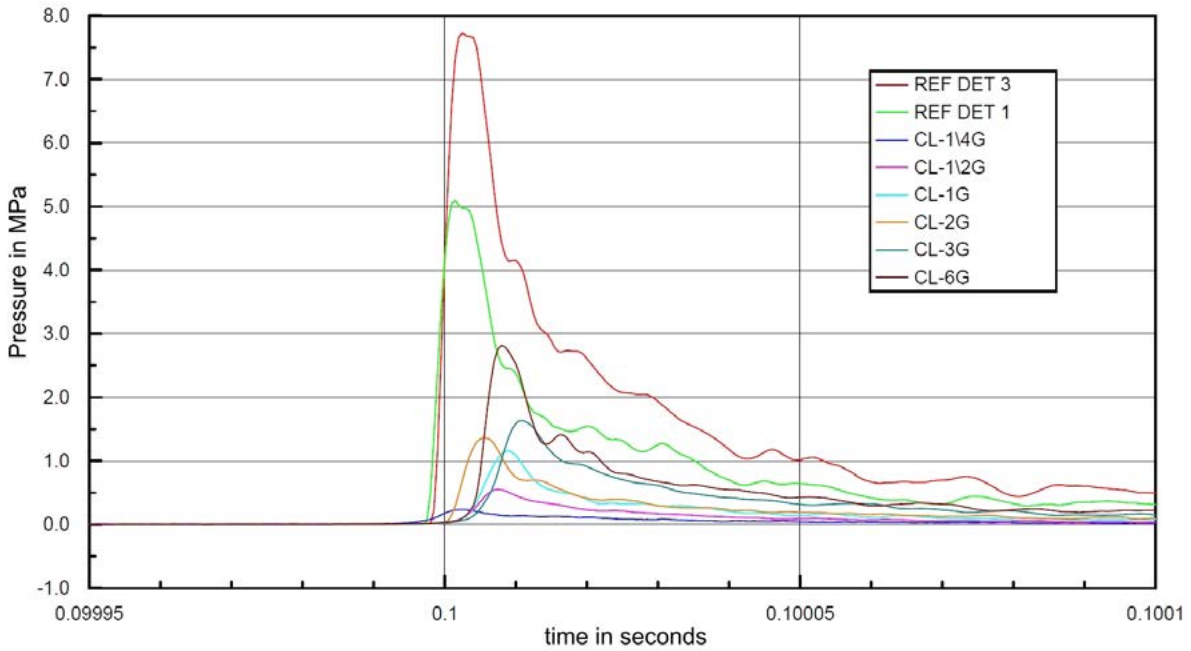

Figure 6. *Time pressure curves of the investigated squibs 'Cl series' and the two reference detonators.*

with the following definitions: p – pressure; M – mass of charge; E – energy of shock wave; T – subscript indicating test; R – subscript indicating reference.

For formula 3 the maximum pressure and for formula 4 the shock energy were taken as the basis for the calculation of the equivalent initiation capability. For the squib 'HE 4', the following values were achieved:

0.20 g PETN on the basis of the maximum pressure (see formula 3);

0.24 g PETN on the basis of the shock energy (see formula 4).

The squib 'Cl-6G' showed the second largest equivalent initiation capability:

0.14 g PETN on the basis of the maximum pressure (see formula 3);

0.08 g PETN on the basis of the shock energy (see formula 4).

The lower value of equivalent initiation capability on the basis of the shock energy in comparison with the reference detonator is due to the slower pressure rise and the lower maximum pressure, see Figure 6.

Since the other squibs showed much lower equivalent initiation capabilities, an initiation of the secondary explosive with direct contact was therefore not performed. Only the squib 'HE 4' with its high equivalent initiation capability led to the assumption that an initiation of sensitive explosives is likely. However, the results of the underwater test of the squib 'Cl-6G' were also taken into account for verification purposes.

Initiation of secondary explosives with squibs

For verification of the results of the underwater tests, initiation tests with direct contact of the squibs with the explosive NSP 711 (plastic) were carried out. This secondary explosive is made on the basis of PETN, is cap sensitive, water-resistant and has a density of 1.45 g cm^{-3} and a detonation velocity (VOD) of greater than 7.250 m s^{-1}.

Experiments with the squib 'HE 4'

An NSP 711 explosive charge of 260 g in total was formed, which was *ca*. 50 cm long, *ca*. 3 cm wide and *ca*. 2 cm high. A resistance sensor (500 ohm m^{-1}) with a length of 0.3 m coming from the side of the ignition point was placed in the centre of the cross-section of the explosive charge. The resistance sensor measures the VOD and was additionally taken to prove that initiation occurred. The run up distance between the bottom of the squib 'HE 4' and the starting point of the VOD measurement was more than 5 times the charge width. The squib 'HE 4' was treated as a strong detonator and was placed cross-sectionally centred into the end of the charge.

As a result of this setup, the squib 'HE 4' functioned properly based on aural observation. However, an initiation of the NSP 711 charge did not occur. After that the charred end of the charge was carefully removed and a detonator 0.25 g PETN was installed in a comparable way into the charge NSP 711. The detonator functioned properly, leading to an initiation of the NSP 711 charge. No further remnants of the explosives remained afterwards and the resistance sensor was completely destroyed.

Since the first experiment did not show an initiation of the NSP 711 charge with the squib 'HE 4', the setup was changed. A charge of 25 g NSP 711 was formed into a 'pear-like' shape and the 'HE 4' was primed into the longish end of this charge, see Figure 7.

For the sake of minimizing the experimental efforts (i.e. finding of explosives in case of non-initiation), the entire charge including the squib was placed in a thick-walled plastic tube. This tube was buried in the ground, see also Figure 7. The charge was placed at the bottom of the tube on the soil with no contact with the wall.

The first trial in this setup revealed also a complete functioning of the squib 'HE 4' without an initiation of the 'pear-shaped' NSP 711 charge. One third of the explosive charge was dispersed, whereas the other two thirds were found flattened at the bottom of the tube. However, the repetition trial of this setup showed with all likelihood an initiation of the 'pear-shaped' NSP 711 charge. The significantly different aural observation revealed a corresponding reaction. The observed damage also showed signs of at least an initiation of NSP 711. The plastic tube extensively ruptured from the bottom to the top and was found displaced at one side of the soil ground, see Figure 8. The

Figure 7. *Setup of the 'pear-shaped' charge NSP 711.*

Figure 8. *Ruptured plastic tube as a result of the second trial with the combination of squib 'HE 4' and the 'pear-shaped' NSP 711 charge.*

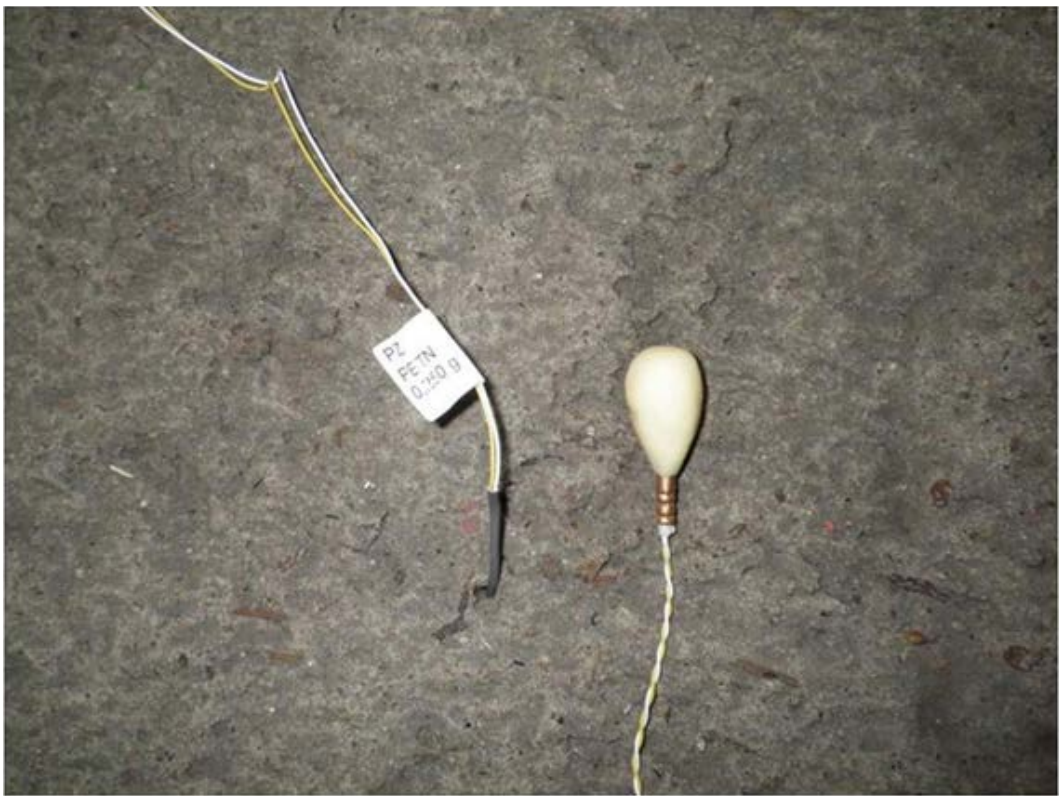

Figure 9. *Proof of the cap sensitivity of the NSP 711 charge with the detonator 0.25 g PETN.*

fragments of the plastic tube and the observations imply that the reaction occurred as a deflagration.

Experiments with the squib 'Cl-6G'

The setup with the squib 'Cl-6G' was identical to the ones with the combination 'HE 4' and 'pear-shaped' NSP 711 charge, as described above. The only difference in the setup occurred in the first out of four trials, where the reference detonator 0.25 g PETN and the explosive charge were not introduced into the plastic tube, as an initiation of the charge was likely to occur. The NSP 711 charge including the detonator was directly placed on the soil ground, see Figure 9. The charge was initiated by the detonator in the first trial as expected.

The other three trials with the squib 'Cl-6G' showed no initiation of the NSP 711 charges in any of the cases. The squibs functioned properly, which was acoustically observed. Almost the entire masses of the NSP 711 charges were always found on the bottom of the plastic tube, in some cases partly dispersed. The thick-walled plastic tube was found completely intact and it remained in its initial position.

Summary and conclusions

The results of this study reveal that the squibs investigated were not able to reliably initiate a plastic explosive on the basis of PETN. The combination of this reference detonator and the sensitive explosives corresponds to a worst-case assessment with regard to the capability of initiating secondary explosives.

The categorization of the squibs as theatrical pyrotechnic articles of the category T2 under the European Directive 2007/23/EC can be justified based on the results of this study. The new requirements according to the recast of this Directive (2013/29/EU; essential safety requirements no. 4) can be seen as fulfilled for the tested articles.

It was furthermore proved that the underwater test according to EN 13763-15 reveals meaningful results in order to demonstrate that squibs and comparable pyrotechnics are generally not able to initiate secondary explosives. The performance parameters of these pyrotechnics achieved from these tests allow a direct comparison with common detonators for explosives.

For a general assessment of the initiation capability of squibs an equivalent initiation capability in grams of PETN in connection with the underwater tests was determined. The results of the experiments with direct contact of the squibs on the secondary explosives confirm the assessments of the results of the underwater tests in the context of the definition of a threshold range for the equivalent initiation capability of squibs. As a conclusion it appears to be possible to substitute the initiation test by the underwater tests in combination with the calculation of an equivalent initiation capability.

It appears to be sensible that these findings and conclusions can also be applied to other comparable pyrotechnic articles.

Therefore, squibs and other comparable pyrotechnic articles are not able to initiate secondary explosives, if the equivalent initiation capability determined from the underwater test is less than 0.25 g PETN.

For the assessment of the capability of initiating a secondary explosive, the equivalent initiation capabilities of both the maximum pressure based and the shock energy based values should be taken into account. This appears to be particularly important in those cases where the equivalent initiation capability is greater than 0.2 g PETN. For those cases where the equivalent initiation capability is smaller than 0.2 g PETN (based on shock energy values), an initiation of secondary explosives by the pyrotechnic article is not expected.

The results achieved reveal that in most cases a setup with direct contact of the article with the secondary explosive can be avoided. In consequence, the problems associated with the performance of such experiments (e.g. finding of unexploded substances) do not occur.

Finally, it should be noted that the chosen configuration and setup of the underwater test in this study are only applicable for pyrotechnic articles with small net explosive contents. In cases where large net explosive contents are investigated, appropriately bigger water tanks should be used.

References

1 Directive 2007/23/EC of the European Parliament and of the Council of 23 May 2007 on the placing on the market of pyrotechnic articles, *Official Journal of the European Union*, 14.6.2007.

2 Directive 2013/29/EU of the European Parliament and of the Council of 12 June 2013 on the harmonisation of the laws of the Member States relating to the making available on the market of pyrotechnic articles (recast), *Official Journal of the European Union*, 28.6.2013.

3 EN 13763-15:2004 Explosives for civil uses - Detonators and relays - Part 15: Determination of equivalent initiating capability, European Committee for Standardization CEN, 2004.

Visual and Near Infrared Mass Extinction Coefficient of Five Pyrotechnic Screening Smokes

Matti Harkoma
Finnish Defence Forces Technical Research Centre, Explosives and CBRN Protection Technology, P.O.Box 5, FIN-34111 Lakiala, Finland.
Email: matti.harkoma@mil.fi

Abstract: *The screening properties of five different obscurants were compared at relative humidities of 30%, 50% and 85% and mass extinction coefficients were calculated. The obscurants were five military smokes: 1) a traditional hexachloroethane, Zn powder and TNT based screening smoke, the HC smoke as a reference, 2) a potassium chlorite, Mg powder and azodicarbonamide based screening smoke, the KM smoke, 3) a Mg powder based HC smoke, 4) a potassium chlorate, lactose and terephthalic acid based white coloured screening smoke, the TPA smoke, and 5) a titanium oxide based HC smoke. The apparatus was a CCD (Charge-Coupled Device) detector based dispersive spectrometer with a sample chamber and a humidity generator. The wavelength region was 450 to 850 nm. The important variable in determining how a military smoke retains its screening properties over time is the mass extinction coefficient. According to the results, the Zn based HC smoke has the best screening properties at low relative humidity. When the relative humidity is high the Mg based HC smoke has the best screening properties at first, but the KM type smoke retains its screening properties well, being the best of these three smokes after 20 seconds. After 60 seconds, the mass extinction coefficient of the KM smoke is 33% higher than the mass extinction coefficient of the reference smoke, when the mass extinction coefficient of the Mg based HC smoke is 20% lower than the mass extinction coefficient of the reference smoke.*

Keywords: *Screening smoke, obscurant, extinction coefficient, infrared*

1. Introduction

The reason for measuring transmission is to investigate the extinction properties of obscurants such as military smokes as a function of wavelength in the visual and near infrared region of 450 to 850 nm. The commonly known wavelength limits are 380 to 760 nm for the visual range (VIS) and 0.76 to 1.3 μm for the near infrared range (NIR), respectively. The wavelength limits may vary depending on the reference. Reliable and repeatable laboratory scale transmission measurement of obscurants in the visual and near infrared wavelength region requires an apparatus specially designed for this research.

In practice, humidity noticeably affects the extinction of light in an aerosol medium such as military smokes, and therefore measurements have to be performed in a controlled humidity environment. A humidity generator and the capability to measure the relative humidity and temperature are necessary. On the basis of experience the calculated absolute humidity values for each military smoke using the measured values of relative humidity and temperature should be taken into account when analysing the screening properties.

The extinction research on obscurants such as military screening smokes was performed in the visual and infrared wavelength region using an FTIR spectrometer and an experimental

Article Details	***Article No:- 0101***
Manuscript Received:- 30/09/2013	***Final Revisions:-18/01/2014***
Publication Date:-19/01/2014	***Archive Reference:- 1637***

chamber with humidity adjustment.[1] Some studies were carried out using the whole broad visual wavelength band of the QTH lamp for the extinction measurements of screening smokes.[2] An infrared camera was also a very useful instrument for research into the infrared screening capability of military smoke clouds.[3,4] The chemistry of military screening smokes for known compositions has been described by many authors.[5–7]

2. Transmission measurements of aerosols

An aerosol in the gaseous medium consists of solid state particles and/or liquid droplets, which have a particular diametric distribution, e.g. the HC type military smoke has a typical particle diameter of about 0.1 μm,[8] but at high humidity it rises to values of 3 to 7.6 μm after several seconds. As a point of comparison typical natural clouds contain water droplets with mean radii of about 20 μm.[9]

The interaction mechanisms between electromagnetic radiation and aerosol particles in the visible and infrared region are scattering and absorption. In the scattering phenomenon, an electromagnetic wave changes its direction of propagation randomly in every collision with aerosol particles. In absorption a photon loses its energy totally or partly to the vibrational or rotational movement of a molecule. Absorption is a potential interaction mechanism with gaseous molecules and with solid particles or with liquid droplets.

The variables in the transmission of the radiation through a medium containing aerosol particles are spectral radiance $L_\lambda(\lambda,s)$ at a point s with coordinates (x,y,z), mass concentration of the aerosol ρ [g cm^{-3}], spectral mass absorption coefficient $\alpha_a(\lambda,s)$ and spectral mass scattering coefficient $\alpha_s(\lambda,s)$. The wavelength of the radiation is λ. Thus the spectral radiance has the equation:

$$dL_\lambda(\lambda,s) = -\alpha(\lambda,s)L_\lambda(\lambda,s)\rho ds \qquad (1)$$

where $\alpha(\lambda,s) = \alpha_a(\lambda,s) + \alpha_s(\lambda,s)$ is the spectral mass extinction coefficient. The extinction of the radiation is the combined effect of the absorption and the scattering phenomena.[10,8]

Here it is assumed that: 1) the aerosol medium is homogenous and thus $\alpha(\lambda,s) = \alpha(\lambda)$; 2) the scattering originating from the side radiation by the aerosol is insignificant and 3) the intrinsic thermal emission of the aerosol and the medium atmosphere is insignificant. The Lambert–Beer law can be written as:

$$\alpha(\lambda)\rho l = -\ln L_\lambda/L_{o\lambda} = \ln L_{o\lambda}/L_\lambda \qquad (2)$$

The transmittance at the wavelength λ is:

$$T_\lambda = L_\lambda/L_{o\lambda} = e^{\alpha(\lambda)\rho l} \qquad (3)$$

The spectral mass extinction coefficient can be calculated from the equation:

$$\alpha(\lambda) = \ln(L_{o\lambda}/L_\lambda)/\rho l = -\ln T_\lambda/\rho l \qquad (4)$$

The variables $L_{o\lambda}$ and L_λ, describing the intensity of the transmitted radiation without aerosol and with aerosol, respectively, can be measured as a function of wavelength. The mass concentration of the aerosol ρ is calculated and the path length of radiation l is known from the geometry of the experimental setup.

The models for the scattering of electromagnetic radiation by a single particle are based either on an exact solution to Maxwell's wave equations or, if there is no analytical solution, on approximative numerical solutions. The Mie theory is an analytical solution to Maxwell's equations in the case of scattering by spherical and ellipsoidal particles. In the case of more complicated geometrical forms of particles, some approximative methods were developed.[11–14]

3. Technical description of the apparatus

The basic setup of the apparatus is a dispersive spectrometer with a multichannel detector for the visible and the near infrared wavelength region. The apparatus is depicted schematically in Figure 1. The monochromator is the 1/8m Oriel 77400 with a 400 lines/mm ruled grating (Oriel 77417). The usable wavelength range of the grating is 270 to 1600 nm, having a primary wavelength range 300 to 1200 nm and a blaze wavelength of 500 nm. Before the exit slit of the monochromator there is a 50 mm diameter diffusing sphere assembly (the integrating sphere Oriel 70505). The CCD (Charge-Coupled Device) detector has 1024 × 256 channels (Oriel model 77193-5 InstaSpec IV) and 180 to 1100 nm spectral response. The usable wavelength region of the spectrometer is thus 270

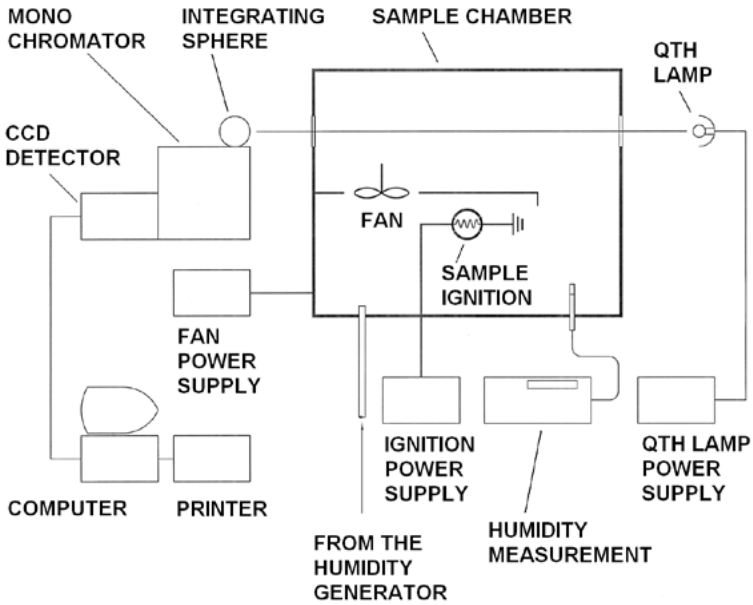

Figure 1. *Schematic picture of the spectrometer for the transmission measurements of aerosols.*

to 1100 nm. The software for the CCD detector system is InstaSpec System IS 401 Version 1.0.

The light source is a QTH lamp, 100 W/12 V Oriel 6358, connected to a stabilized power supply. The sample chamber has a volume of 150 L with dimensions of 840 × 300 × 600 mm. The material is stainless steel AISI 314 with a wall thickness of 1 mm. The optical windows are made of quartz glass. The wavelength calibration of the spectrometer was performed using the well-known mercury lines of a fluorescent lamp.

The weight of a military smoke sample was 2 g. The specific weight of the military smoke mixture varied depending on the specific weight of the used components. Typically the net weight of the military smoke canister is 425 g. That's why it is reasonable to use constant sample weight for all studied obscurants. The pressed sample pellets have been ignited with electric current using 0.25 mm thick AlCr wire.

4. Humidity of air and humidity generator

The relative humidity RH of an air and water vapour mixture is defined as the ratio of the partial vapour pressure of water P_w to the saturated vapour pressure of water P_{ws} at a prescribed temperature. It is normally expressed as a percentage according to the equation RH = $P_w/P_{ws}\times 100\%$.

The saturated vapour pressure can be calculated from the equation[15]

$$P_{ws} = A \cdot 10^{\left(\frac{m \cdot t}{t+T_n}\right)}$$

where temperature dependent variables A, m and T_n are given values from Table 1

The absolute humidity α is the quantity of water in a particular volume of air. Usually it is the mass of water vapour m_w in grams per cubic meter of air V_a: $a = m_w/V_a$.

The absolute humidity is a function of temperature and can be expressed using the saturated vapour

Table 1. Values of variables A, m and T_n at temperatures from −40 to +180 °C.

t/°C	A	m	T_n
−40 to +50	6.1078	7.5000	237.3
+50 to +100	5.9987	7.3313	229.1
+100 to +150	5.8493	7.2756	225.0
+150 to +180	6.2301	7.3033	230.0

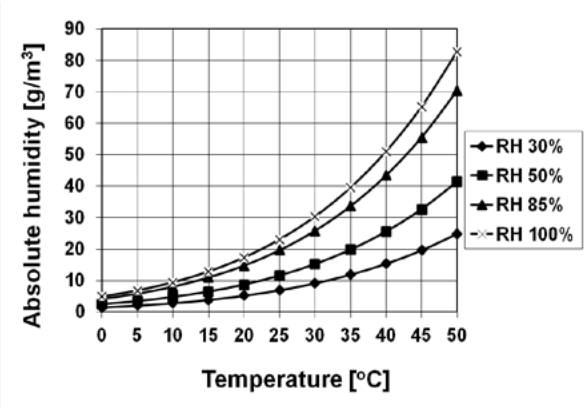

Figure 2. *Absolute humidity of air as a function of temperature calculated using equation of α when relative humidity is 30%, 50%, 85% and 100%.*

pressure of water and the relative humidity of air in the form

$$a = 216.68 \cdot \mathrm{RH} \cdot P_{ws} / (100 \cdot p - \mathrm{RH} \cdot P_{ws}).$$ [12]

Figure 2 describes the absolute humidity of air as a function of temperature calculated using this equation for *a* when the relative humidity is 30%, 50%, 85% and 100%.

The setup of the humidity generator is represented in Figure 3. It consists of three 500 ml electrically warmed gas washing bottles connected in series using silicone rubber pipes.

The adjustment of humidity is performed by mixing dry air and damp air in a three way valve. The air, having suitable humidity for the research, is connected to the sample chamber. The humidity is measured in the condensed water extraction container and in the sample chamber using humidity transducers (Vaisala HMP230).

5. Results

Several transmission measurements of military screening smokes have been performed by varying the humidity in the sample chamber. In Figure 4, a transmission spectrum of HC smoke in the visible and very near infrared region of 402 to 884 nm is depicted, when the relative humidity was 30%. The maximum intensity of the spectrum in this setup is typically 266 000 counts. Measuring the spectrum without extinction, the background spectrum, it is possible to work out the net effect of an aerosol. It is the difference between the background spectrum and the extinction spectrum of the aerosol. Typically the maximum intensity of a background spectrum is 4.5×10^6 counts, which

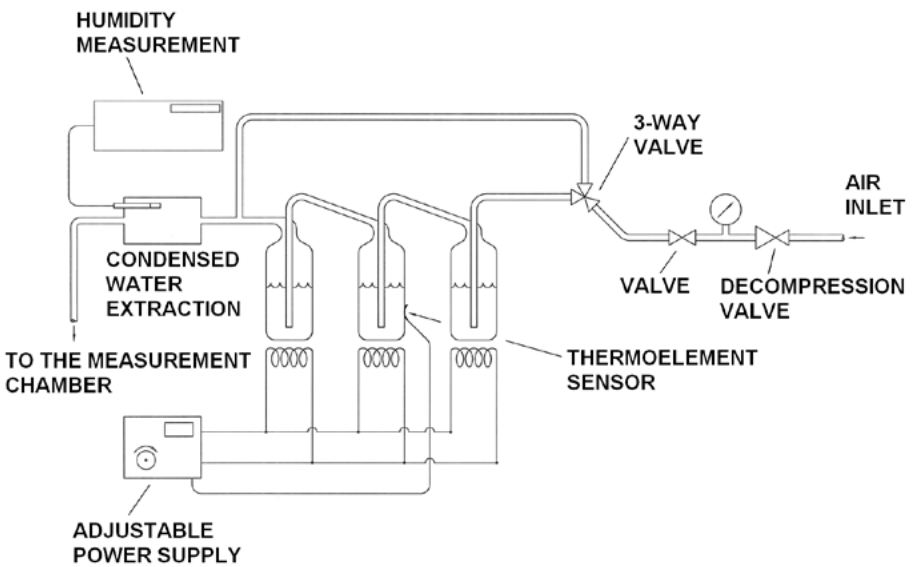

Figure 3. *The schematic picture of the humidity generator.*

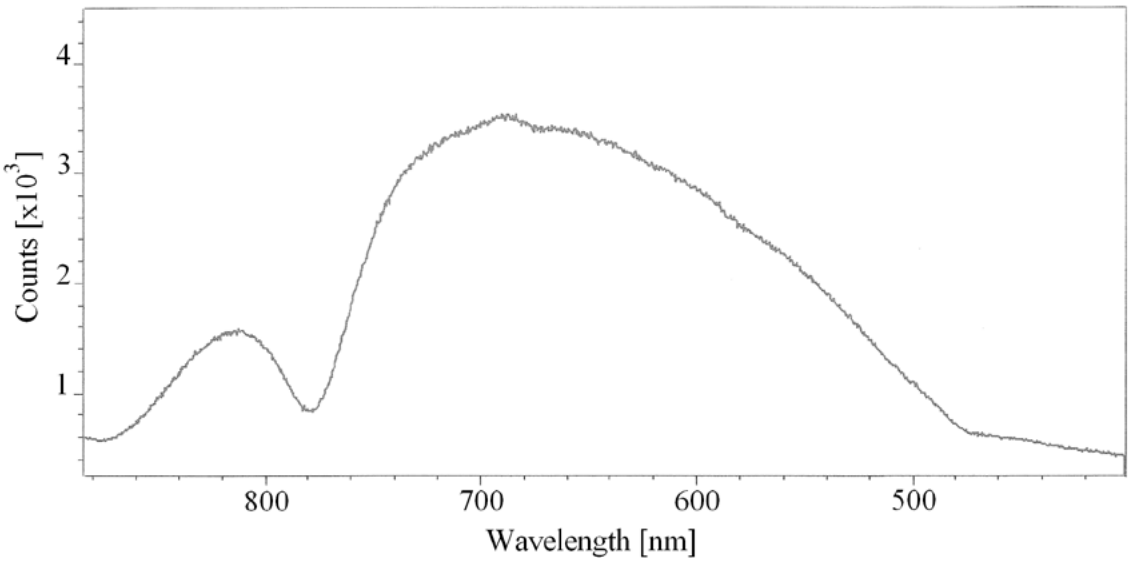

Figure 4. *A single spectrum of an HC/Zn type military smoke in the wavelength region 884 to 402 nm.*

corresponds to zero absorption. Those values are relative and depend on the intensity of the QTH lamp and on the setup of the apparatus.

The measurement of the kinetic series of an aerosol gives the extinction coefficients as a function of time. In Figure 5, a kinetic series of a HC/Zn type military smoke is depicted on a time scale of up to 190 s. The aerosol pellet is ignited between 30 and 40 seconds after the start of the measurement.

Details of the military smoke compositions studied are given in Table 2. HC/Zn is the traditional hexachloroethane, metallic Zn powder and TNT based military smoke, which was usually used as a reference.

Kinetic measurements make it possible to compare the extinction properties of aerosols in a certain fixed wavelength as a function of time. The mass concentration of the aerosol ρ was calculated using a sample chamber of 0.150 m^3 in volume and a mass of 2 g for the pressed smoke pellet. Here it was assumed that the smoke pellet burns perfectly without producing any ash. The path length l of the radiation was 0.84 m. The relative

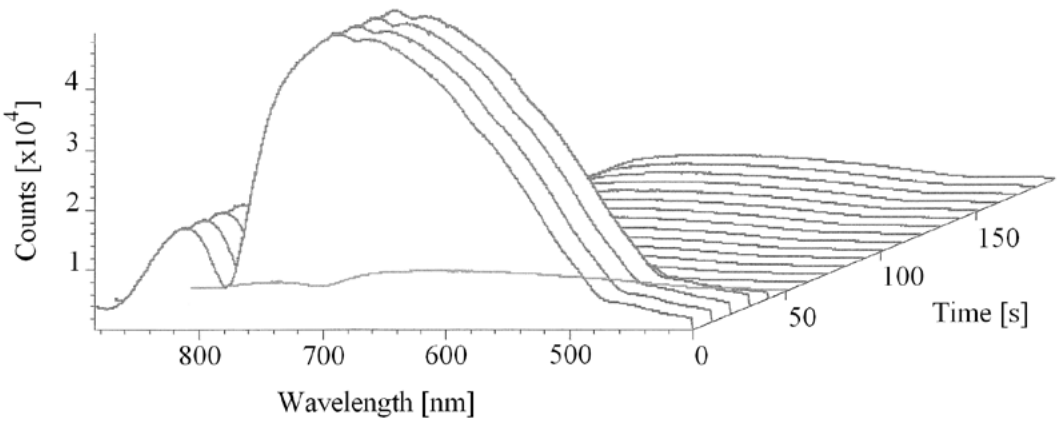

Figure 5. *The kinetic series of a HC/Zn type military smoke between 0 and 190 seconds. The time difference between the two spectra is 10 seconds. The ignition took place between 30 s and 40 s after the start of the measurement.*

Table 2. *The studied military smoke compositions.*

Symbol	Type	Composition	Manufactured by
HC/Zn	HC smoke	C_2Cl_6, Zn, TNT [a]	Haapajärvi Ordnance Depot, Finland
KM	KM smoke	KCl, KNO_3, Mg, $NH_2CON{=}NCONH_2$,[b] $KClO_4$[16]	NICO GmBH, Germany
HC/Mg	HC smoke	C_2Cl_6, Mg[17]	TNO, Netherlands
TPA	White coloured smoke	$KClO_3$, lactose, terephthalic acid (TPA)[18]	PVTT
TIO	HC smoke	C_2Cl_6, Al, TiO_2	Haapajärvi Ordnance Depot, Finland

[a] C_2Cl_6 is hexachloroethane (HC), TNT is trinitrotoluene. [b] Azodicarbonamide.

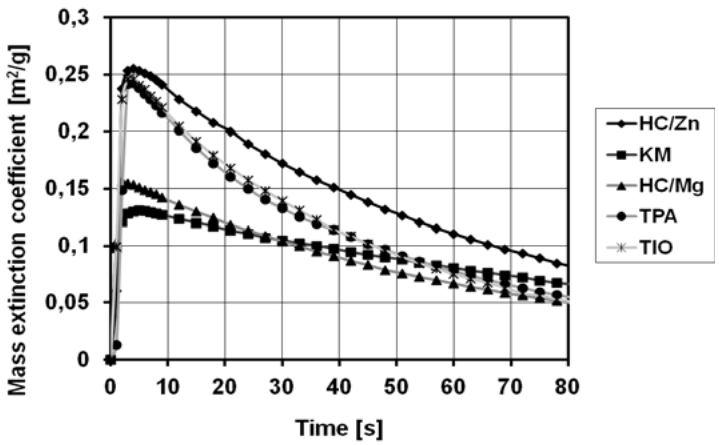

Figure 6. *The relative mass extinction coefficient of five military smokes as a function of time with a fixed wavelength of 600 nm and relative humidity of 30%.*

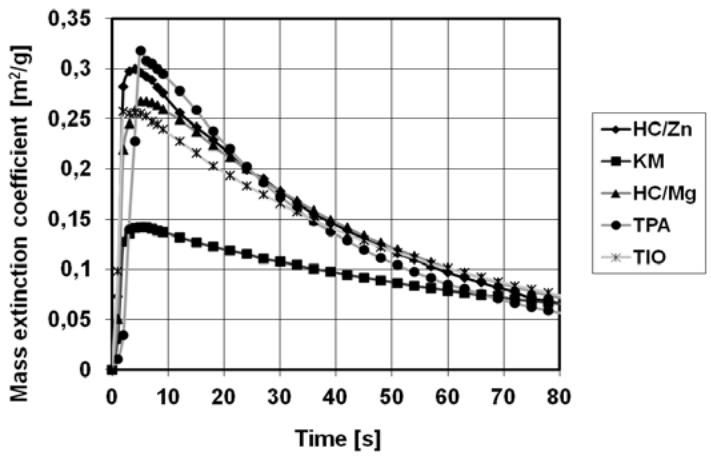

Figure 7. *The relative mass extinction coefficient of five military smokes as a function of time with a fixed wavelength of 600 nm and relative humidity of 50%.*

mass extinction coefficient was calculated using equation (4) for $\alpha(\lambda)$ as in section 2.

In Figures 6–8, the relative mass extinction coefficient of the five military smokes with a fixed wavelength of 600 nm is depicted up to 80 s after ignition, when the relative humidity was 30%, 50% and 85%.

In Figures 9–13, the maximum value of relative mass extinction coefficient for five military smokes is depicted as a function of wavelength 450 to 650 nm, when the relative humidity was 30%, 50% and 85%. The mass extinction coefficient has been calculated as a mean value of three measurements.

In Tables 3–5, the absolute humidity values α for each military smoke are calculated using the measured values of relative humidity RH and temperature t. The nominal value of relative humidity was 30%, 50% and 85%.

According to the equation for α and Figure 2 the absolute humidity mean value of 22.1 g m^{-3} in Table 5.4 corresponds to a relative humidity of 100% when the temperature is 24.3 °C.

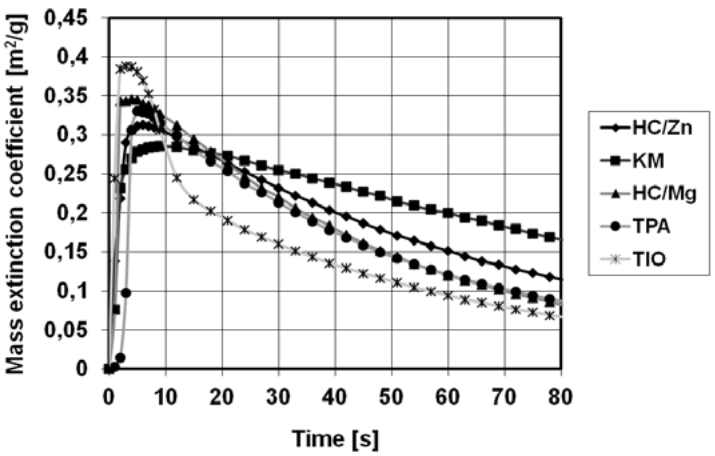

Figure 8. *The relative mass extinction coefficient of five military smokes as a function of time with a fixed wavelength of 600 nm and relative humidity of 85%.*

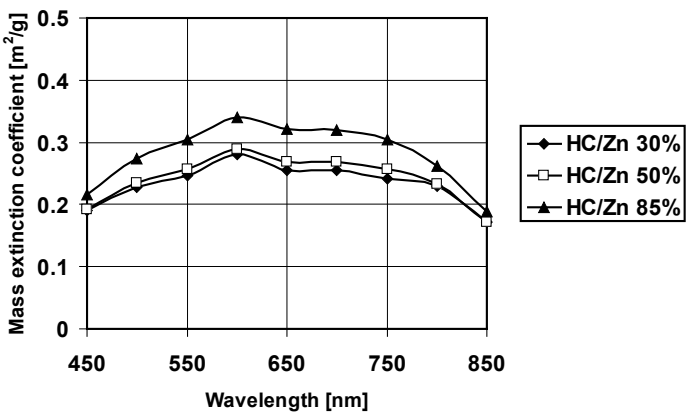

Figure 9. *The relative mass extinction coefficient of HC/Zn military smoke as a function of wavelength, when the relative humidity was 30%, 50% and 85%.*

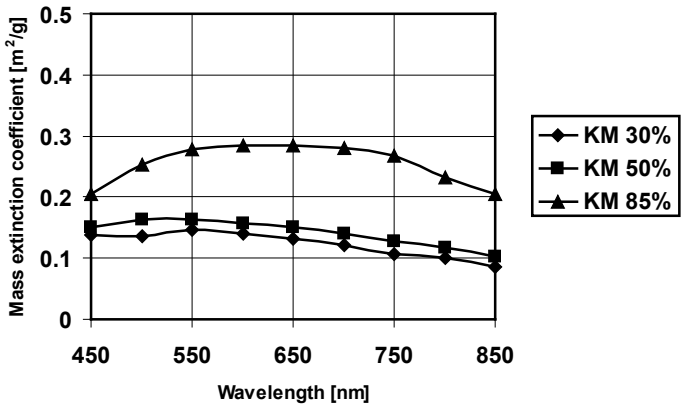

Figure 10. *The relative mass extinction coefficient of KM military smoke as a function of wavelength, when the relative humidity was 30%, 50% and 85%.*

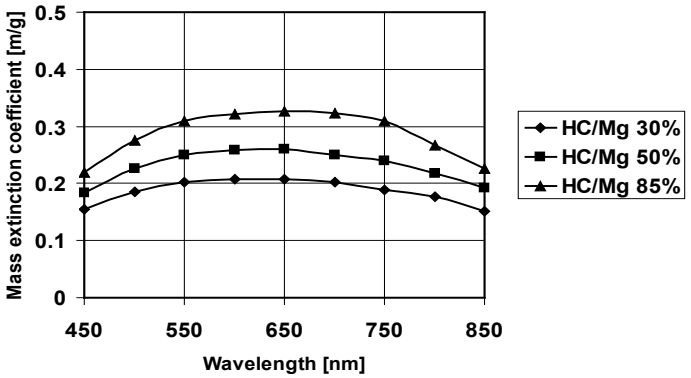

Figure 11. *The relative mass extinction coefficient of HC/Mg military smoke as a function of wavelength, when the relative humidity was 30%, 50% and 85%.*

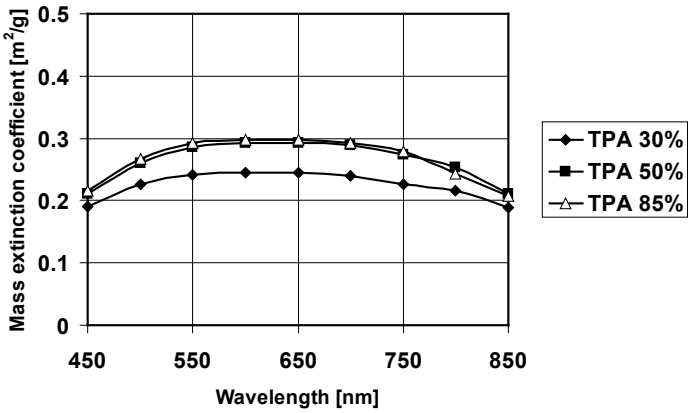

Figure 12. *The relative mass extinction coefficient of TPA military smoke as a function of wavelength, when the relative humidity was 30%, 50% and 85%.*

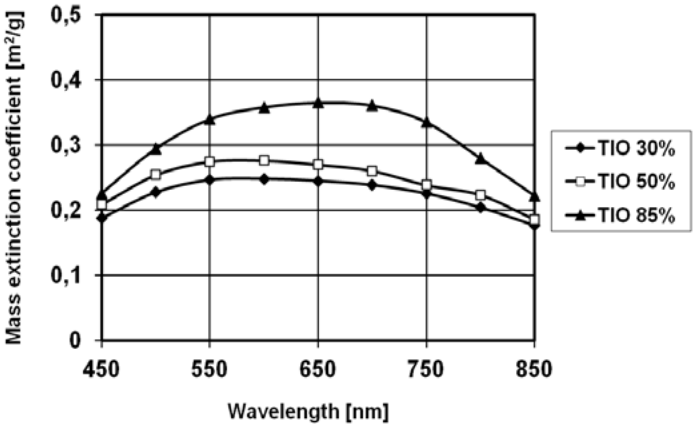

Figure 13. *The relative mass extinction coefficient of TIO military smoke as a function of wavelength, when the relative humidity was 30%, 50% and 85%.*

Table 3. *Measured values of relative humidity and temperature and calculated absolute humidity values for each military smoke with mean value and variation of absolute humidity α when the nominal value of the relative humidity was 30%.*

	RH (%)	*t*/°C	α/g m^{-3}
HC/Zn	50.5	24.2	11.1
KM	50.7	24.3	11.2
HC/Mg	50.2	23.3	10.5
TPA	50.4	24.7	11.4
TIO	50.3	24.4	11.2
Mean value			**11.1**
Variation (%)			**8.2**

Table 4. *Measured values of relative humidity and temperature and calculated absolute humidity values for each military smoke with mean value and variation of absolute humidity α when the nominal value of the relative humidity was 50%.*

	RH (%)	*t*/°C	α/g m^3
HC/Zn	30.3	24.0	6.6
KM	29.7	23.0	6.1
HC/Mg	30.3	24.0	6.6
TPA	30.3	24.3	6.7
TIO	30.4	23.3	6.4
Mean value			**6.5**
Variation (%)			**9.3**

Table 5. *Measured values of relative humidity and temperature and calculated absolute humidity values for each military smoke with mean value and variation of absolute humidity α when the nominal value of the relative humidity was 85%.*

	RH (%)	*t*/°C	α/g m^3
HC/Zn	85.0	27.9	23.0
KM	85.0	27.8	22.9
HC/Mg	85.0	25.7	20.3
TPA	85.1	27.7	22.8
TIO	85.0	26.8	21.6
Mean value			**22.1**
Variation (%)			**11.9**

6. Discussion

The laboratory scale extinction measurement as a function of wavelength is a method for comparing the screening and protection properties of military smokes. Using the CCD-detector, the whole wide wavelength region was measured simultaneously. Our interest is in comparing the screening properties of military smokes as a function of time and as a function of wavelength. In the real life environment, temperature and humidity change constantly. The measurement of extinction when the relative humidity is, for example, 30%, 50% and 85% provides a useful range for comparing the screening properties of aerosols such as military smokes. The calculated absolute humidity values

for each military smoke using the measured values of relative humidity and temperature (Tables 3–5) were taken into account analysing the screening properties. The water has a well known absorption minimum at the wavelength 460 to 480 nm.[8]

Strong absorption by CO_2 exists in the 2.7 μm region, the 4.3 μm region and the region between 11.4 μm and 20 μm. Weaker absorption bands are present at 1.4 μm, 1.6 μm, 2.0 μm, 4.8 μm, 5.2 μm, 9.4 μm, and 10.4 μm. Absorption bands by CO exist in the 2.3 μm and in the 4.7 μm region. Weaker absorption bands are present at the wavelength 1.560 to 1.633 μm.[11] Thus the distinctive absorption bands of CO_2 and CO are outside the wavelength region of 450 to 850 nm.

Analysis of screening properties as a function of time (Figures 6–8) shows, for example, that the traditional HC/Zn smoke and TIO have the best extinction properties inside a time period of 80 seconds when the relative humidity is 30%. Unexpectedly, the traditional HC/Zn smoke, the TPA smoke and the HC/Mg smoke have virtually equal screening properties when the relative humidity is 50%. The screening properties are better compared with the KM smoke and the TIO smoke up to 80 seconds at that relative humidity. At a relative humidity of 85% the TIO smoke has the best screening properties inside the first 7 seconds, but it loses screening properties rapidly compared with the other smokes, the HC/Zn, the KM, the HC/Mg and the TPA smoke. The HC/Mg smoke and the TPA smoke have the second best screening properties inside the first 18 seconds. After that the HC/Mg smoke and the HC/Zn smoke have better screening properties. The TIO based military aerosol is probably better at producing bigger particles when compared, for example, with the other smokes studied here. According to those results (Figure 8), the KM smoke retains its screening properties best when the relative humidity is high. As a general observation one could say that the screening properties of military smokes are better when the humidity of the air is rising, which is in good agreement with other references.

Considering the values of the relative mass extinction coefficient as a function of wavelength 450 to 850 nm (Figures 9–13), when the relative humidity was 30%, 50% and 85%, it can be seen that the extinction properties are, in general, better in the visual range when the wavelength is longer, except for HC/Zn, which seems to have a maximum value at about 600 nm (orange).

In general the measured temperature values were about 3 degrees higher for all five military smokes when the relative humidity was 85% in comparison with the measurements at relative humidity 30% and 50%. The absolute humidity mean value of 22.1 g m^{-3} (Table 5) corresponds to a relative humidity of 100% when the temperature is 24.3 °C. Conversely, the temperature value of 24.3 °C corresponds to the absolute humidity value of 18.8 g m^{-3} when the relative humidity is 85%. The difference is 3.3 g m^{-3}, which is 17.6% of the humidity value of 18.8 g m^{-3}. This may emphasize the relative influence of humidity. The mean variation of the absolute humidity in the measurements was about 10% and it may have influenced the individual extinction coefficient values but not the order of measured military smokes, when the variable was the mass extinction coefficient.

6. Acknowledgments

I would like to thank my co-workers and colleagues Ms. Maija Hihkiö, Ms. Tellervo Vormisto, Ms. Hanna Kariniemi, Mr. Matti Hemmilä, Mr. Paavo Raerinne and Mr. Petri Wallgren.

References

1 F. Hopfgarten and P. Collvin, 'Studies of IR- and visible screening smoke', *Proceedings of 16th International Annual Conference of ICT*, Karlsruhe, FRG, 1985.

2 B. Doescher, 'A Dynamic Performance Test of Military Screening Smokes', *Proceedings of 35th International Annual Conference of ICT*, Karlsruhe, FRG, 2004.

3 S. Cudzilo, 'Studies of IR-Screening Smoke Clouds', *Propellants, Explosives, Pyrotechnics*, Vol. 26, 2001, pp. 12–16.

4 M. O. Hemmilä, M. K. Hihkiö, M. J. Harkoma and M. K. Hagfors, 'Training Smokes Evaluation Program', *Proceedings of Twenty-Third International Pyrotechnics Seminar*, Tsukuba, Japan, 1997.

5 J. A. Conkling, *Chemistry of Pyrotechnics*, Marcel Dekker Inc, New York, 1985.

6 A. A. Shidlovsky, *Principles of Pyrotechnics*, Mashinostroyeniye Press, 1964.

7 H. Ellern, *Military and Civilian Pyrotechnics*, Chemical Publishing Company Inc., New York, 1968.

8 G. Heimburger, 'Toxikologisk undersoekning av zink- och titanroeksatser' (Toxicological Investigation of Zinc and Titanium Smoke Compositions. A Literature Study), FOA report C 40072-H2, 1977.

9 E. J. McCartney, *Optics of the Atmosphere – Scattering by Molecules and Particles*, John Wiley & Sons, New York, 1976, p. 225.

10 F. G. Smith, *The Infrared & Electro-Optical Systems Handbook, Volume 2, Atmospheric Propagation of Radiation*, Infrared Information Analysis Center, Ann Arbor, Michigan, SPIE Optical Engineering Press, Bellingham, Washington, 1993.

11 W. L. Wolfe and G. J. Zissis, *The Infrared Handbook*, The Infrared Information Analysis (IRIA) Center, Environmental Research Institute of Michigan, 1993.

12 A. Ishimaru, *Wave Propagation and Scattering in Random Media*, Vol 1 and 2, Academic Press, New York, 1978.

13 V. I. Rakov, L. T. Sushkova and M. Z. Korytnyy, 'Simulating the IR Radiation Extinction Process in the Atmosphere', *Radio engineering and electronic physics*, Vol. 20, 1975, p. 7.

14 C. F. Bohren and D. R. Huffman, *Absorption and Scattering of Light by Small Particles*, John Wiley & Sons, New York, 1983, p. 82.

15 Vaisala Inc., *Manual of the Humidity and Temperature Transmitter Series HMP230*, Vaisala, 1997-02-28.

16 U. Krone, 'A non-toxic pyrotechnic screening smoke for training purposes', *Proceedings of the 15th International Pyrotechnics Seminar*, 581, 1990.

17 C. A. Van Driel, A. P. M. Leenders, A. B. Leeuwenburgh and E. Schonevilee, Composition for generating smoke, WO 98/40330, PCT/NL/98/00149.

18 G.V. Tracy, J.A. Domanico and G. P. Young, U.S. Stationery Invention Registration H227, 1987.

Information for Readers

Editorial Policy

Articles accepted for publication in the *Journal of Pyrotechnics* can be on any technical subject in pyrotechnics. However, a strong preference will be given to articles reporting on research (conducted by professional or serious individual experimenters) and to review articles (either at an advanced or tutorial level). Both long and short articles will be gladly accepted. Also, responsible letters commenting on past Journal articles will be published along with responses by the authors.

Back Issues

Back issues of the Journal will be kept in print permanently as reference material. In addition all past articles and issues are available at the *Journal of Pyrotechnics* - http://archive.jpyro.com.

New Publication Procedures

As announced in Issue 26, the JPyro Board has decided that the Journal will be first published in electronic form and that the hard copy will be published annually. This has been driven by three main factors - the needs of authors to have their papers published in a reasonable timescale, the success of the JPyro archive, and the costs and time required to produce hard copies. In addition the modern publishing and research worlds increasing rely on early electronic publication to provide information to others in the most timely manner and, as appropriate, to be able to claim Intellectual Property rights on material published (which are taken from the date of publication).

In future articles accepted for publication in the Journal will be published, in the first instance, electronically on the JPyro archive website (http://archive.jpyro.com) within a target timescale of three weeks from acceptance (i.e. when all editing is complete) and eight weeks from original submission. All articles will be dated and published in acceptance order. The timescales rely, of course, on referees and authors responding in a reasonable timescale to any queries raised.

In this way no article will be held up awaiting the collation of all the other material necessary for economic and efficient production of the hard copy. Instead, a hard copy of the Journal will be available to those who require it, in most cases annually - incorporating all the articles published within the previous year - for an additional charge. In addition, the JPyro archive will continue to offer online purchase of single articles from the Journal and other publications, or time-limited access to the entire archive.

If you have any questions regarding the new approach please do contact any of the production team

Publication Frequency

Articles in the *Journal of Pyrotechnics* will appear first electronically at http://archive.jpyro.com and will subsequently be produced in hard copy annually in the early spring of the year following publication.

Subscriptions

The following subscription types are available

- Electronic only - access to the electronic versions of articles published during the subscription period indefinitely
- Electronic and Hard copy - as above + hard copy when published
- Single article access - indefinite access to the specified article
- Access to the entire archive - annual access to the full archive

Events and Sponsors

Now that the Journal of Pyrotecnics is published, primarily, electronically the forthcoming events are available on the archive website http://archives.jpyro.com.

If you have any events you would like included in that list please contact the publisher.

Please note

It is our intention in the future to maintain an up-to-date list of current sponsors on the JPyro archive website - http://archives.jpyro.com.

If there are any changes to your details please email sponsors@jpyro.com.

Sponsors of the Journal get unlimted electronic access to the issues which they have sponsored, details online and in the hard copy and a discounted rate for hard copy editions. Please contact the publisher for more details.

Caution

The experimentation with, and the use of, pyrotechnic materials can be dangerous and may require licences or permits in certain countries; it is felt to be important for the reader to be duly cautioned. Without the proper training and experience no one should ever experiment with or use pyrotechnic materials. Also, the amount of information presented in this Journal is not a substitute for necessary training and experience, nor does it remove the relevant application of national or local laws and regulations.

A major effort has been undertaken to review all articles for correctness. However it is possible that errors remain. It is the responsibility of the reader to verify any information herein before applying that information in situations where death, injury or property damage could result.